

(NASA-TM-X-3336) SUBSONIC AND TRANSONIC
DYNAMIC STABILITY CHARACTERISTICS OF THE
SPACE SHUTTLE LAUNCH VEHICLE (NASA) 68 p HC
\$4.50

N76-19051

CSCL 01A

Unclassified
21091

H1/01

1. Report No. NASA TM X-3336	2. Government Accession No.	3. Recipient's Catalog No.	
4. Title and Subtitle SUBSONIC AND TRANSONIC DYNAMIC-STABILITY CHARACTERISTICS OF THE SPACE SHUTTLE LAUNCH VEHICLE		5. Report Date March 1976	
6. Performing Organization Code		7. Author(s) Delma C. Freeman, Jr., Richmond P. Boyden, and Edwin E. Davenport	
8. Performing Organization Report No. L-10378		9. Performing Organization Name and Address NASA Langley Research Center Hampton, Va. 23665	
10. Work Unit No. 506-26-30-01		11. Contract or Grant No.	
12. Sponsoring Agency Name and Address National Aeronautics and Space Administration Washington, D.C. 20546		13. Type of Report and Period Covered Technical Memorandum	
14. Sponsoring Agency Code			
15. Supplementary Notes			
16. Abstract <p>An investigation has been conducted to determine the subsonic and transonic dynamic-stability characteristics of a 0.015-scale model of the space shuttle launch vehicle. These tests were conducted in the Langley 8-foot transonic pressure tunnel over a Mach number range from 0.3 to 1.2. Forced-oscillation equipment was used to determine the damping characteristics of several configurations about all three axes.</p> <p>The test results show that the model exhibited positive damping in pitch except at the highest Mach number (1.2) where there was a region of negative damping at 2° angle of attack. The yawing-oscillation tests show that the model exhibited nonlinearities and negative damping at Mach numbers of 0.3 and 0.6. The model exhibited positive roll damping throughout the test angle-of-attack and Mach range.</p>			
17. Key Words (Suggested by Author(s)) Dynamic stability Shuttle launch vehicle Aerodynamics		18. Distribution Statement Unclassified - Unlimited	
		Subject Category 01	
19. Security Classif. (of this report) Unclassified	20. Security Classif. (of this page) Unclassified	21. No. of Pages 66	22. Price* \$4.25

SUBSONIC AND TRANSONIC DYNAMIC-STABILITY CHARACTERISTICS OF THE SPACE SHUTTLE LAUNCH VEHICLE

Delma C. Freeman, Jr., Richmond P. Boyden,
and Edwin E. Davenport
Langley Research Center

SUMMARY

An investigation has been conducted to determine the subsonic and transonic dynamic-stability characteristics of a 0.015-scale model of the space shuttle launch vehicle. These tests were conducted in the Langley 8-foot transonic pressure tunnel over a Mach number range from 0.3 to 1.2. Forced-oscillation equipment was used to determine the damping characteristics of several configurations about all three axes.

The test results show that the model exhibited positive damping in pitch except at the highest Mach number (1.2) where there was a region of negative damping at 2° angle of attack. The yawing-oscillation tests show that the model exhibited nonlinearities and negative damping at Mach numbers of 0.3 and 0.6. The model exhibited positive roll damping throughout the test angle-of-attack and Mach range.

INTRODUCTION

As part of the space shuttle development effort, the Langley Research-Center has sponsored a program to determine experimentally the dynamic-stability characteristics of the space shuttle vehicle. Aerodynamic damping derivatives have been determined for the orbiter at subsonic to hypersonic speeds (refs. 1 to 3) and for the launch vehicle at supersonic speeds (ref. 4).

As part of this study, subsonic and transonic forced-oscillation tests of a 0.015-scale model of the space shuttle launch vehicle configuration (orbiter designation 140 A/B) were conducted in the Langley 8-foot transonic pressure tunnel. These tests were conducted for several configurations over a Mach number range from 0.3 to 1.2; the tests measured pitch, roll, and yaw damping, the normal force due to pitch rate, and the cross derivatives: yawing moment due to roll rate and rolling moment due to yaw rate. Tests were conducted for the complete launch vehicle configuration and also for the orbiter external-tank configuration which simulated an abort situation. Dynamic derivatives were measured for two center-of-gravity locations representative of the shift encountered over the ascent-flight Mach number range.

SYMBOLS

The reference length used to nondimensionalize all of the aerodynamic parameters was the orbiter body length which is 0.4916 m for the 0.015-scale model. The reference area used to nondimensionalize the aerodynamic parameters was the orbiter wing area which is 0.05623 m² for the 0.015-scale model.

All data presented are referred to the body-axis system. (See fig. 1.) The origins of the axes were located to correspond to the center-of-gravity (e.g.) positions shown in figure 2.

Units of measurement are presented in the International System of Units (SI). See reference 5 for details on the use of the SI physical constants and conversion factors.

C_l rolling-moment coefficient, $\frac{\text{Rolling moment}}{q_\infty S\ell}$

$$C_{l_p} = \frac{\partial C_l}{\partial \frac{p\ell}{2V}}, \text{ per radian}$$

$$C_{l\dot{\beta}} = \frac{\partial C_l}{\partial \frac{\dot{\beta}\ell^2}{4V^2}}, \text{ per radian}$$

$C_{l_p} + C_{l\dot{\beta}} \sin \alpha$ damping-in-roll parameter, per radian

$$C_{l_r} = \frac{\partial C_l}{\partial \frac{r\ell}{2V}}, \text{ per radian}$$

$$C_{l\dot{r}} = \frac{\partial C_l}{\partial \frac{\dot{r}\ell^2}{4V^2}}, \text{ per radian}$$

$C_{l_r} - C_{l\dot{\beta}} \cos \alpha$ rolling moment due to yaw rate parameter, per radian

$$C_{l\beta} = \frac{\partial C_l}{\partial \beta}, \text{ per radian}$$

$$C_{l\dot{\beta}} = \frac{\partial C_l}{\partial \frac{\dot{\beta}\ell}{2V}}, \text{ per radian}$$

$C_{l\beta} \sin \alpha - k^2 C_{l\dot{\beta}}$ rolling moment due to roll displacement parameter, per radian

$C_{l\beta} \cos \alpha + k^2 C_{l\dot{\beta}}$ effective dihedral parameter, per radian

C_m pitching-moment coefficient, $\frac{\text{Pitching moment}}{q_\infty S \ell}$

$$C_{m_q} = \frac{\partial C_m}{\partial \frac{q\ell}{2V}}, \text{ per radian}$$

$$C_{m\dot{q}} = \frac{\partial C_m}{\partial \frac{\dot{q}\ell^2}{4V^2}}, \text{ per radian}$$

$C_{m_q} + C_{m\dot{\alpha}}$ damping-in-pitch parameter, per radian

$$C_{m\alpha} = \frac{\partial C_m}{\partial \alpha}, \text{ per radian}$$

$$C_{m\dot{\alpha}} = \frac{\partial C_m}{\partial \frac{\dot{\alpha}\ell}{2V}}, \text{ per radian}$$

$C_{m\alpha} - k^2 C_{m\dot{q}}$ oscillatory longitudinal-stability parameter, per radian

C_N normal-force coefficient, $\frac{\text{Normal force}}{q_\infty S}$

$$C_{N_q} = \frac{\partial C_N}{\partial \frac{q\ell}{2V}}, \text{ per radian}$$

$$C_{N\dot{q}} = \frac{\partial C_N}{\partial \frac{\dot{q}\ell^2}{4V^2}}, \text{ per radian}$$

$$C_{Nq} + C_{N\dot{\alpha}} \quad \text{normal force due to pitch rate parameter, per radian}$$

$$C_{N\dot{\alpha}} = \frac{\partial C_N}{\partial \dot{\alpha}}, \text{ per radian}$$

$$C_{N\dot{\alpha}} = \frac{\partial C_N}{\partial \frac{\dot{\alpha}\ell}{2V}}, \text{ per radian}$$

$$C_{N\alpha} - k^2 C_{Nq} \quad \text{normal force due to pitch displacement parameter, per radian}$$

$$C_n \quad \text{yawing-moment coefficient, } \frac{\text{Yawing moment}}{q_\infty S \ell}$$

$$C_{n_p} = \frac{\partial C_n}{\partial \frac{p\ell}{2V}}, \text{ per radian}$$

$$C_{n_{\dot{p}}} = \frac{\partial C_n}{\partial \frac{\dot{p}\ell^2}{4V^2}}, \text{ per radian}$$

$$C_{n_p} + C_{n\dot{\beta}} \sin \alpha \quad \text{yawing moment due to roll rate parameter, per radian}$$

$$C_{n_r} = \frac{\partial C_n}{\partial \frac{r\ell}{2V}}, \text{ per radian}$$

$$C_{n_{\dot{r}}} = \frac{\partial C_n}{\partial \frac{\dot{r}\ell^2}{4V^2}}, \text{ per radian}$$

$$C_{n_r} - C_{n\dot{\beta}} \cos \alpha \quad \text{damping-in-yaw parameter, per radian}$$

$$C_{n\dot{\beta}} = \frac{\partial C_n}{\partial \dot{\beta}}, \text{ per radian}$$

$$C_{n\dot{\beta}} = \frac{\partial C_n}{\partial \frac{\beta\ell}{2V}}, \text{ per radian}$$

$C_{n\beta} \cos \alpha + k^2 C_{n\dot{\beta}}$	oscillatory directional-stability parameter, per radian
$C_{n\beta} \sin \alpha - k^2 C_{n\ddot{\beta}}$	yawing moment due to roll displacement parameter, per radian
f	frequency of oscillation, hertz
k	reduced frequency parameter $\omega\ell/2V$ in pitch, yaw, and roll, radians
ℓ	reference length, orbiter length, meters
M	free-stream Mach number
p.d.r.	angular velocity of model about X-, Y-, and Z-axis, respectively, radians/second
q_∞	free-stream dynamic pressure, kPa
R	Reynolds number based on orbiter body length, ℓ
S	reference area, meters ²
V	free-stream velocity, meters/second
X,Y,Z	body reference axes
α	angle of attack, degrees or radians
β	angle of sideslip, radians
ϕ	model roll orientation angle, degrees
ω	angular velocity, $2\pi f$, radians/second

A dot over a quantity indicates a first derivative with respect to time.

APPARATUS AND MODEL

The 0.015-scale model used in the investigation consisted of the orbiter (designated 140 A+B), the external propellant tank, and the solid rocket boosters arranged together in the complete launch configuration shown in figure 2. The model could be tested without the solid rocket motors as a tank-orbiter combination which simulated an abort situation. The moment reference center could be varied and data were measured about the two positions shown in figure 2. Details of the propellant tank, solid rocket motors, and the front and rear attachment points are presented in figure 3.

The subsonic and transonic forced-oscillation tests were conducted in the Langley 8-foot transonic pressure tunnel. The model was mounted with the balance and sting in the external propellant tank. A photograph of the model mounted in the tunnel for the forced-oscillation tests is presented in figure 4. A description of the techniques and apparatus for the forced-oscillation tests is given in reference 2.

TESTS

The forced-oscillation tests were conducted to determine the pitch ($C_{m_q} + C_{m\dot{\alpha}}$), yaw ($C_{n_r} - C_{n\dot{\beta}} \cos \alpha$), and roll ($C_{l_p} + C_{l\dot{\beta}} \sin \alpha$) damping; the changes in normal force due to pitch rate ($C_{N_q} + C_{N\dot{\alpha}}$) and the cross derivatives: yaw due to rolling velocity ($C_{n_p} + C_{n\dot{\beta}} \sin \alpha$) and roll due to yawing velocity ($C_{l_r} - C_{l\dot{\beta}} \cos \alpha$).

The values of the nominal amplitude of the oscillation and of the range of the reduced frequency parameter (determined as discussed in ref. 2) during the dynamic-stability tests were:

Oscillation axis	Amplitude of oscillation, degrees	Reduced frequency parameter, k, radians
Pitch	1	0.0152 to 0.0655
Yaw	1	.0186 to .0608
Roll	2.5	.0199 to .0947

Dynamic tests were conducted with two center-of-gravity (c.g.) locations: the aft moment reference center representing the center-of-gravity position of the complete configuration for the lift-off flight conditions and the forward moment reference center representing the c.g. position of the complete configuration under conditions of maximum dynamic pressure. The tests for

the orbiter external-tank configuration were conducted for the forward location only. Multiple data points were taken at each test condition and are presented to show the repeatability of the data.

The forced-oscillation tests were conducted over an angle-of-attack range of approximately $\pm 10^\circ$. The test conditions follow:

Mach number	q_∞ , kPa	R
0.3	5.98	2.87×10^6
.6	20.01	5.11
.9	33.94	6.40
1.2	21.11	3.40

For the entire Mach number range, the model was tested with transition strips fixed by application of No. 120 grit located 2.54 centimeters aft on the nose of the orbiter, of the external tank, and of the solid rocket boosters and 1.27 centimeters streamwise aft of the leading edge on the wing and vertical tail. All transition strips were approximately 0.25 centimeter wide.

RESULTS AND DISCUSSION

Pitching-Oscillation Test Results

The oscillatory stability parameters measured in the pitching-oscillation tests at Mach numbers of 0.3, 0.6, 0.9, and 1.2 are presented in figures 5 to 8. The pitch-damping characteristics of the complete configuration ($C_{m_q} + C_{m\dot{\alpha}}$) and the in-phase with displacement parameters ($C_{m\alpha} - k^2 C_{m\dot{q}}$) are presented as a function of angle of attack in figure 5 for the two moment reference centers. The data indicate that the effect of c.g. locations on the pitch damping was small and produced an increment in $C_{m\alpha} - k^2 C_{m\dot{q}}$ about equal to that expected on the basis of the magnitude of the c.g. shift. Comparisons between the in-phase parameter measured in the forced-oscillation tests and the $C_{m\alpha}$ determined from static tests (unpublished data) of a similar model for the same test conditions are also presented in figures 5(b), 5(c), and 5(d). These comparisons show good agreement between the static and dynamic test results.

In general, the launch vehicle configuration exhibited positive damping (negative values of $C_{m_q} + C_{m\dot{\alpha}}$) throughout the test angle-of-attack range for Mach numbers of 0.3, 0.6, and 0.9. At a Mach number of 1.2 there is a marked region of negative damping (positive

values of $C_{m_q} + C_{m\dot{\alpha}}$) at angles of attack around 2^0 . The appearance of this region of negative damping is not surprising for this blunt body in the mixed flow regime at transonic speeds. The positive angle-of-attack range was limited to 6^0 at a Mach number of 1.2 because of reflected shock impingement upon the vertical tail of the model.

The pitch-damping characteristics of the orbiter external-tank configuration for the forward moment center are presented in figure 6. These results show that for the orbiter external-tank combination, the model exhibited positive damping throughout the test angle-of-attack and Mach range. Note that the negative damping that occurred with the complete launch configuration at $M = 1.2$ (fig. 5(d)) did not occur for the orbiter external-tank configuration.

The normal force due to pitch rate parameter ($C_{N_q} + C_{N\dot{\alpha}}$) and the normal force due to pitch displacement parameter ($C_{N\alpha} - k^2 C_{N\dot{q}}$) for the complete vehicle and the orbiter external-tank configurations are presented in figures 7 and 8. The data of figure 7 show that for the complete launch configuration, $C_{N_q} + C_{N\dot{\alpha}}$ is generally positive and exhibits a non-linearity for the condition where pitch damping is negative (fig. 5(d)). Comparisons between the in-phase $C_{N\alpha} - k^2 C_{N\dot{q}}$ and the $C_{N\alpha}$ computed from the static test measurements are also presented in figure 7. This comparison shows good agreement between the static and forced-oscillation test results. For the orbiter external-tank combination the data (fig. 8) show the normal-force parameter $C_{N_q} + C_{N\dot{\alpha}}$ to be positive and linear throughout the Mach number and angle-of-attack range tested.

Yawing-Oscillation Test Results

The oscillatory stability parameters measured in the yawing-oscillation tests are presented in figures 9 to 11. The in-phase with displacement ($C_{n\beta} \cos \alpha + k^2 C_{n_f}$) and out-of-phase with displacement ($C_{n_f} - C_{n\dot{\beta}} \cos \alpha$) parameters are presented in figures 9 and 10. The damping data of figure 9 measured for the complete launch vehicle show that at Mach numbers of 0.3 and 0.6 there are regions of negative damping over a large portion of the test angle-of-attack range. However, the model exhibited positive damping at the higher transonic Mach numbers. A comparison of the in-phase $C_{n\beta} \cos \alpha + k^2 C_{n_f}$ with the $C_{n\beta} \cos \alpha$ computed from the static data is also presented in figure 9. This comparison shows that in general, the values measured in the forced-oscillation tests are higher than those measured in the static tests but the trends with angle of attack appear to be the same.

The yaw-damping results for the orbiter external-tank combination are presented in figure 10. These results show trends similar to those obtained for the complete vehicle. In

particular, the orbiter external-tank configuration exhibited significant regions of negative damping in yaw at Mach numbers of 0.3 and 0.6. At the higher Mach numbers, the orbiter external-tank configuration exhibited positive values of damping in yaw; there was an exception when $\alpha = 1^\circ$ at $M = 0.9$. Results obtained for the orbiter external-tank configuration with the vertical tail removed are also presented in figures 10(a) and 10(b). Analysis of these data shows that the vertical tail provides a nearly constant increment to the damping in yaw, except for angles of attack greater than 6° for $M = 0.6$.

The rolling moment due to yaw rate parameter $(C_{l_r} - C_{l\dot{\beta}} \cos \alpha)$ is presented in figures 11 and 12. Data are also presented in figure 11 showing a comparison of the in-phase $C_{l\dot{\beta}} \cos \alpha + k^2 C_{l_r}$ and the $C_{l\dot{\beta}} \cos \alpha$ computed from the static data. The comparison shows excellent agreement between the static and forced-oscillation results. The forced-oscillation results show that for both the complete configuration and the orbiter external-tank combination, the rolling moment due to yawing velocity was positive and the vertical tail added a nearly constant increment. One nonlinearity occurred at a Mach number of 0.6 for the orbiter external-tank configuration (fig. 12); this nonlinearity corresponds to that in yaw damping at $M = 0.6$ (fig. 10(b)).

Rolling-Oscillation Test Results

The oscillatory stability parameters measured in the rolling-oscillation tests are presented in figures 13 to 16. The in-phase with displacement $(C_{l\dot{\beta}} \sin \alpha - k^2 C_{l_p})$ and out-of-phase with displacement $(G_{T_p} + C_{l\dot{\beta}} \sin \alpha)$ parameters are presented in figures 13 and 14. Comparisons of the in-phase $C_{l\dot{\beta}} \sin \alpha - k^2 C_{l_p}$ with the $C_{l\dot{\beta}} \sin \alpha$ computed from the static data are presented in figures 13(b), 13(c), and 13(d). The comparison shows excellent agreement between the forced-oscillation and static results. The roll-damping parameter $(C_{l_p} + C_{l\dot{\beta}} \sin \alpha)$ shows that for both the launch vehicle configuration (fig. 13) and the orbiter external-tank combination (fig. 14), the model exhibited positive damping throughout the test angle-of-attack and Mach range.

The yawing moment due to roll rate parameter $(C_{n_p} + C_{n\dot{\beta}} \sin \alpha)$ is presented in figures 15 and 16. The data show that $C_{n_p} + C_{n\dot{\beta}} \sin \alpha$ is generally positive for both the mated vehicle and the orbiter external-tank combination for the angle-of-attack and Mach number range tested. A comparison of the in-phase $C_{n\dot{\beta}} \sin \alpha - k^2 C_{n_p}$ with the $C_{n\dot{\beta}} \sin \alpha$ computed from the static tests is also presented in figures 15(b), 15(c), and 15(d). This comparison shows excellent agreement between the static and forced-oscillation test results.

SUMMARY OF RESULTS

An investigation has been conducted to determine the subsonic and transonic dynamic-stability characteristics of a 0.015-scale model of the shuttle launch vehicle. The results of this investigation may be summarized as follows:

1. The model exhibited positive damping in pitch throughout the test angle-of-attack range for Mach numbers of 0.3, 0.6, and 0.9. At a Mach number of 1.2, there was a region of negative damping for the complete launch vehicle configuration at angles of attack around 2° .
2. The model exhibited nonlinearities and negative yaw damping over a large portion of the angle-of-attack range at Mach numbers of 0.3 and 0.6 for both the launch vehicle and the orbiter external-tank configuration. At the higher Mach numbers, the model exhibited positive yaw damping throughout the test angle-of-attack range.
3. Both the launch vehicle and orbiter external-tank configuration were positively damped in roll for the test ~~Mach number and~~ angle-of-attack ranges.

Langley Research Center
National Aeronautics and Space Administration
Hampton, Va. 23665
January 16, 1976

REFERENCES

1. Boyden, Richmond P.; and Freeman, Delma C., Jr.: Subsonic and Transonic Dynamic Stability Characteristics of a Space Shuttle Orbiter. NASA TN D-8042, 1975.
2. Freeman, Delma C., Jr.; Boyden, Richmond P.; and Davenport, E. E.: Supersonic Dynamic Stability Characteristics of a Space Shuttle Orbiter. NASA TN D-8043, 1975.
3. Uselton, Bob A.; and Jenke, Leroy M.: Pitch-, Yaw-, and Roll-Damping Characteristics of a Shuttle Orbiter at $M_\infty = 8$. AEDC-TR-74-129, U.S. Air Force, May 1975. (Available from DDC as AD A011 648.)
4. Boyden, Richmond P.; Freeman, Delma C., Jr.; and Davenport, Edwin E.: Supersonic Dynamic-Stability Derivatives of the Space Shuttle Launch Vehicle. NASA TM X-3315, 1976.
5. Mechtly, E. A.: The International System of Units - Physical Constants and Conversion Factors (Second Revision). NASA SP-7012, 1973.

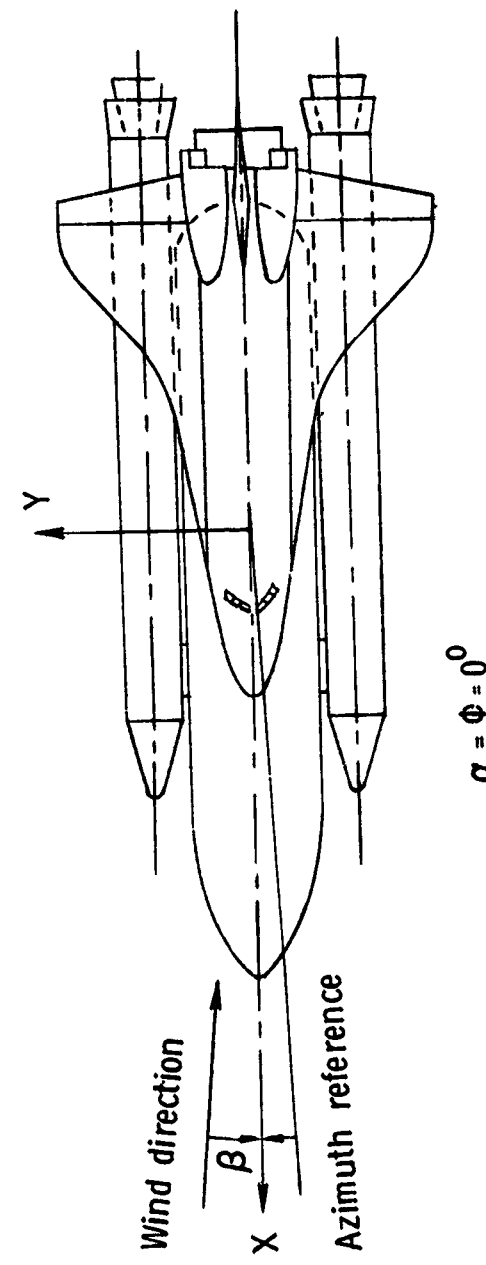
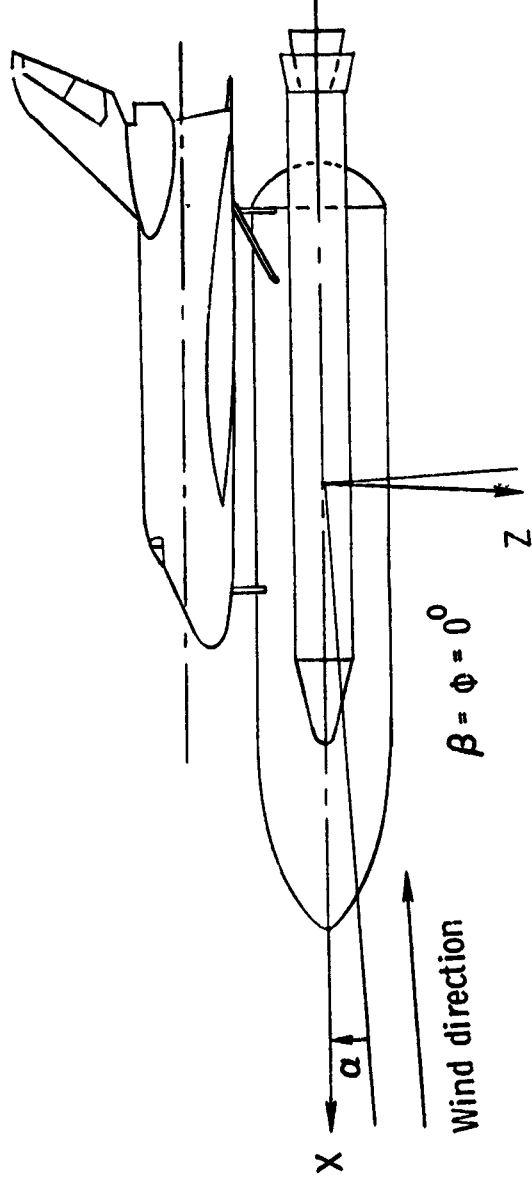


Figure 1.- System of axes used in investigation.

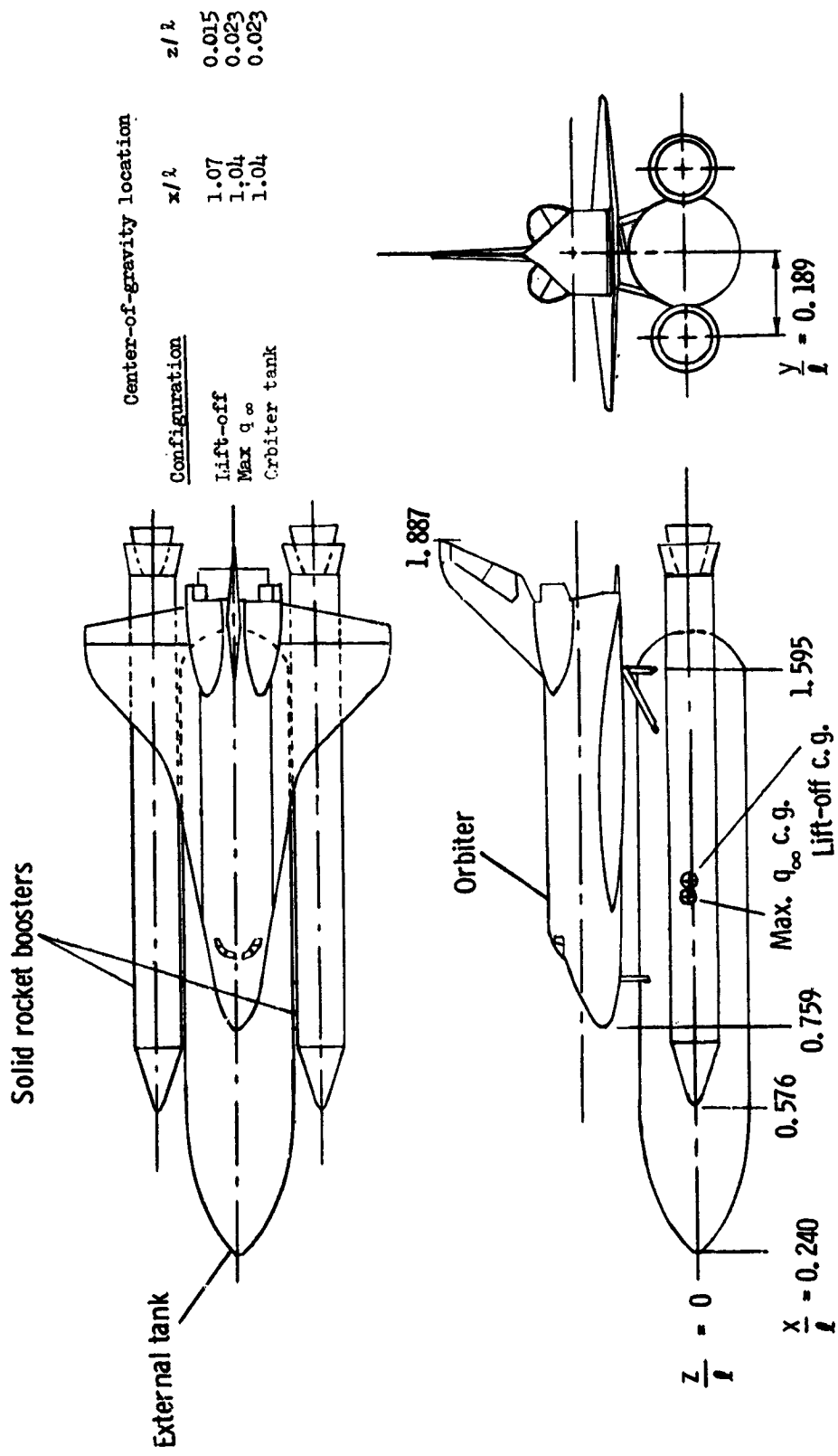
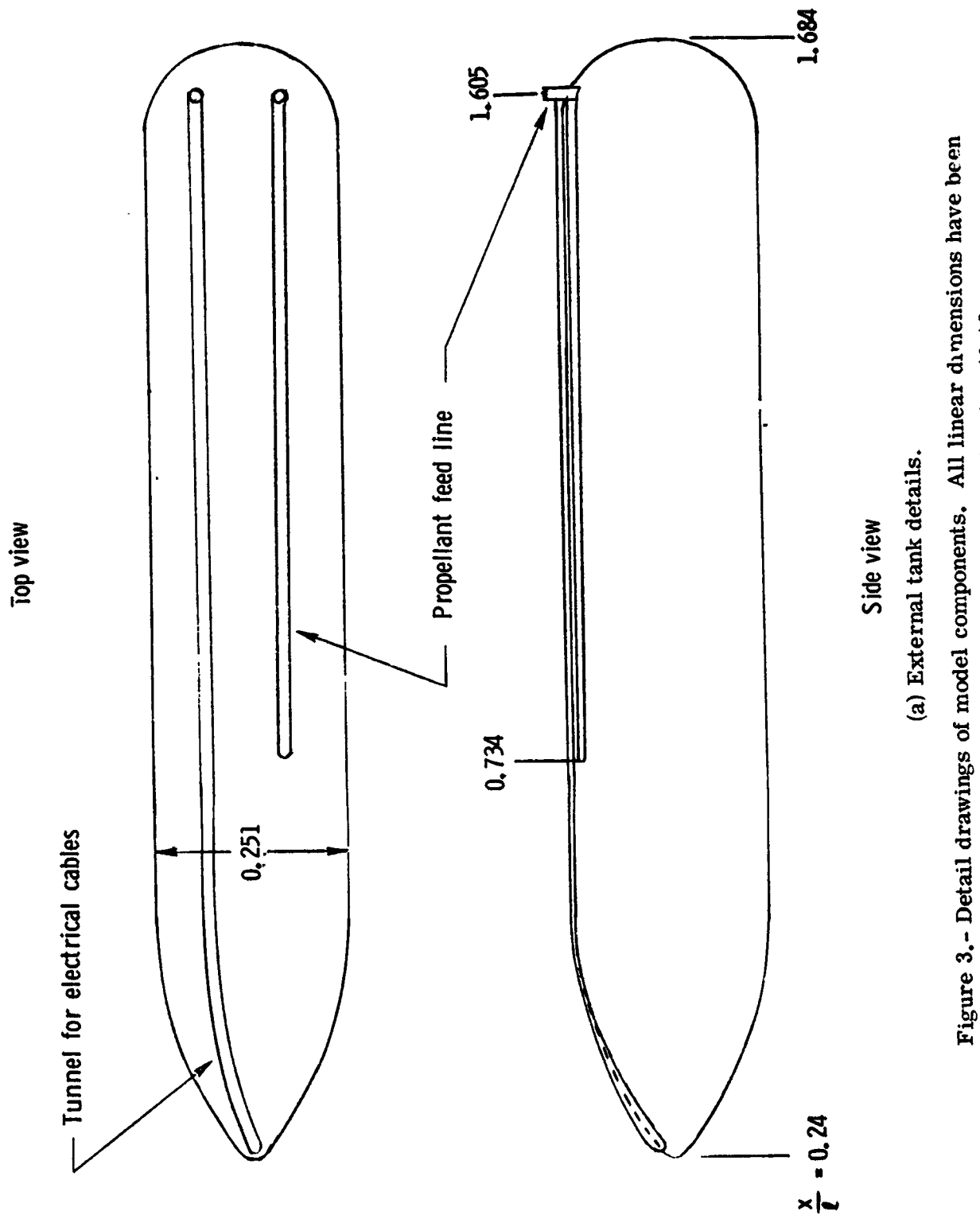
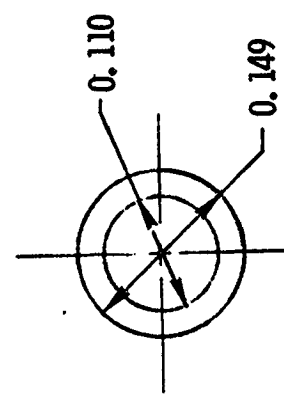


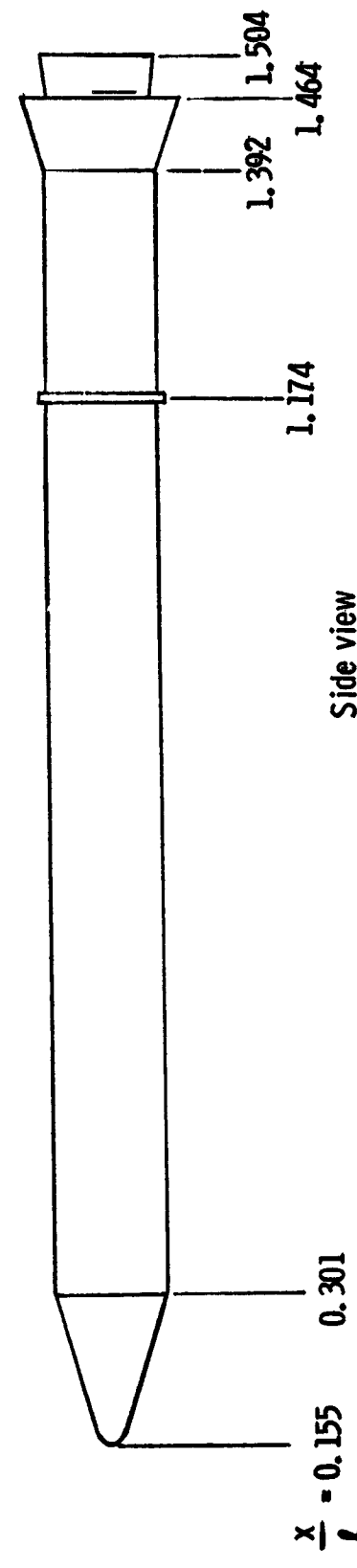
Figure 2.- Three-view drawing of model. All linear dimensions have been nondimensionalized by reference length l ; $l = 49.16$ cm; Max q_{∞} = Maximum free-stream dynamic pressure.



Rear view

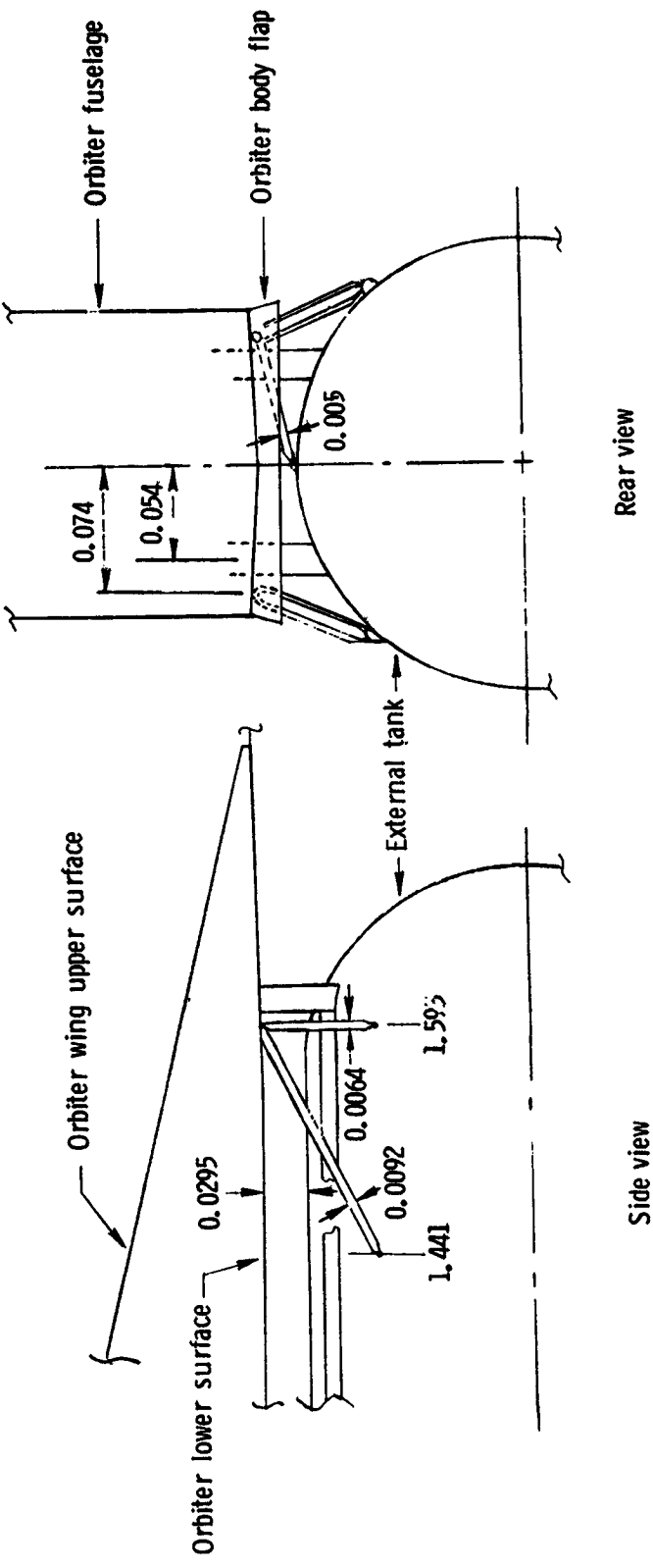


Side view



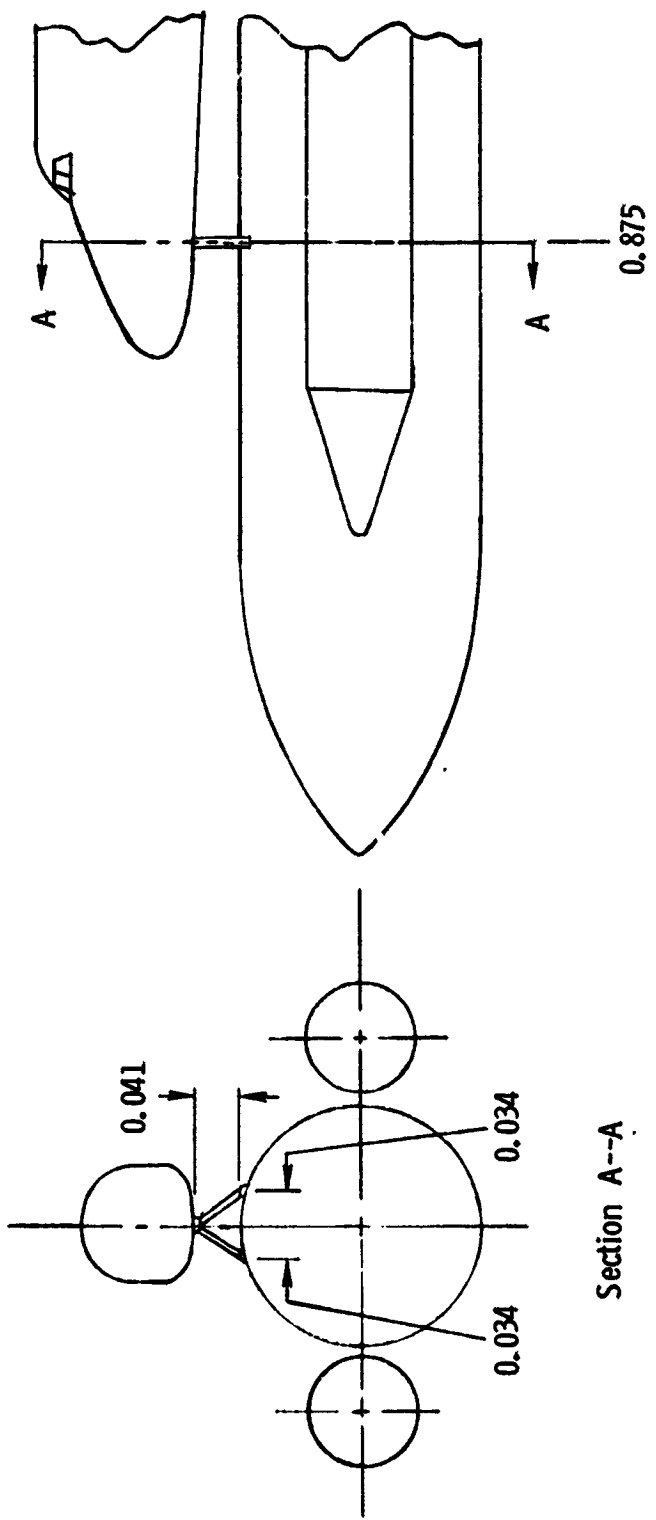
(b) Solid rocket booster details.

Figure 3.- Continued.



(c) Rear orbiter external-tank attachment structure details.

Figure 3.- Continued.



(d) Front orbiter external-tank attachment structure details.

Figure 3.- Concluded.

L-74-5516

Figure 4.- Photograph of model mounted for forced-oscillation tests in 8-foot transonic pressure tunnel.



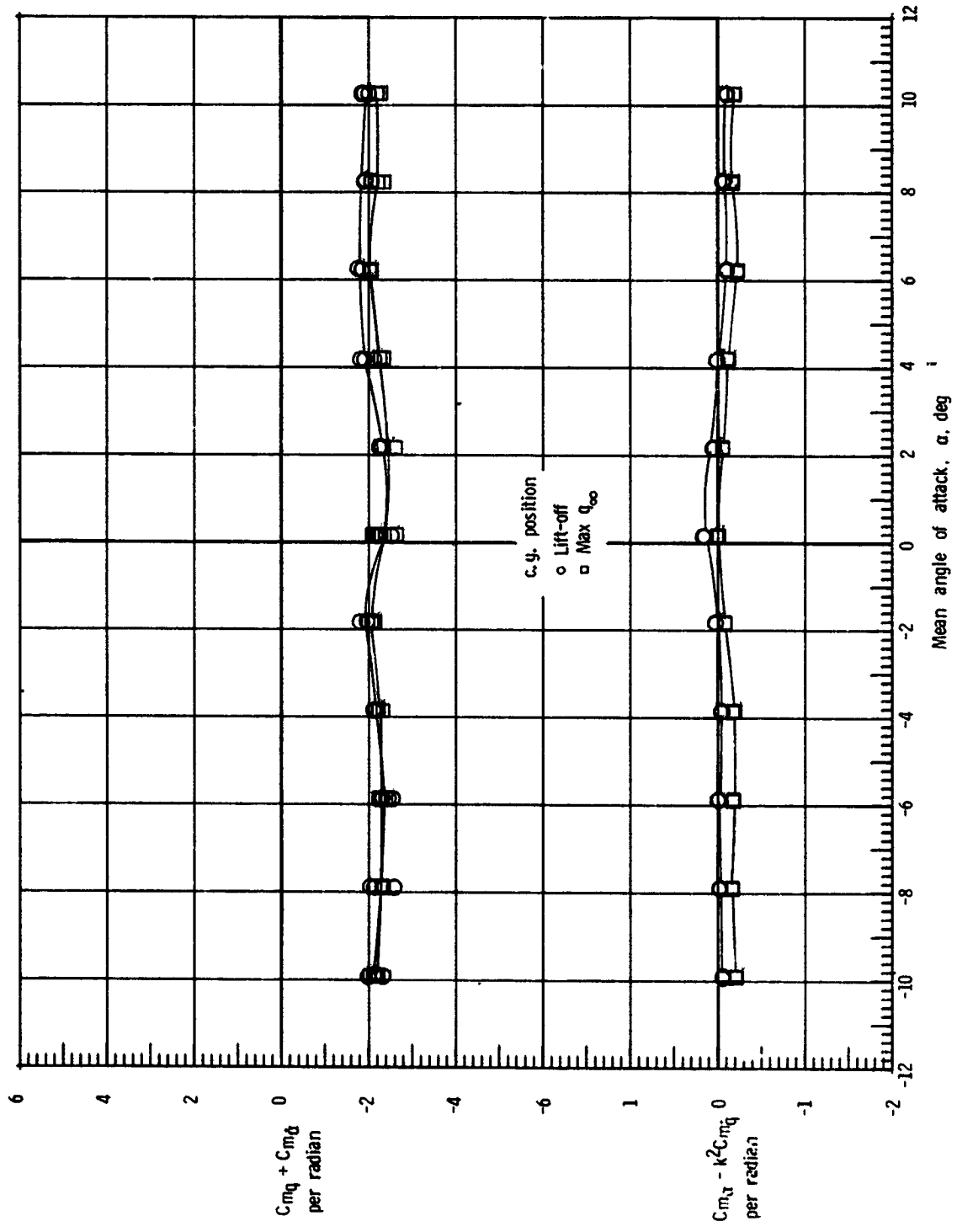
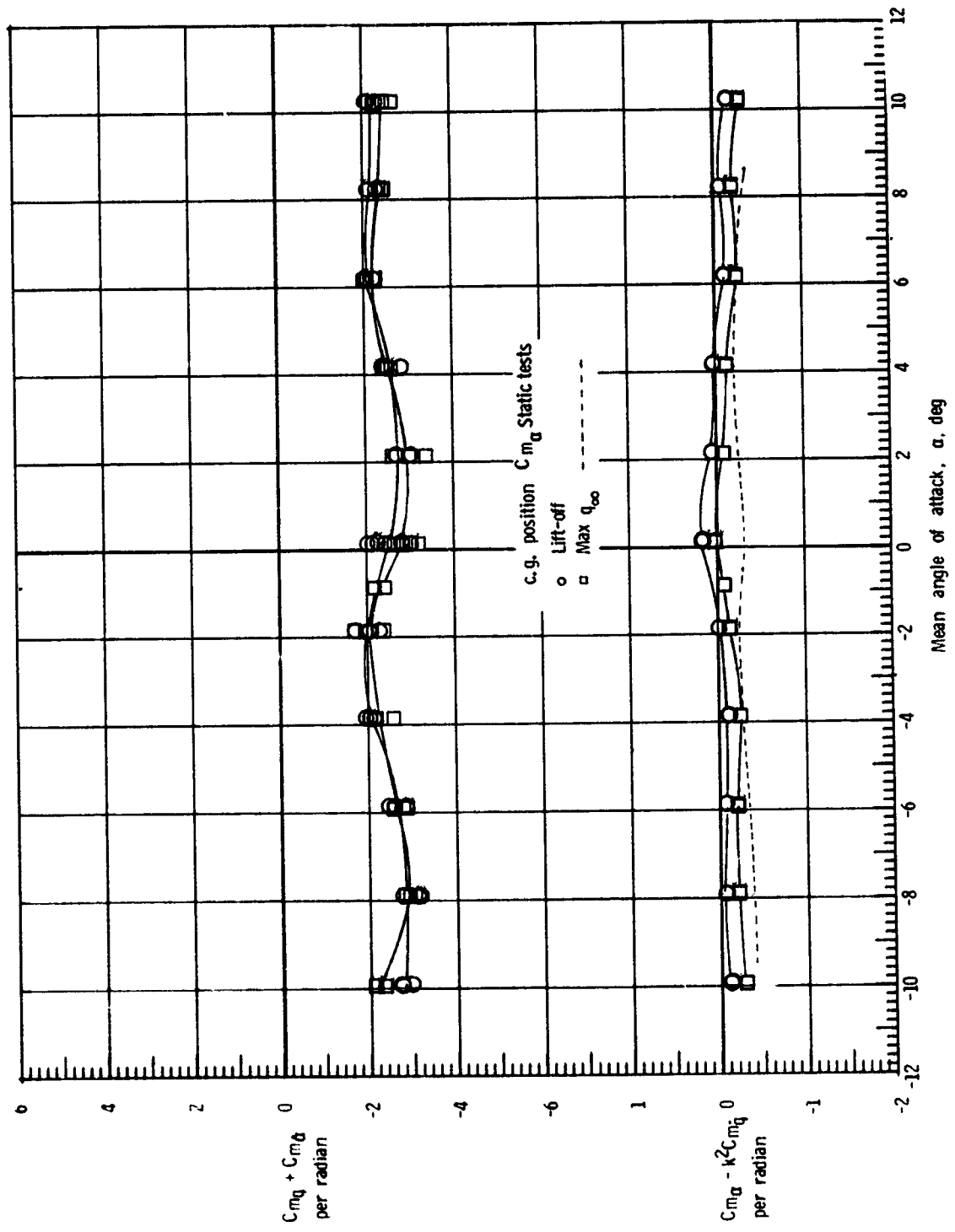
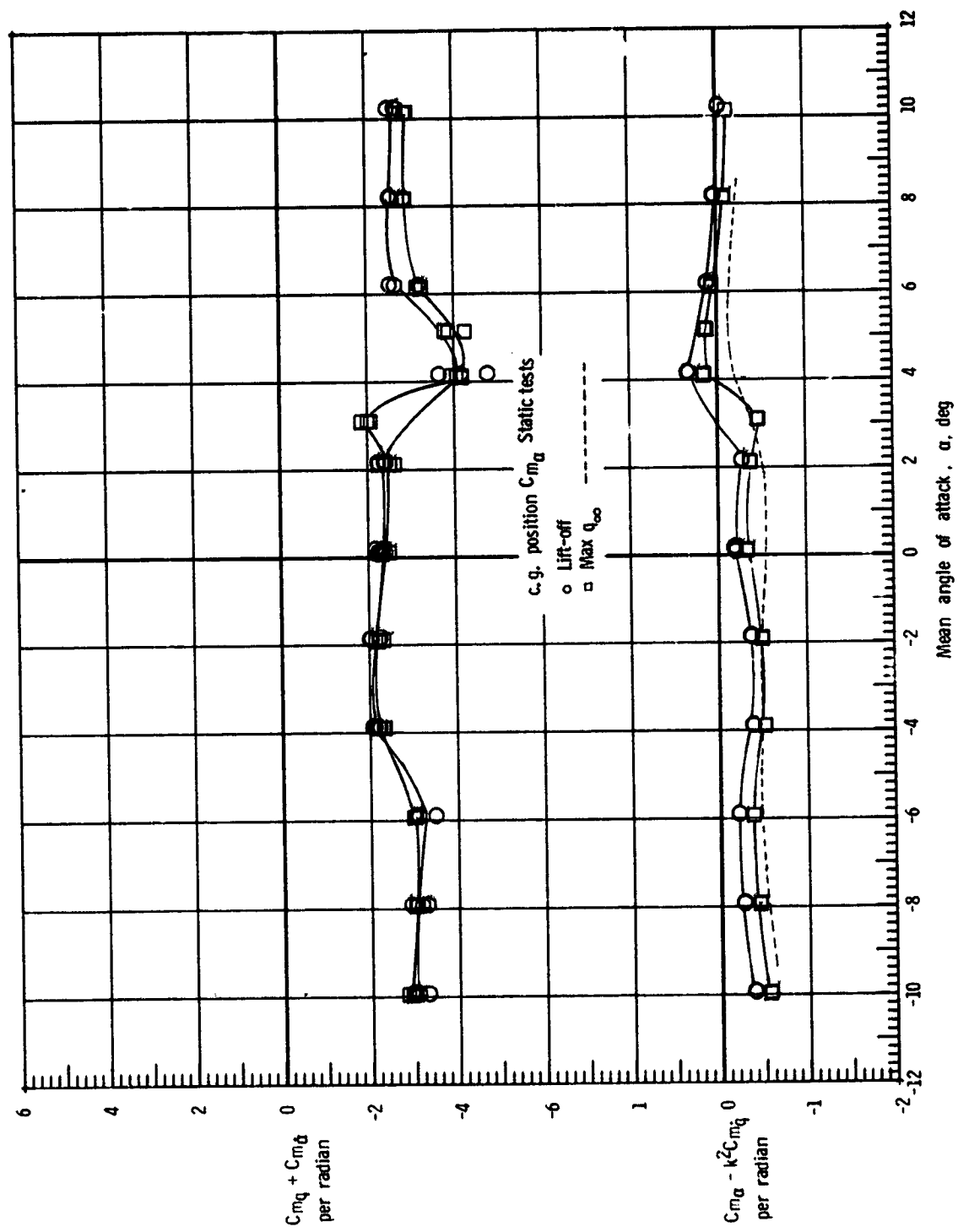


Figure 5.- Effect of center-of-gravity position on damping-in-pitch parameter and oscillatory stability-in-pitch parameter of launch vehicle.
 (a) $M = 0.3$.



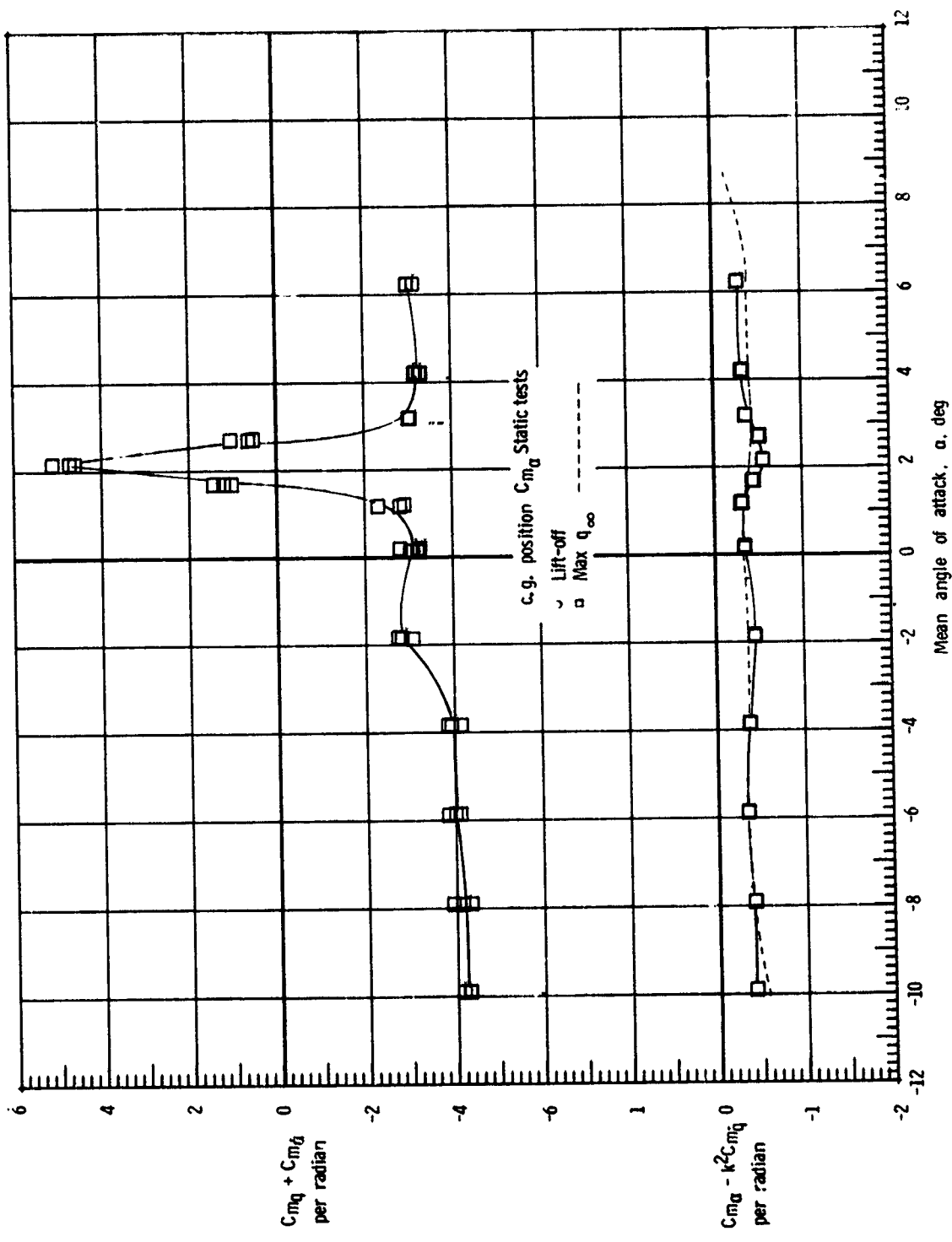
(b) $M = 0.6$.

Figure 5.- Continued.



(c) $M = 0.9$.

Figure 5.- Continued.



(d) $M = 1.2$.

Figure 5.- Concluded.

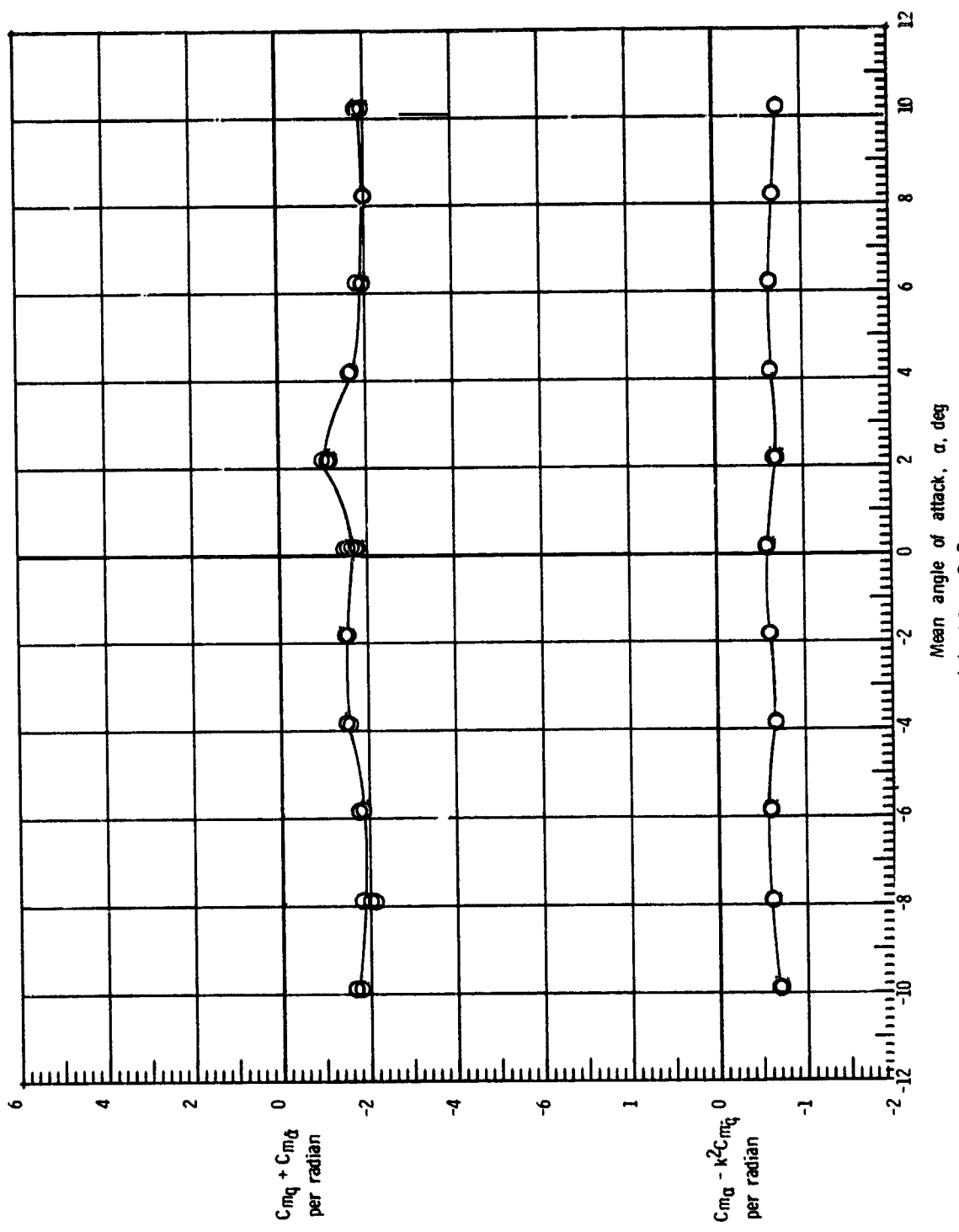
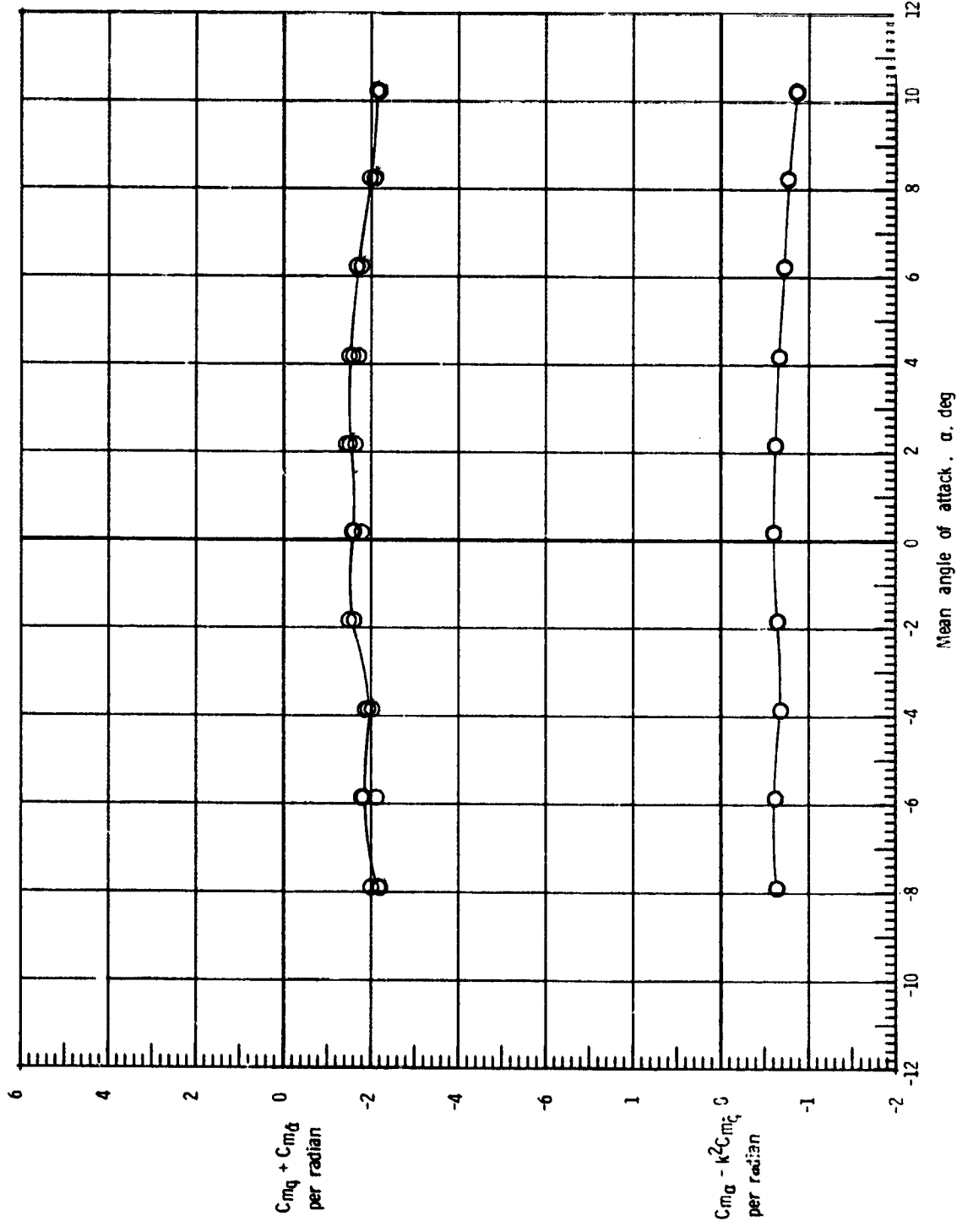


Figure 6.- Damping-in-pitch parameter and oscillatory stability-in-pitch parameter of orbiter external-tank configuration.
 (a) $M = 0.3$.



(b) $M = 0.6$.

Figure 6.- Continued.

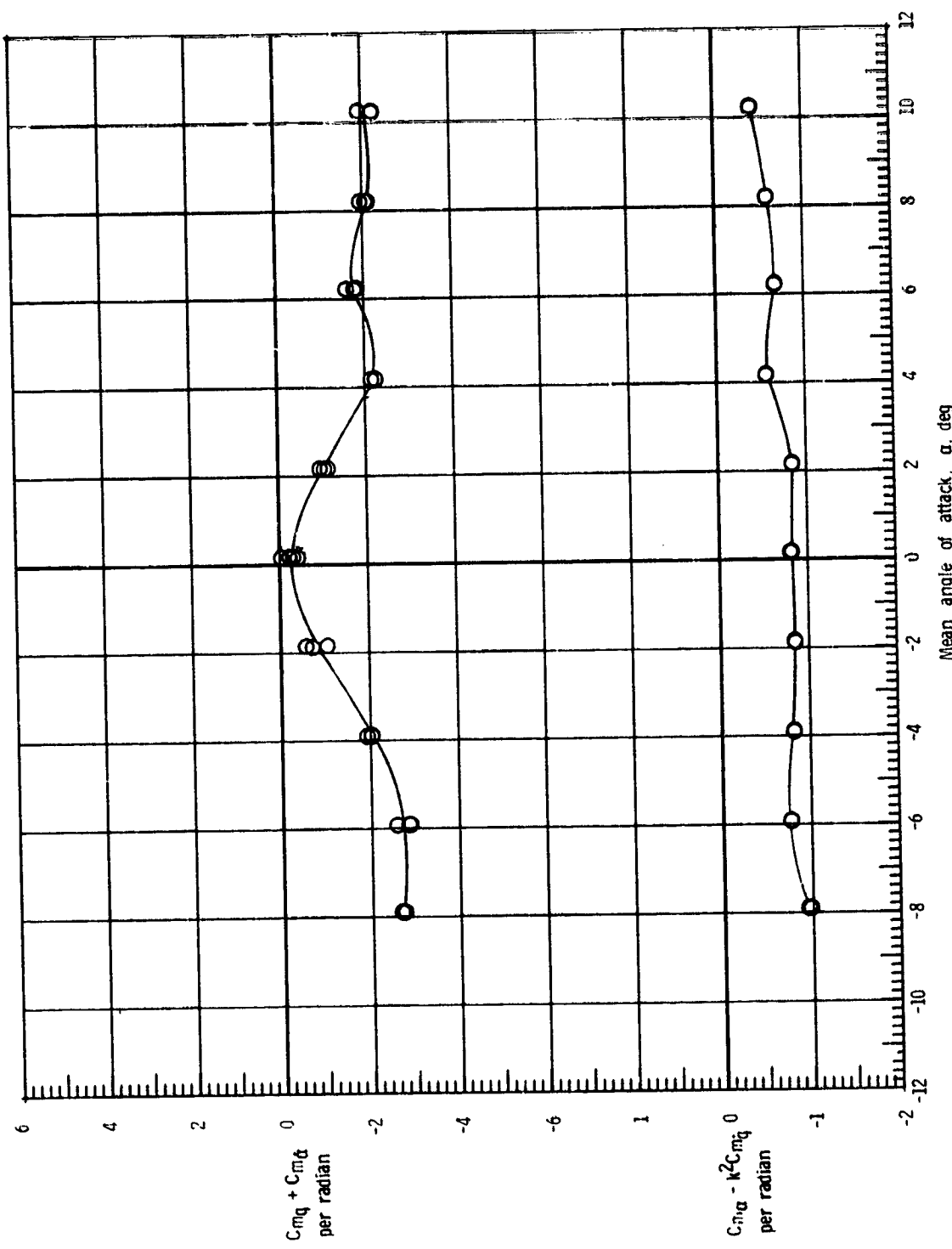
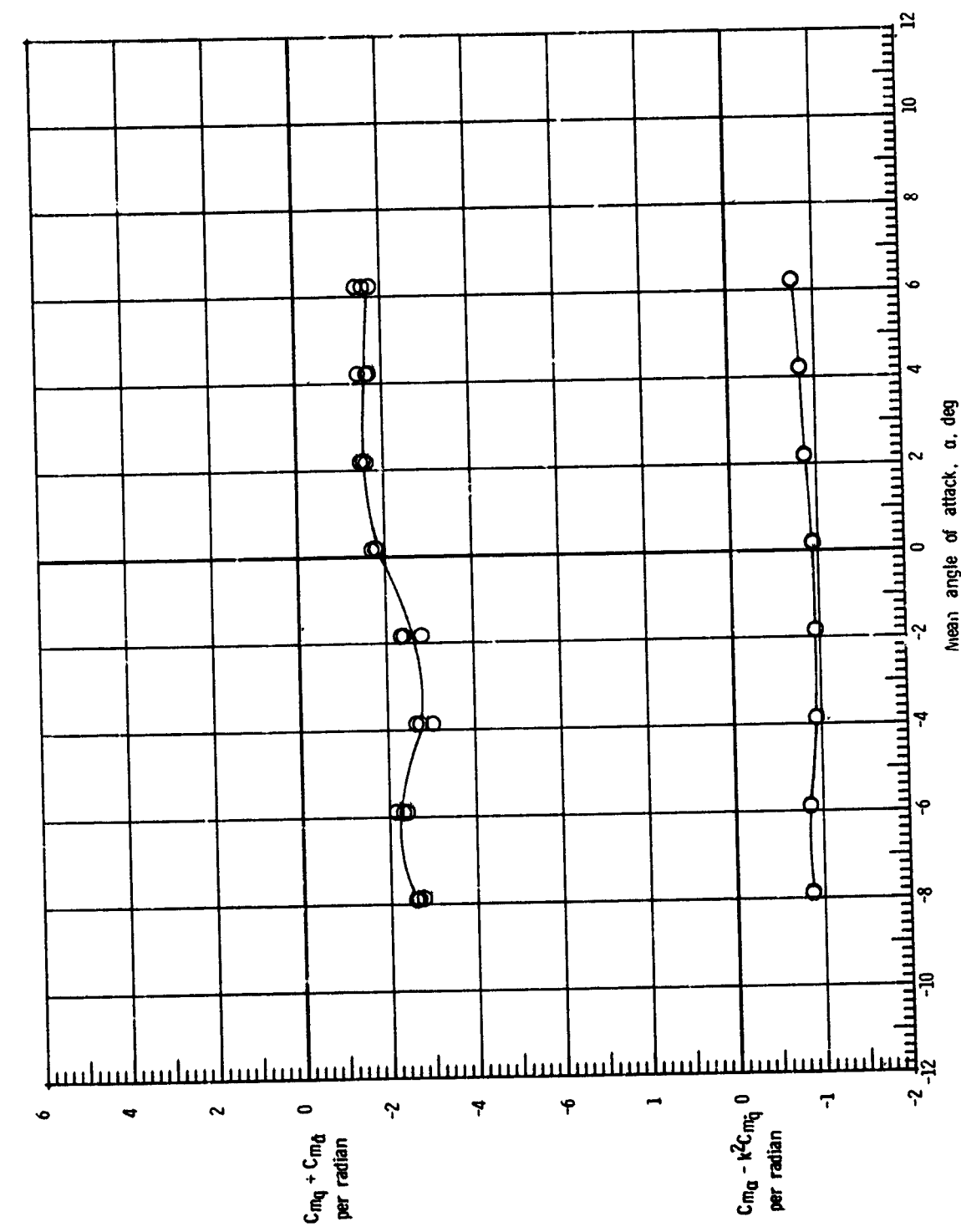


Figure 6.- Continued.
(c) $M = 0.9$.



(d) $M = 1.2$.

Figure 6.- Concluded.

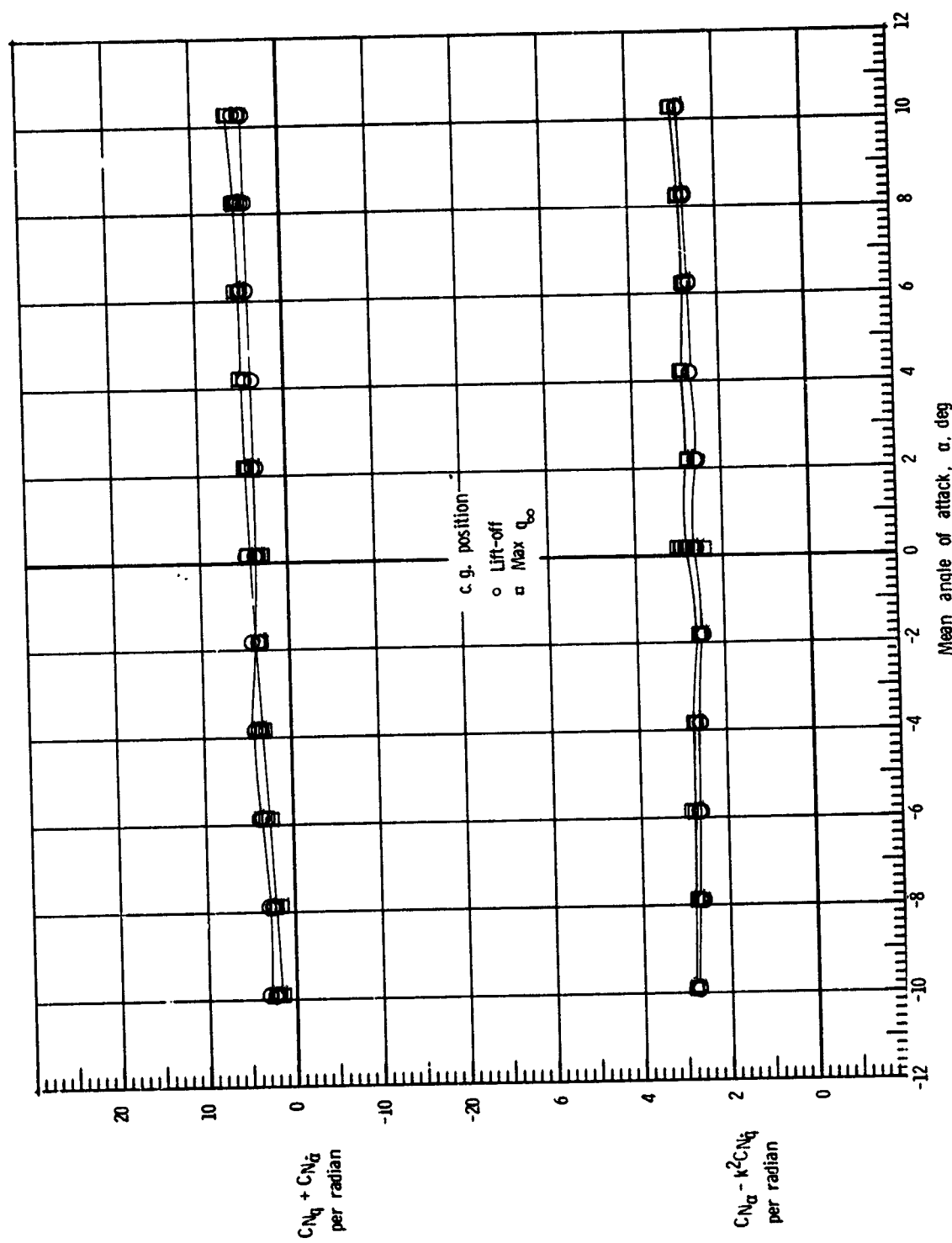
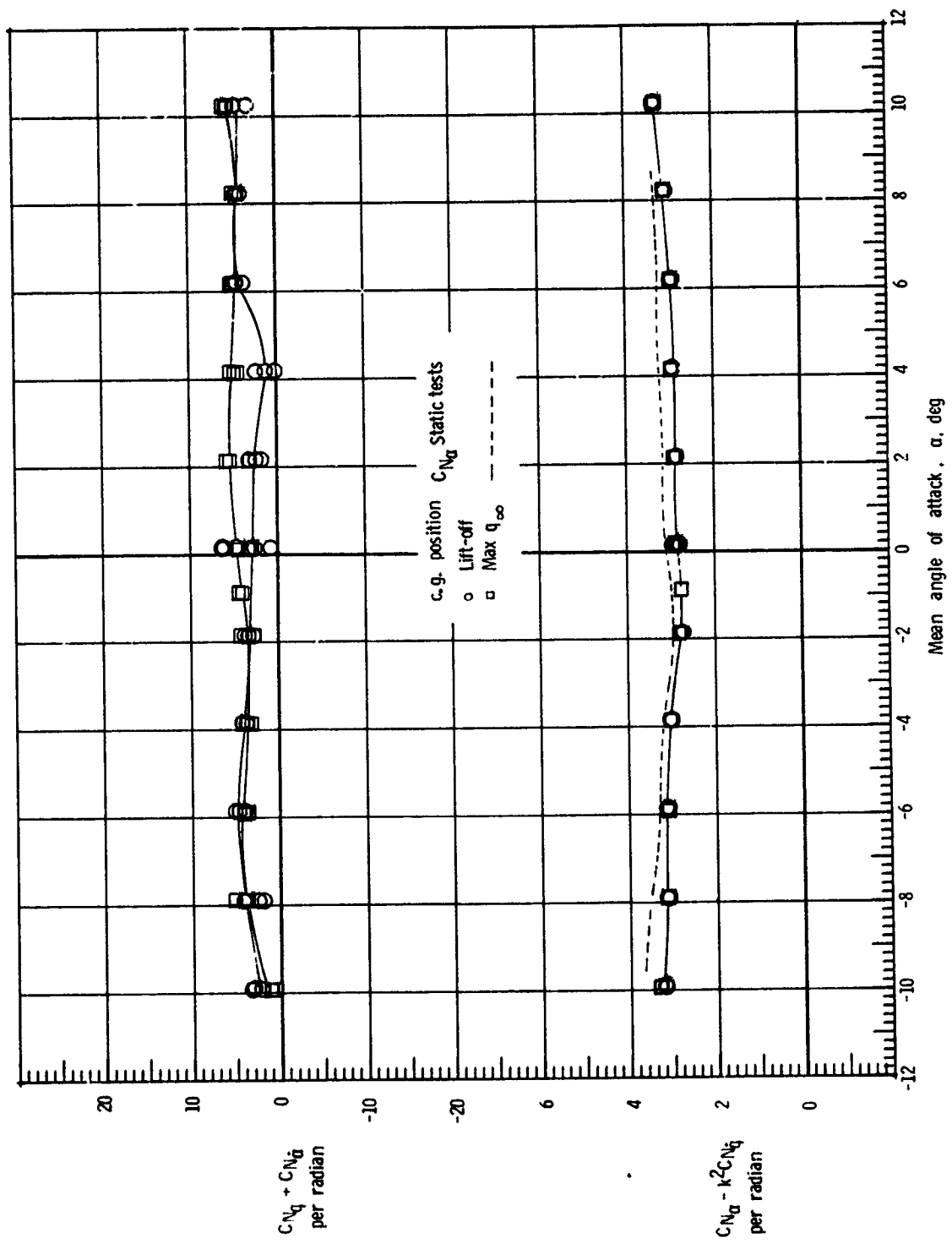


Figure 7.- Effect of center-of-gravity position on normal force due to pitch rate parameter and normal force due to pitch displacement parameter for launch vehicle.
(a) $M = 0.3$.



(b) $M = 0.6$.

Figure 7.- Continued.

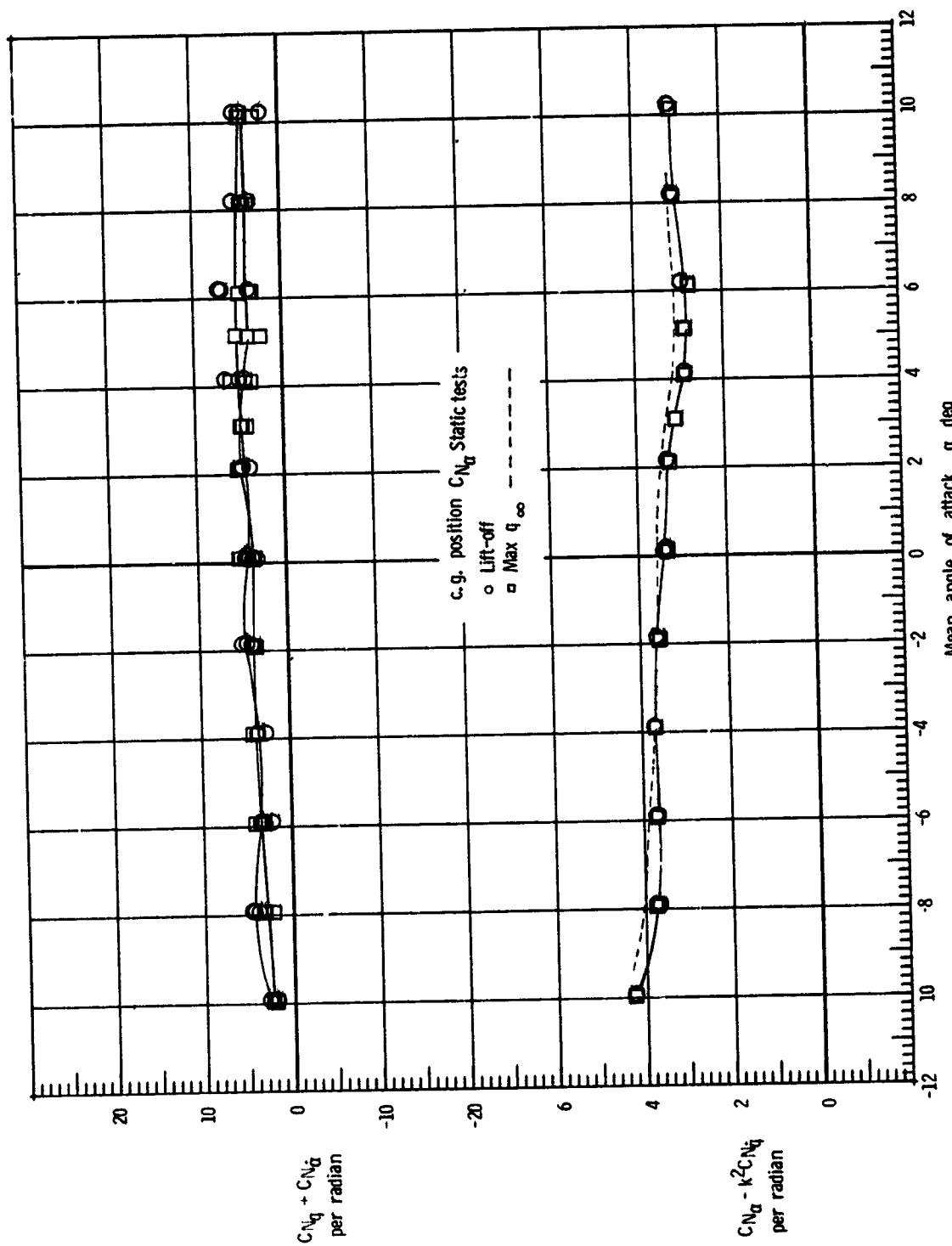
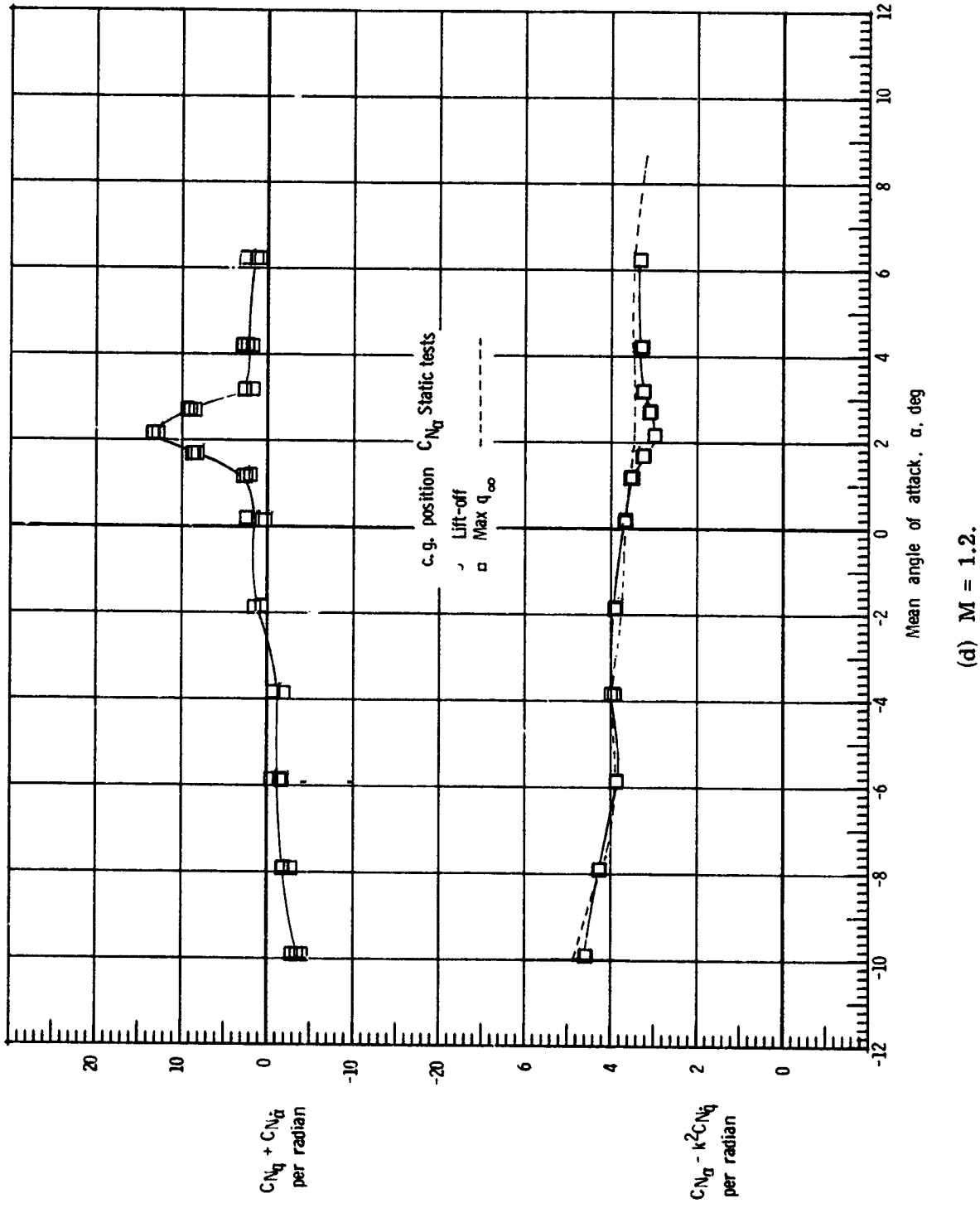


Figure 7.- Continued.
(c) $M = 0.9$.



(d) $M = 1.2$.

Figure 7.- Concluded.

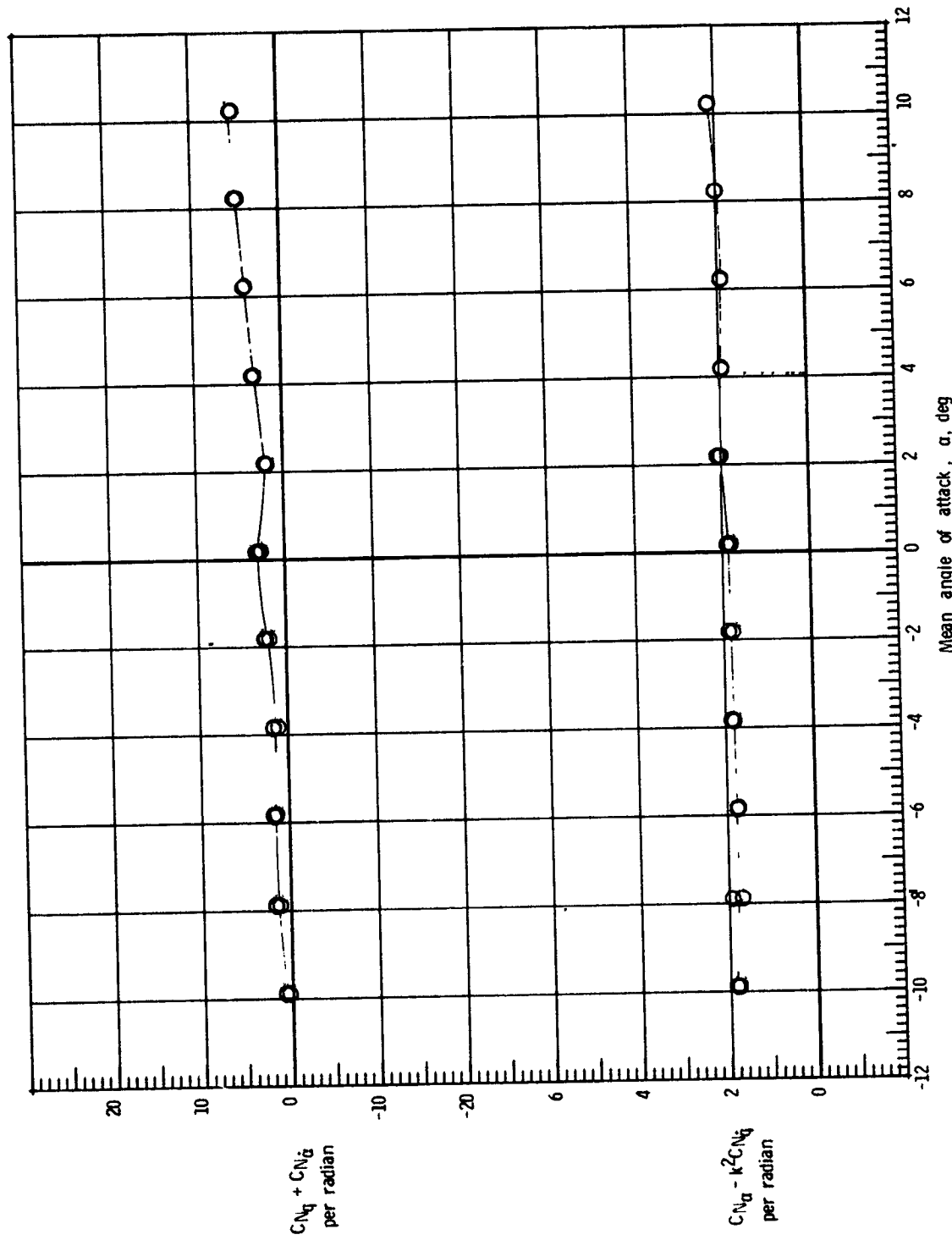
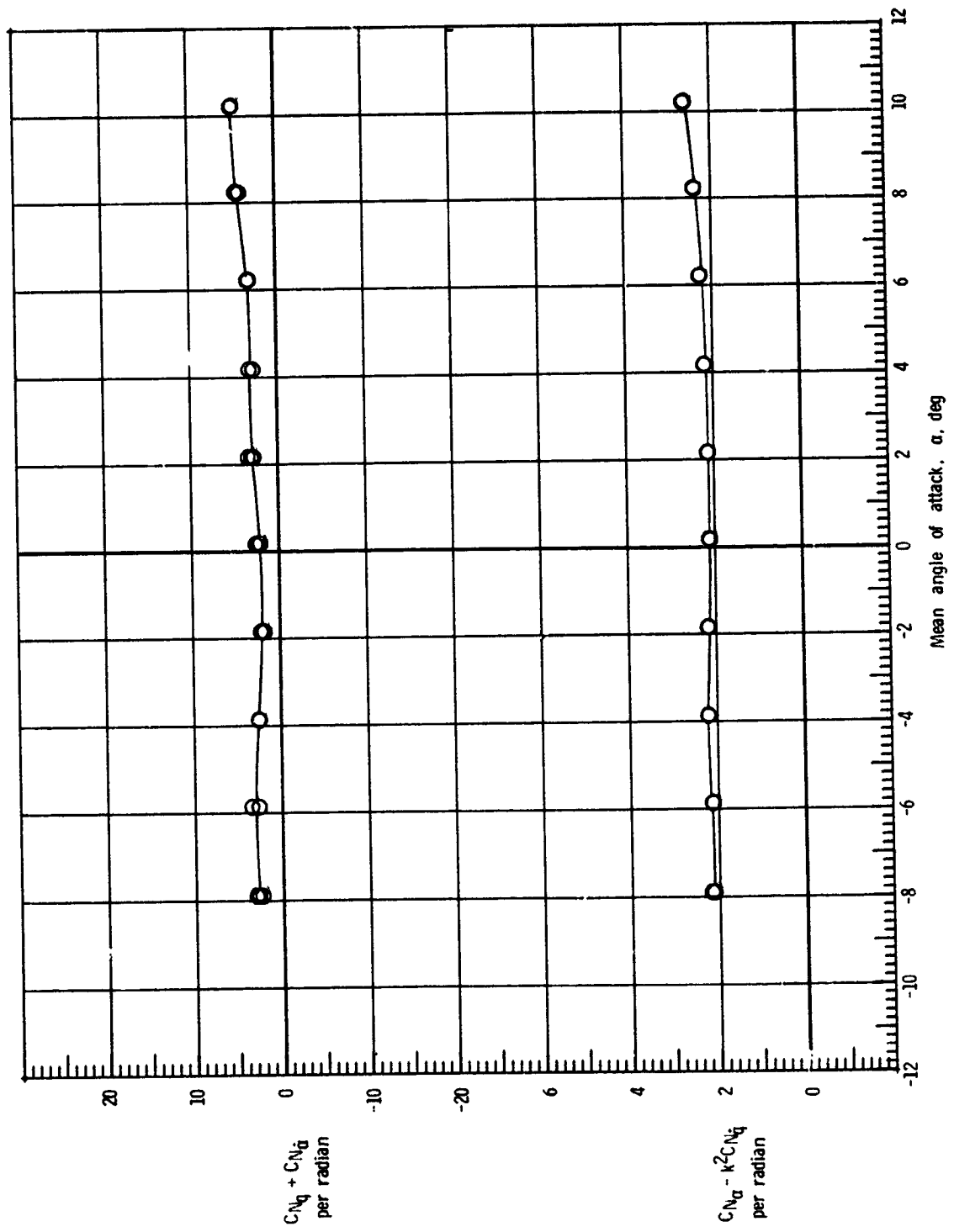
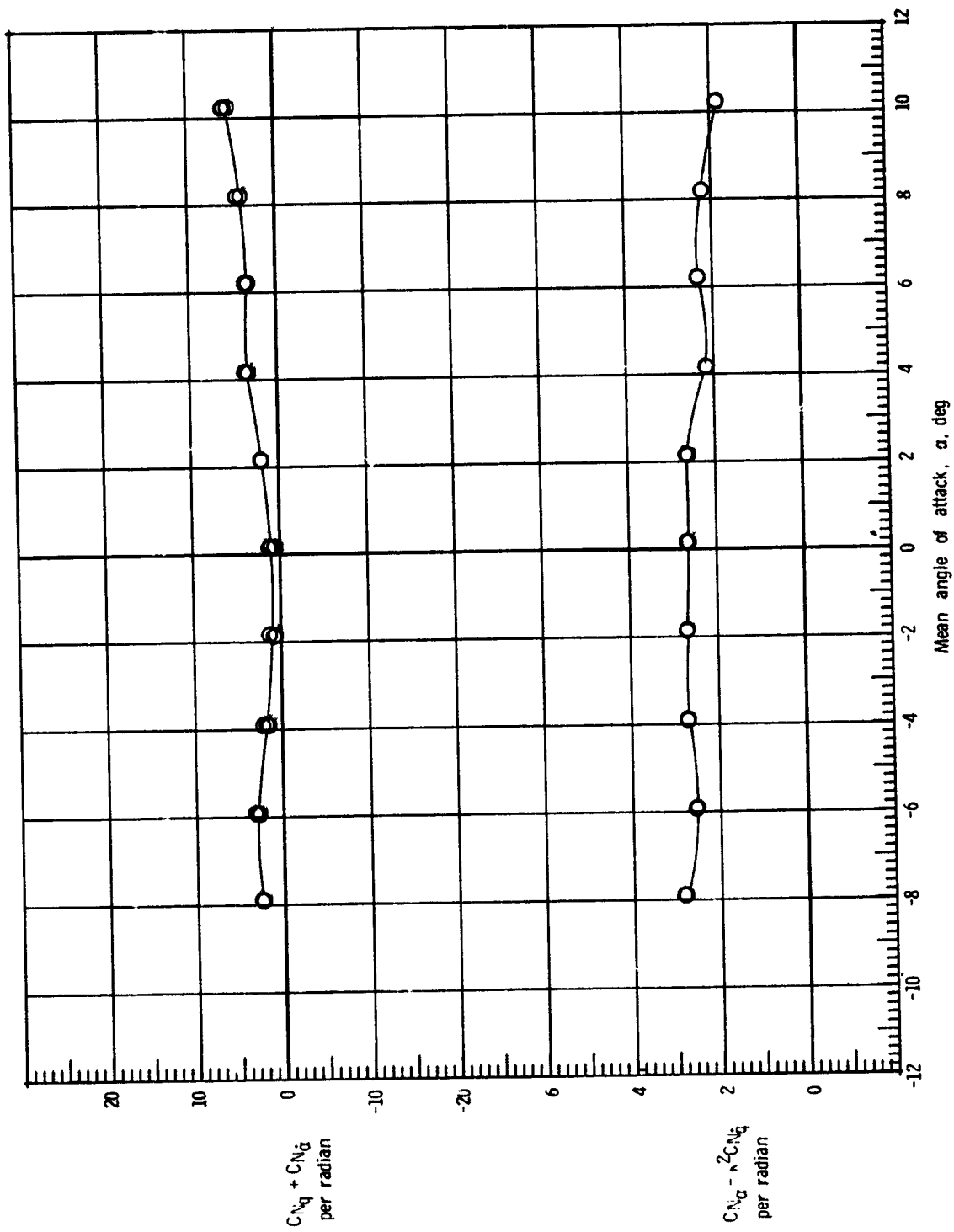


Figure 8.- Normal force due to pitch rate parameter and normal force due to pitch displacement parameter for orbiter external-tank configuration.
(a) $M = 0.3$.



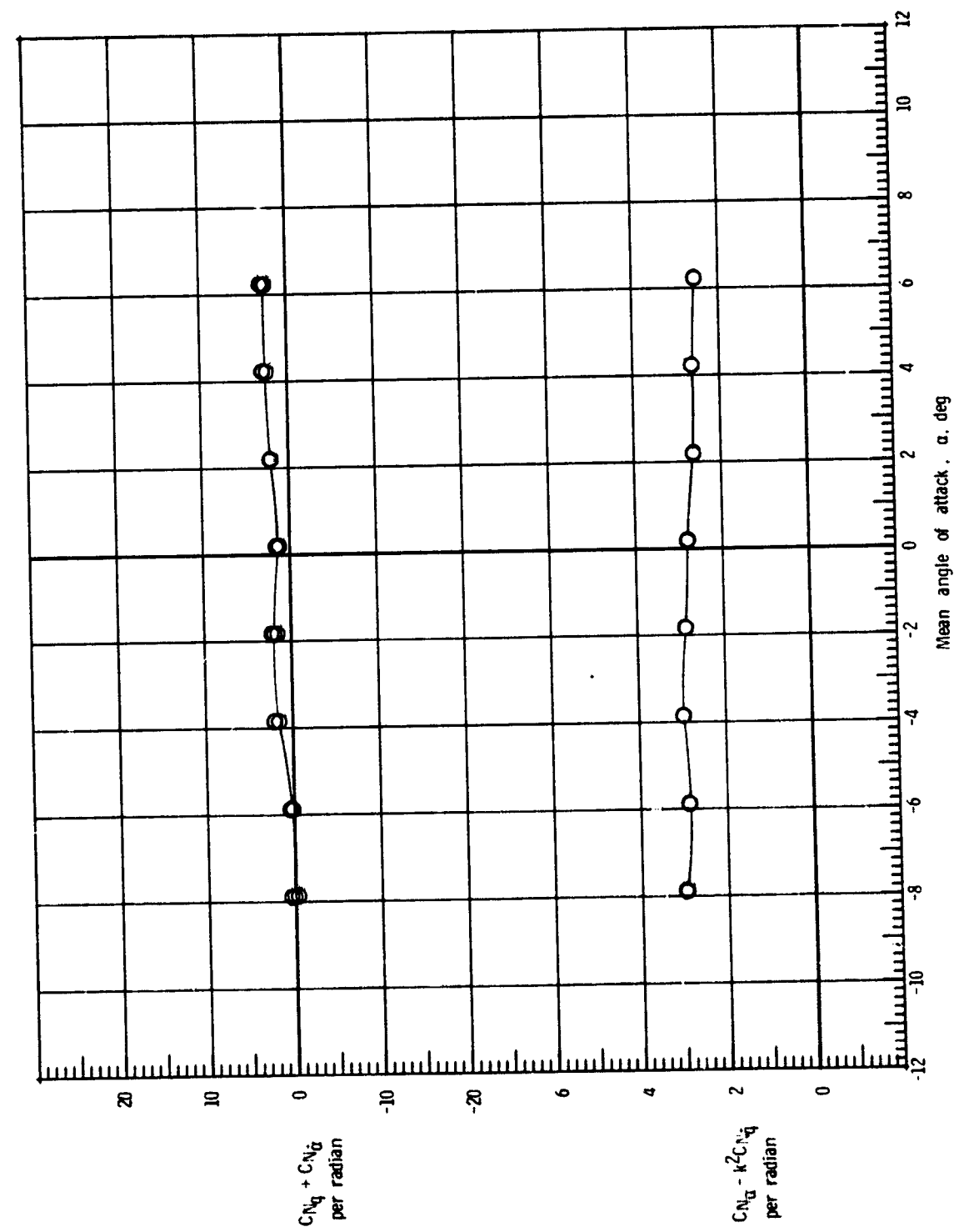
(b) $M = 0.6$.

Figure 8.- Continued.



(c) $M = 0.9$.

Figure 8.- Continued.



(d) $M = 1.2$.

Figure 8.- Concluded.

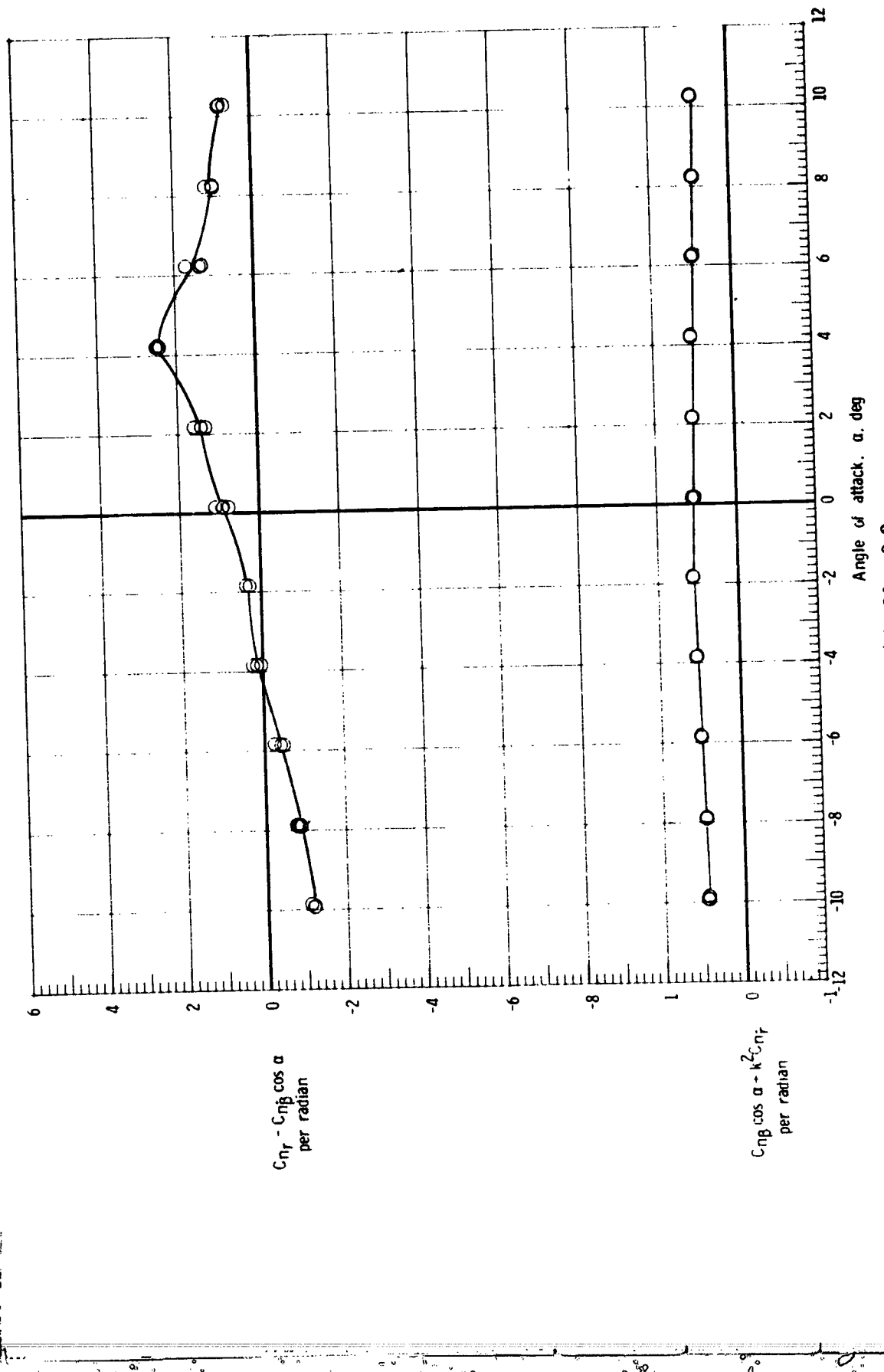
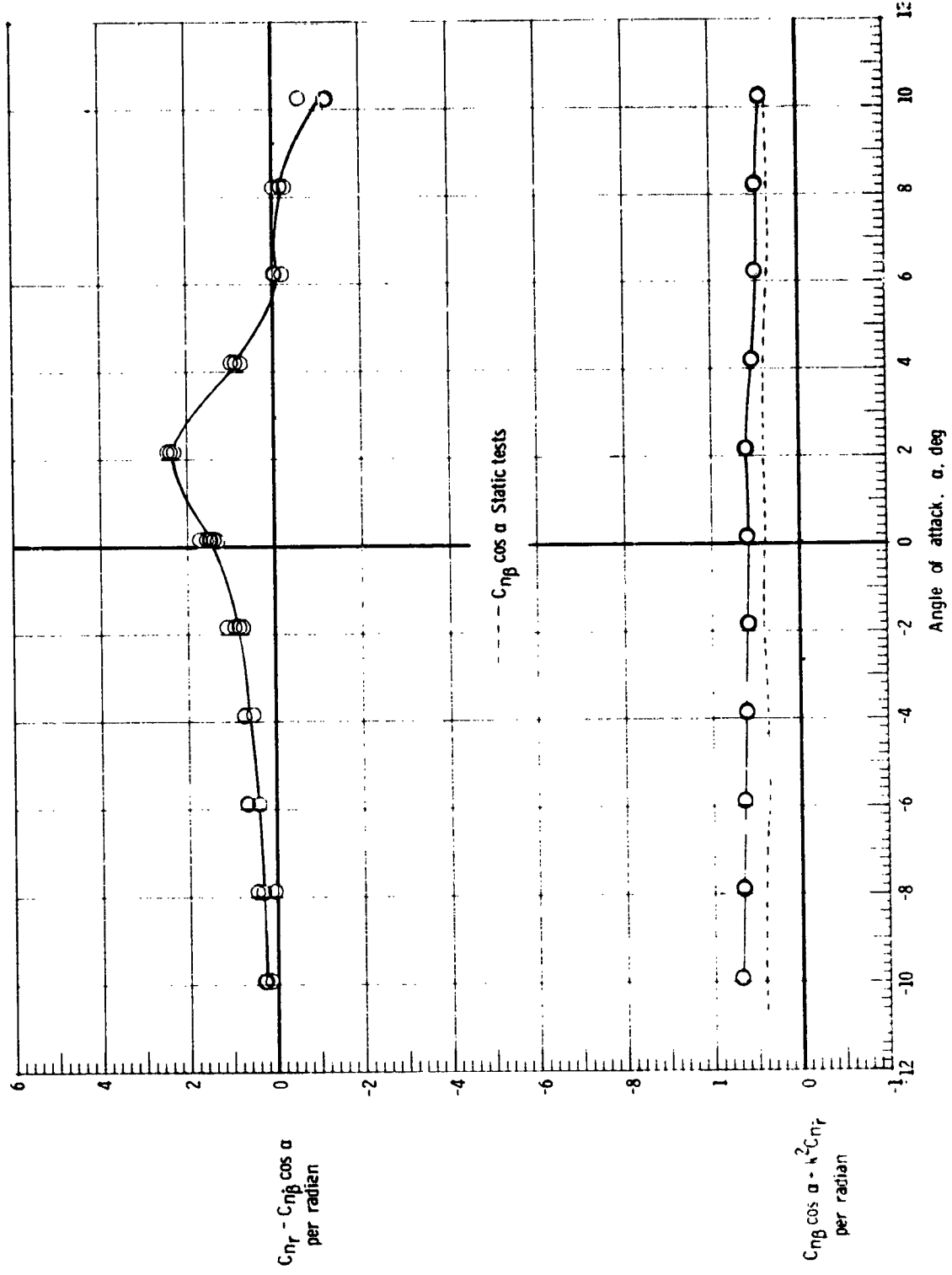
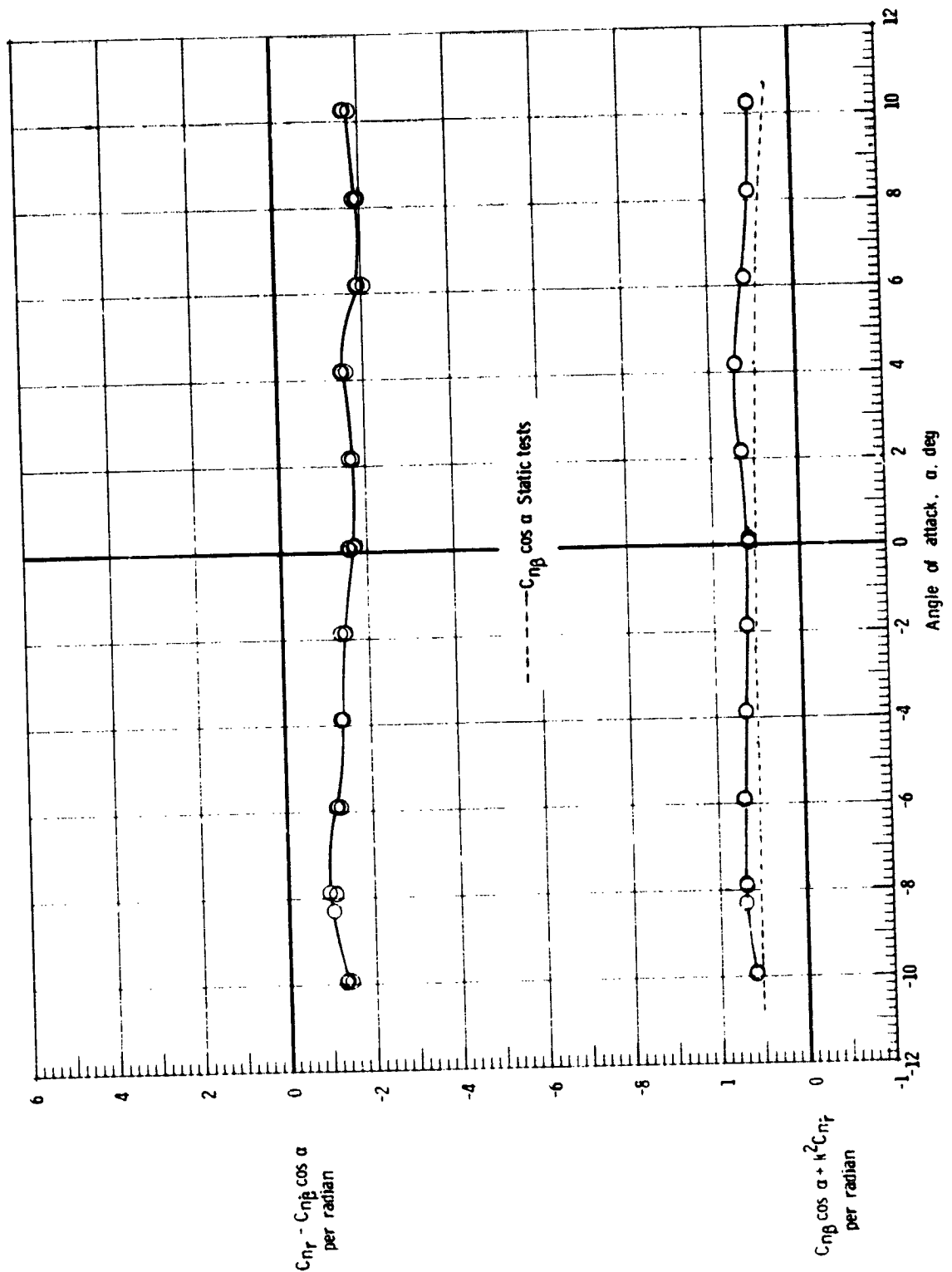


Figure 9.- Damping-in-yaw and oscillatory directional-stability parameters for launch vehicle (Max q_r c.g.).
 (a) $M = 0.3$.



(b) $M = 0.6$.

Figure 9.- Continued.



(c) $M = 0.9$.

Figure 9.- Continued.

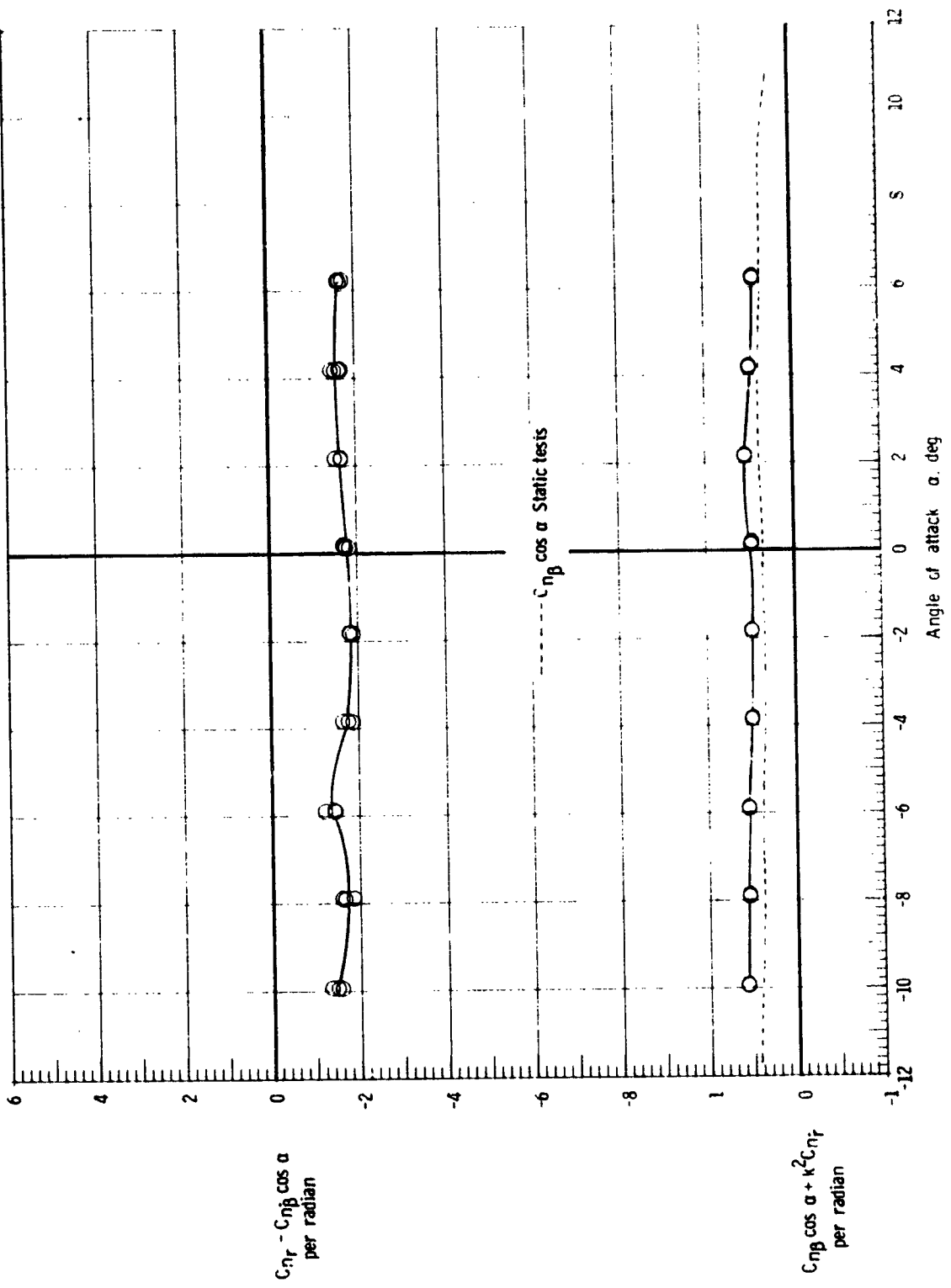


Figure 9.- Concluded.

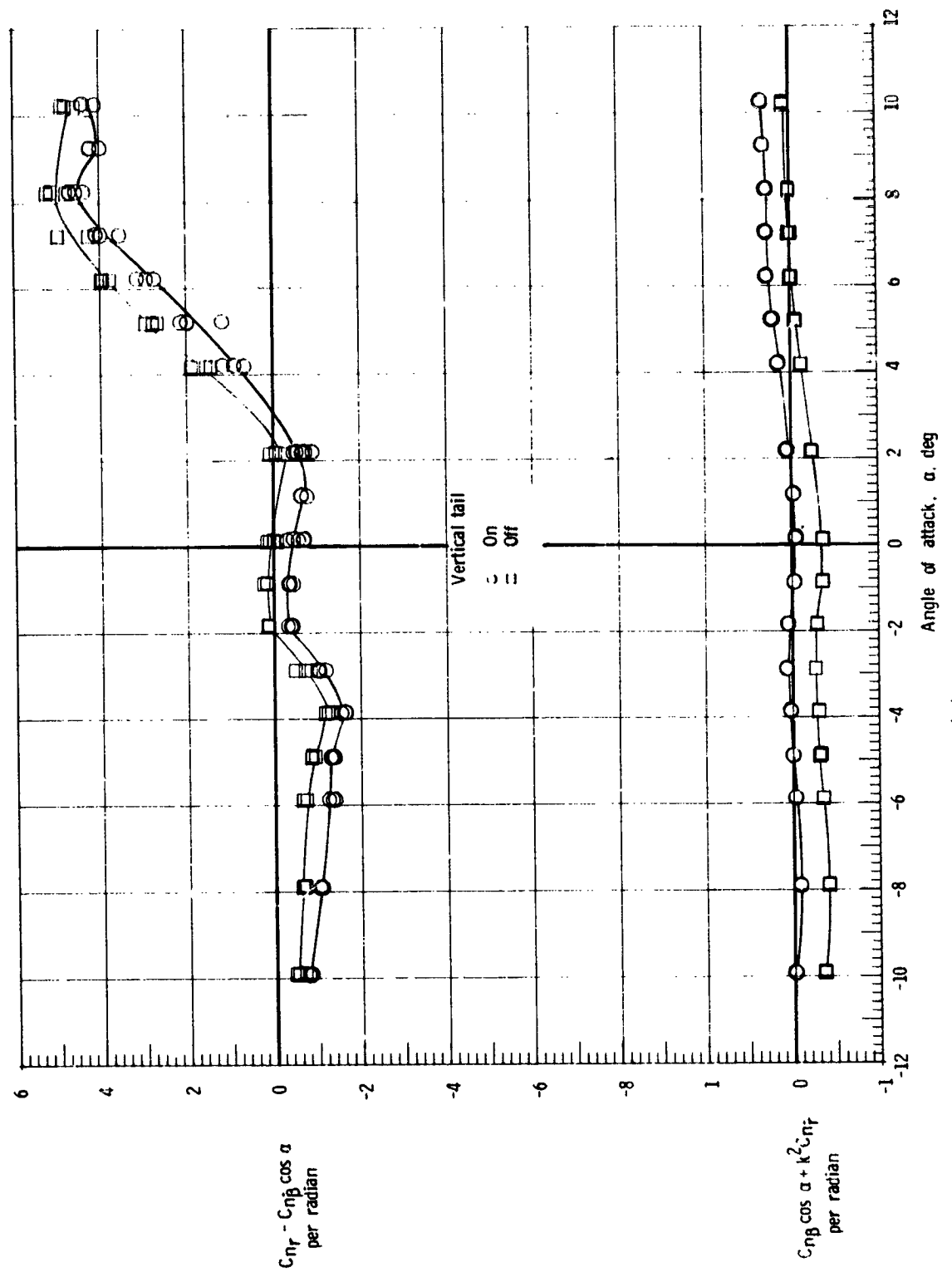
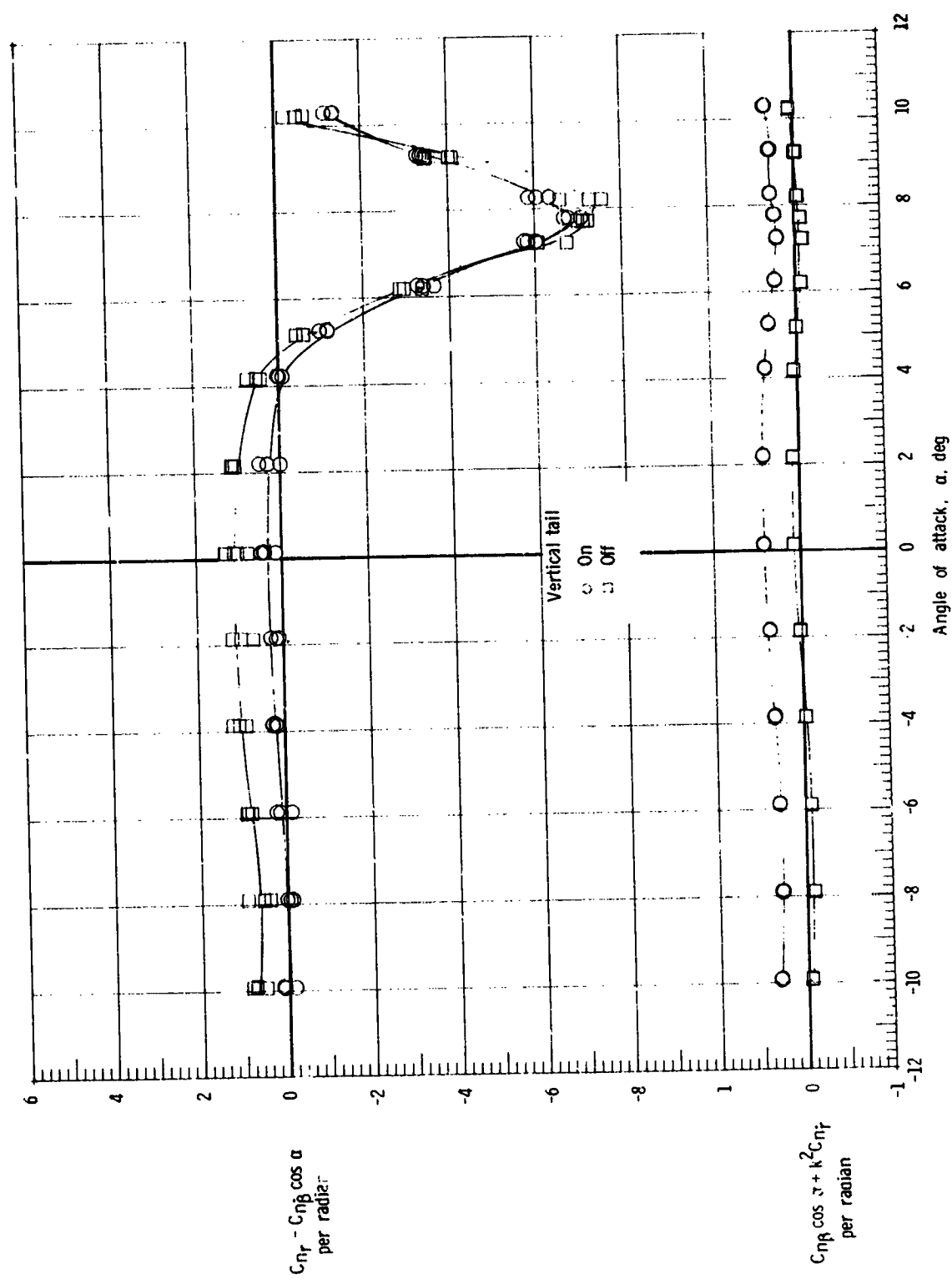
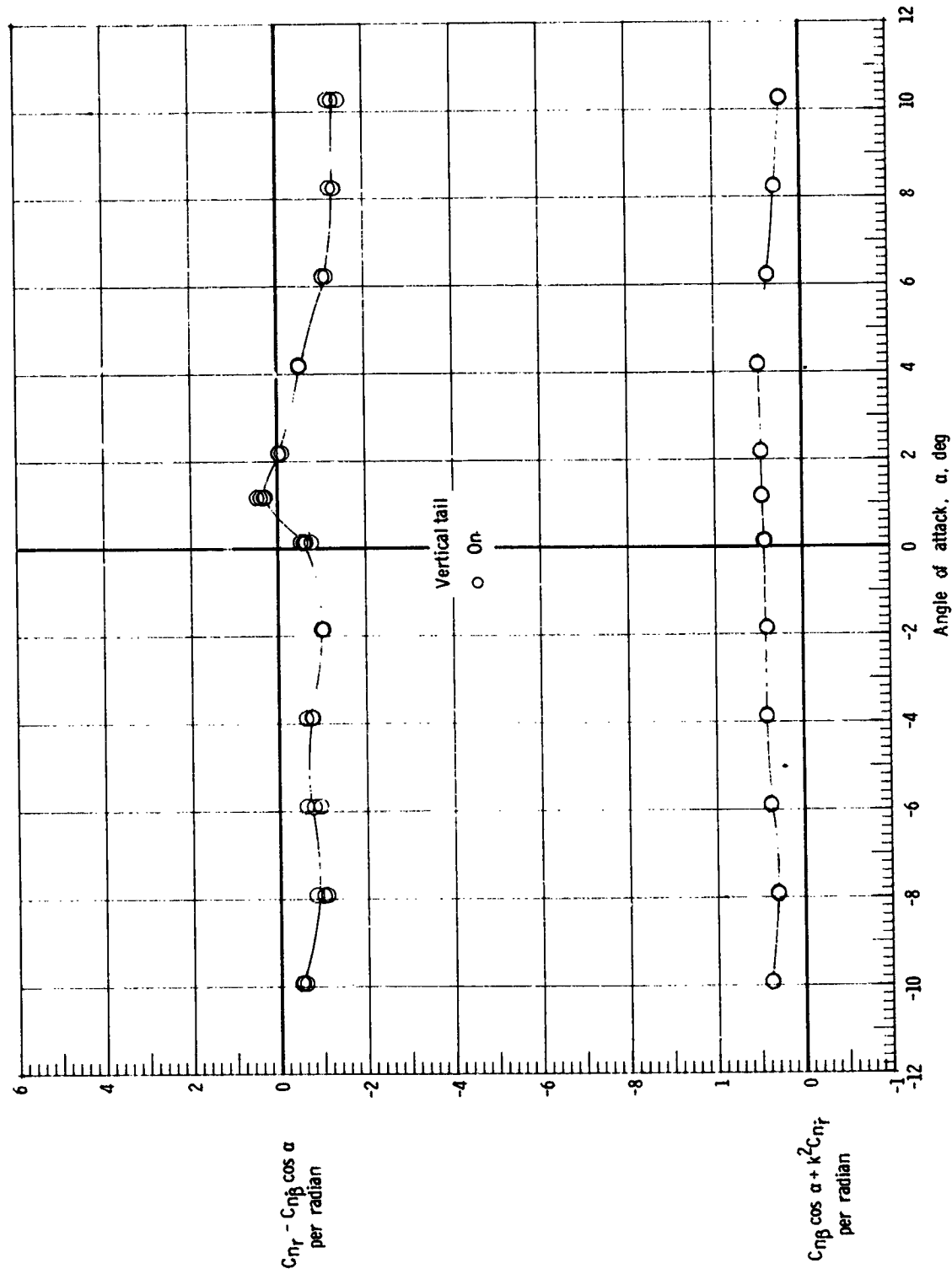


Figure 10.- Damping-in-yaw parameter and oscillatory directional-stability parameter
for orbiter external-tank configuration.
(a) $M = 0.3$.



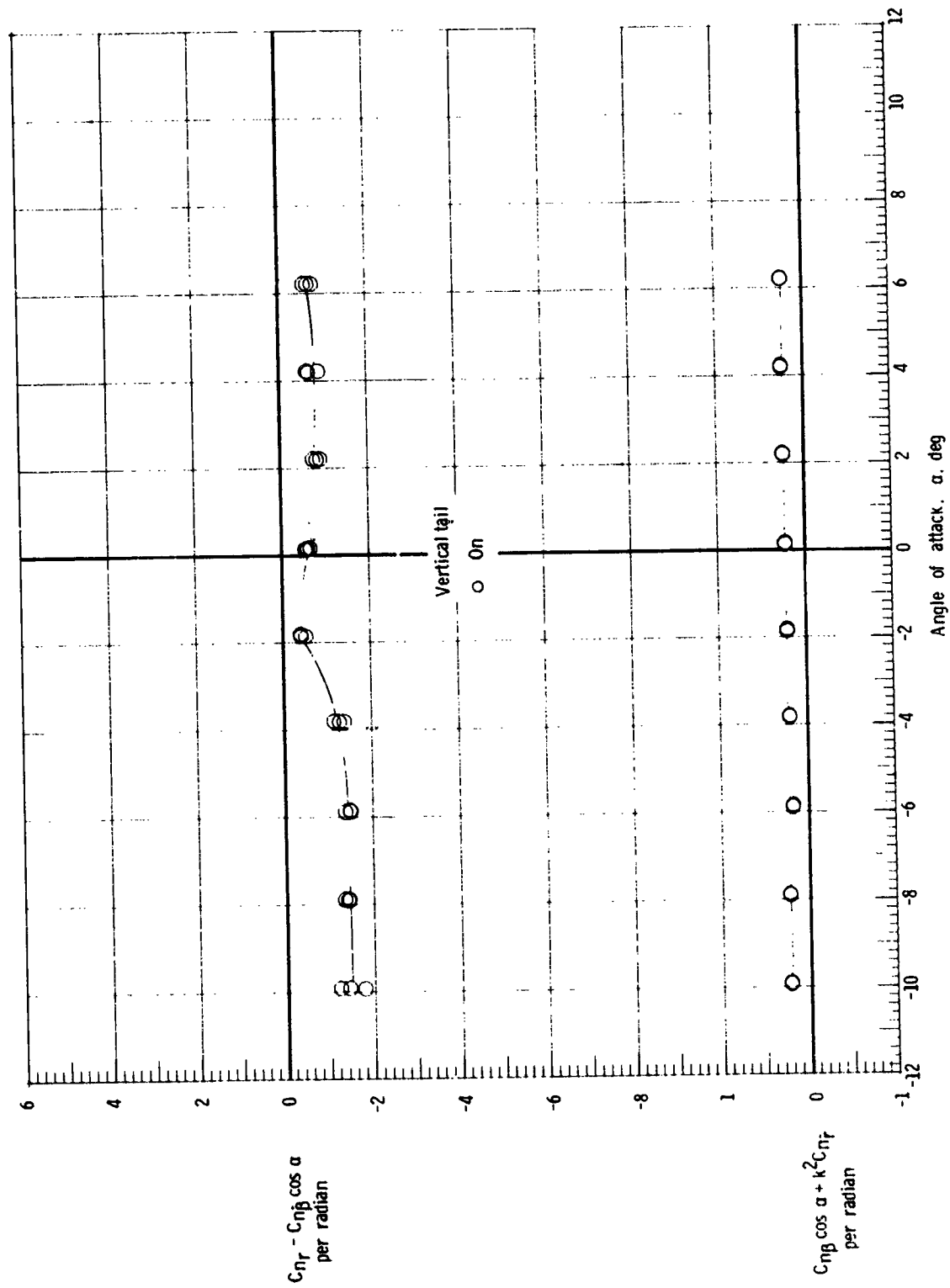
(b) $M = 0.6$.

Figure 10.- Continued.



(c) $M = 0.9$.

Figure 10c - Continued.



(d) $M = 1.2$.

Figure 10.- Concluded.

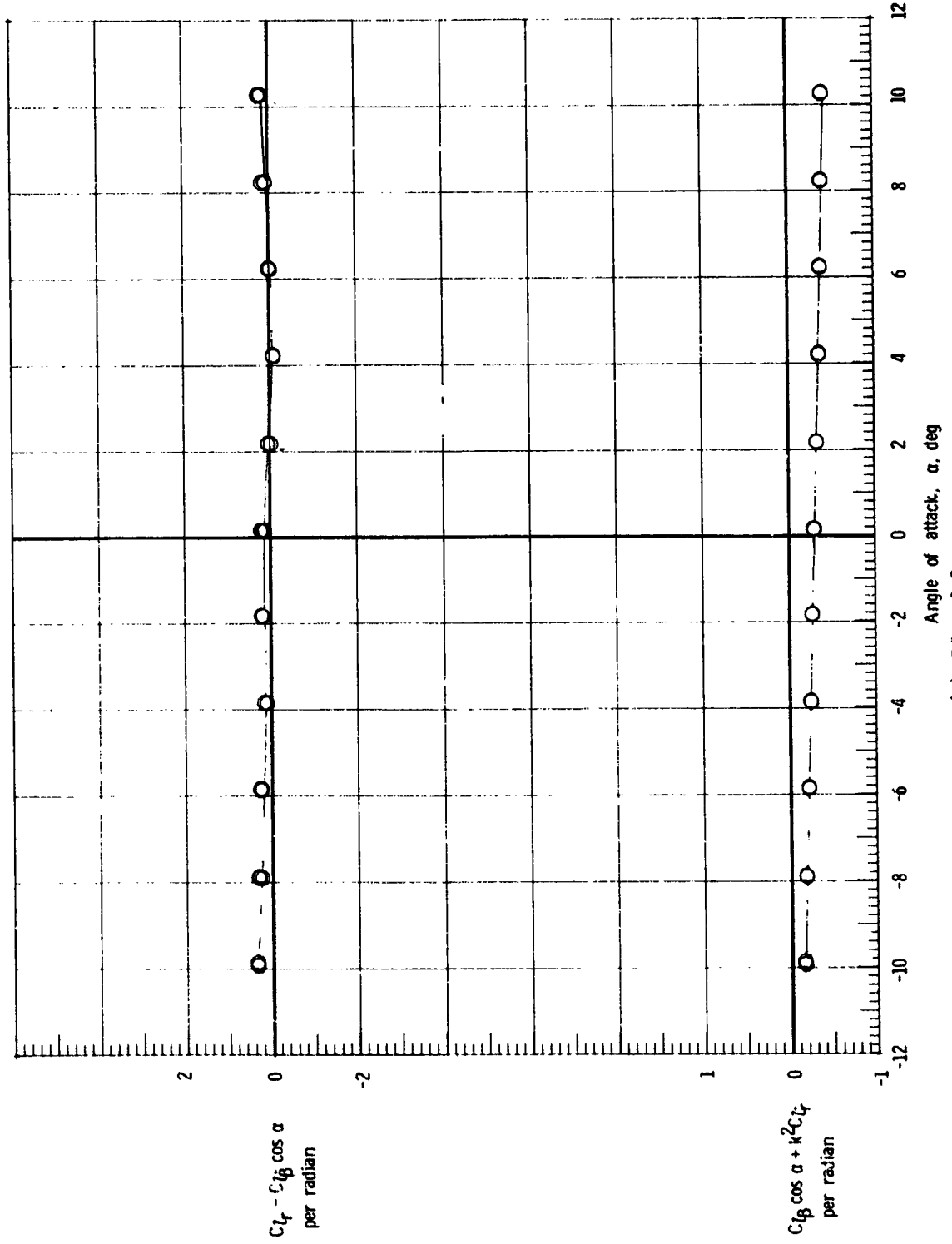


Figure 11.- Rolling moment due to yaw rate parameter and effective dihedral parameter
for launch vehicle (Max q_∞ c.g.).

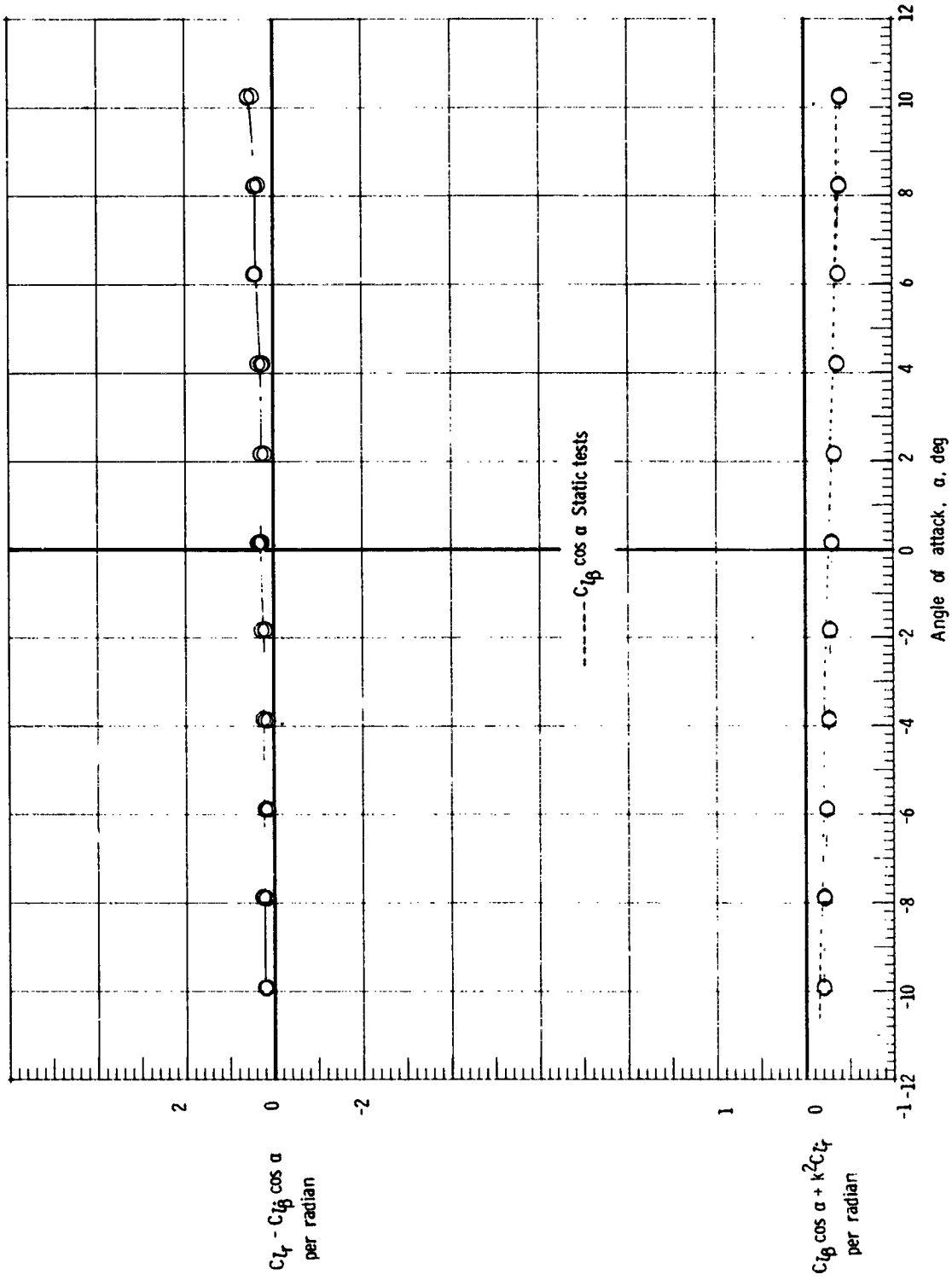
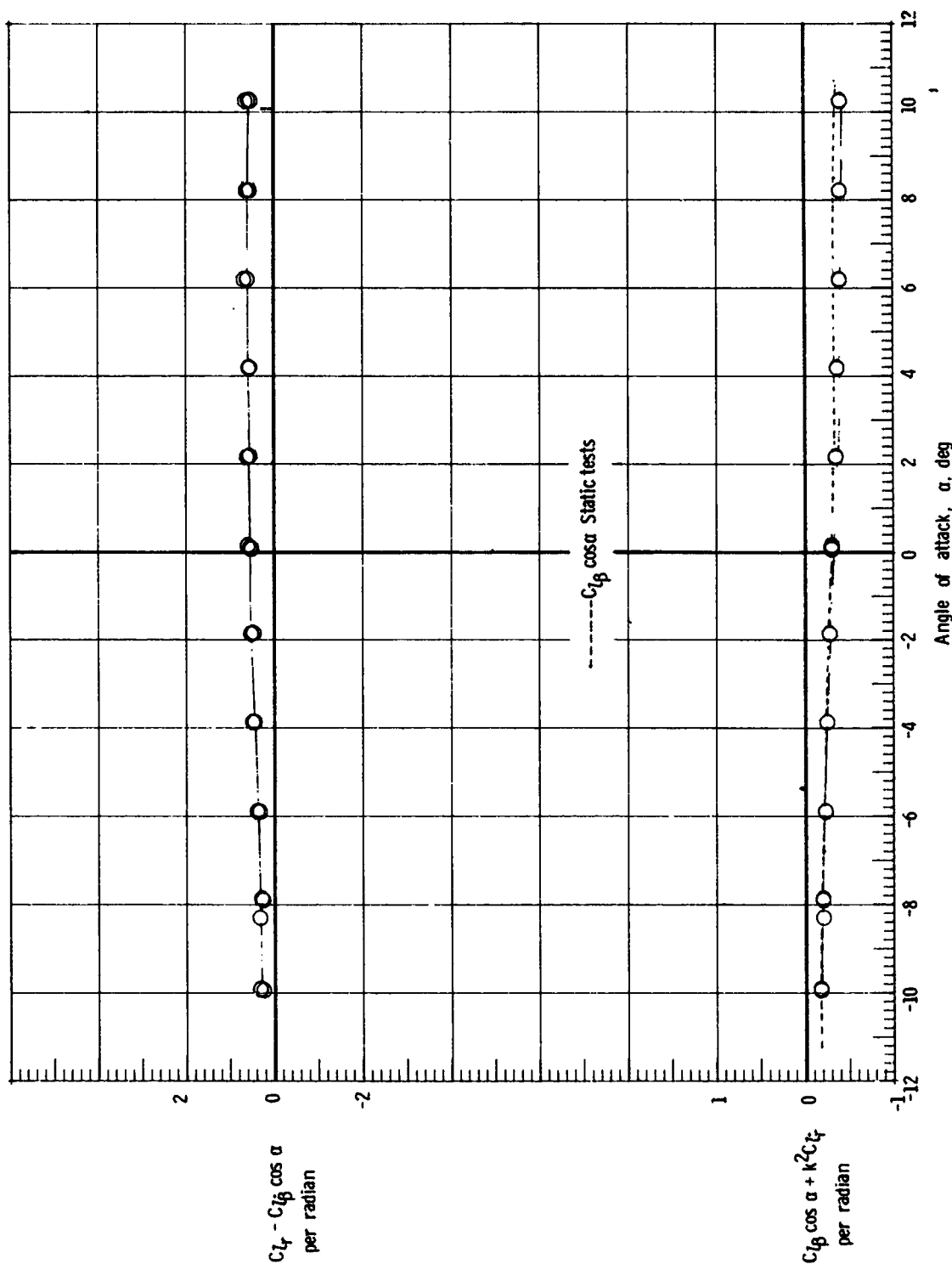
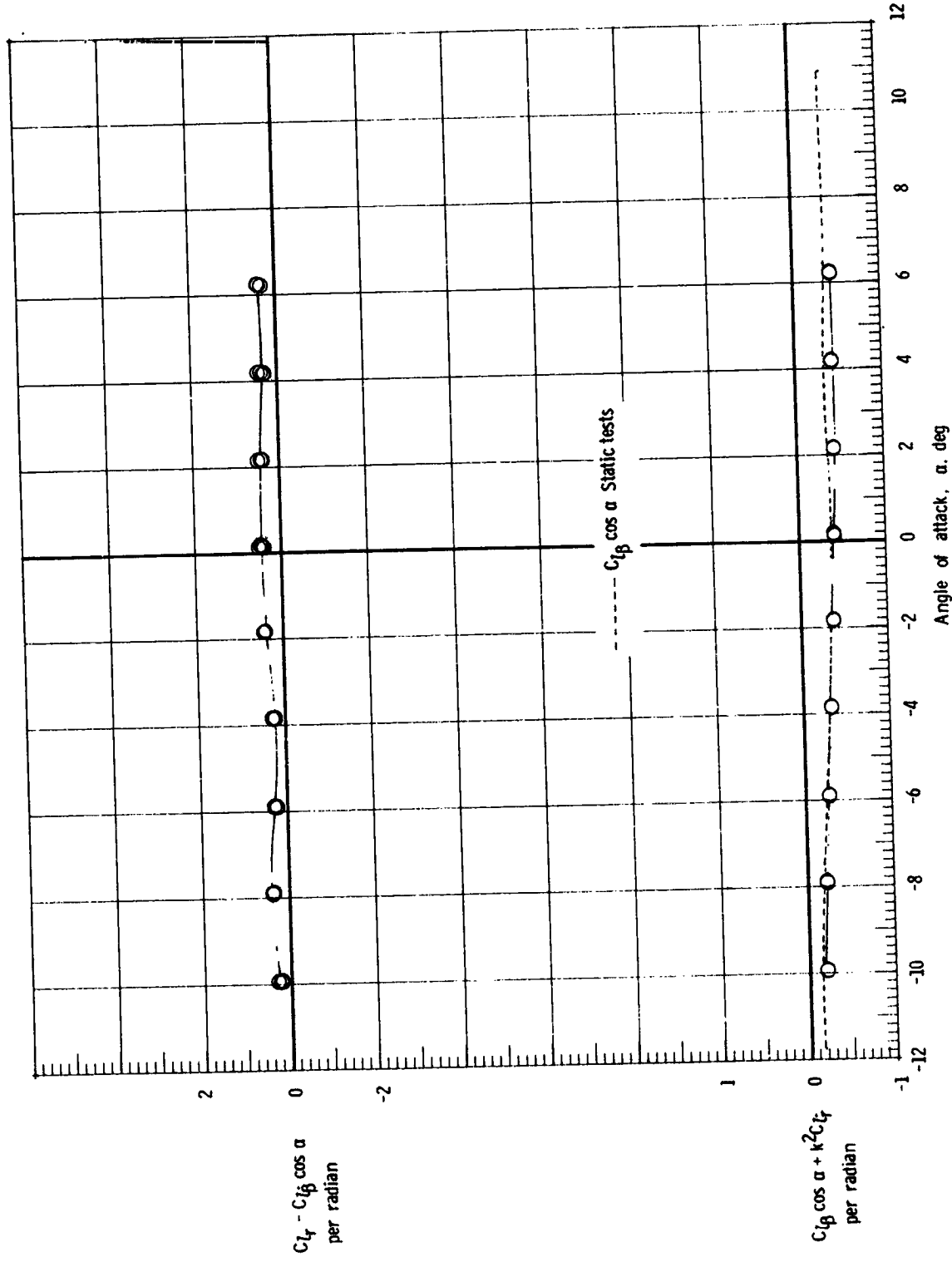


Figure 11.- Continued.



(c) $M = 0.9$.

Figure 11.- Continued.



(d) $M = 1.2$.

Figure 11.- Concluded.

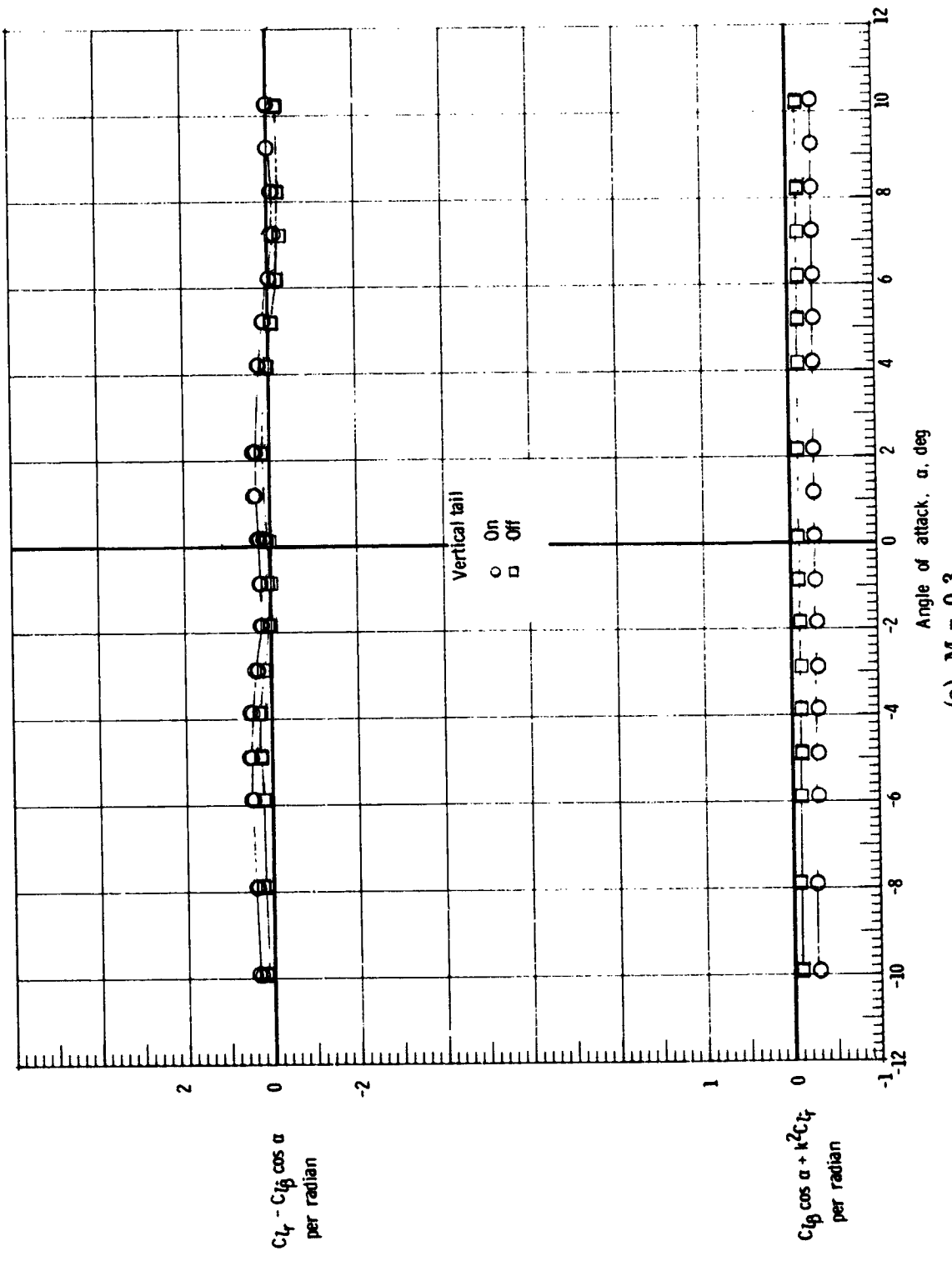
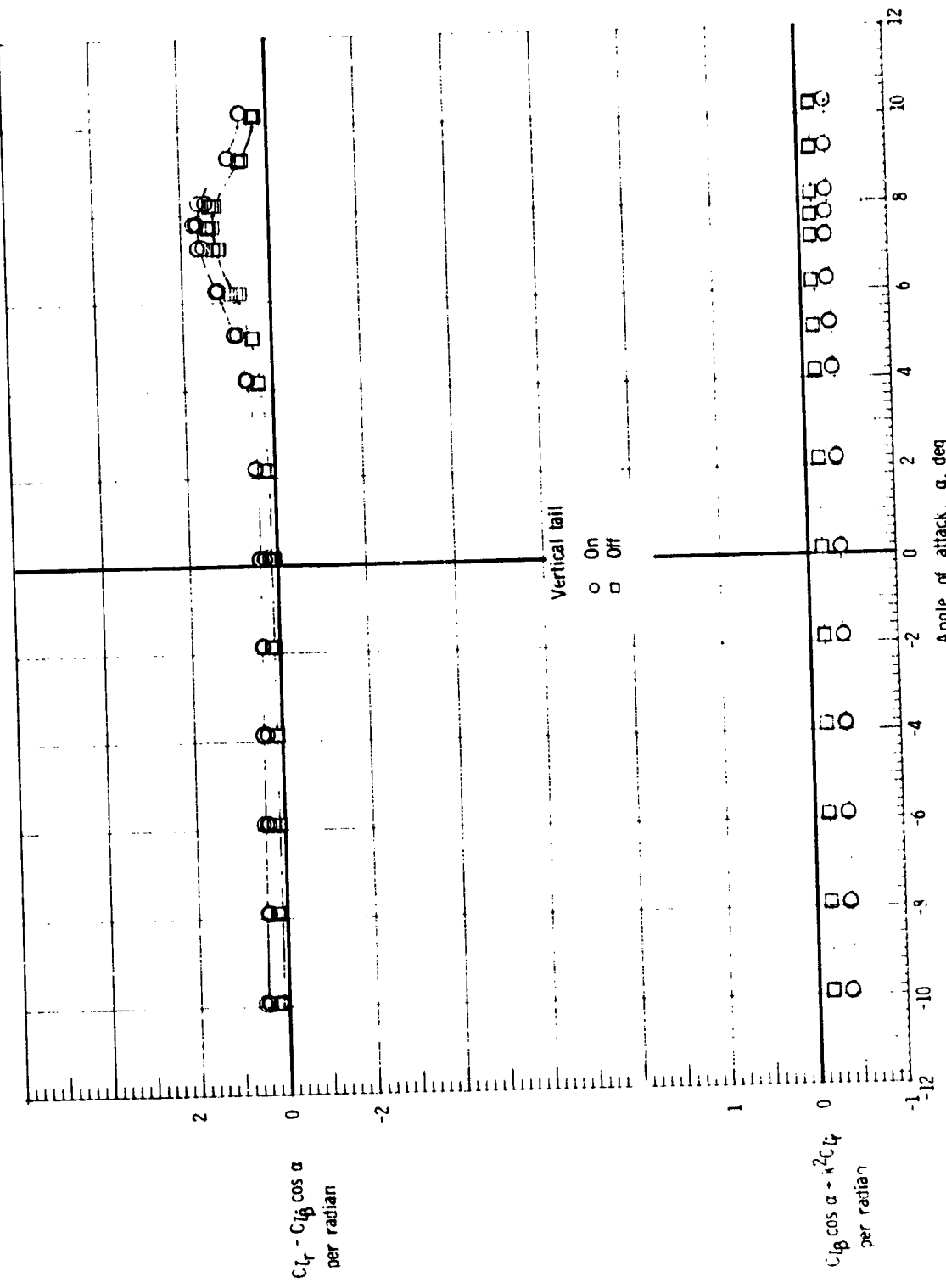
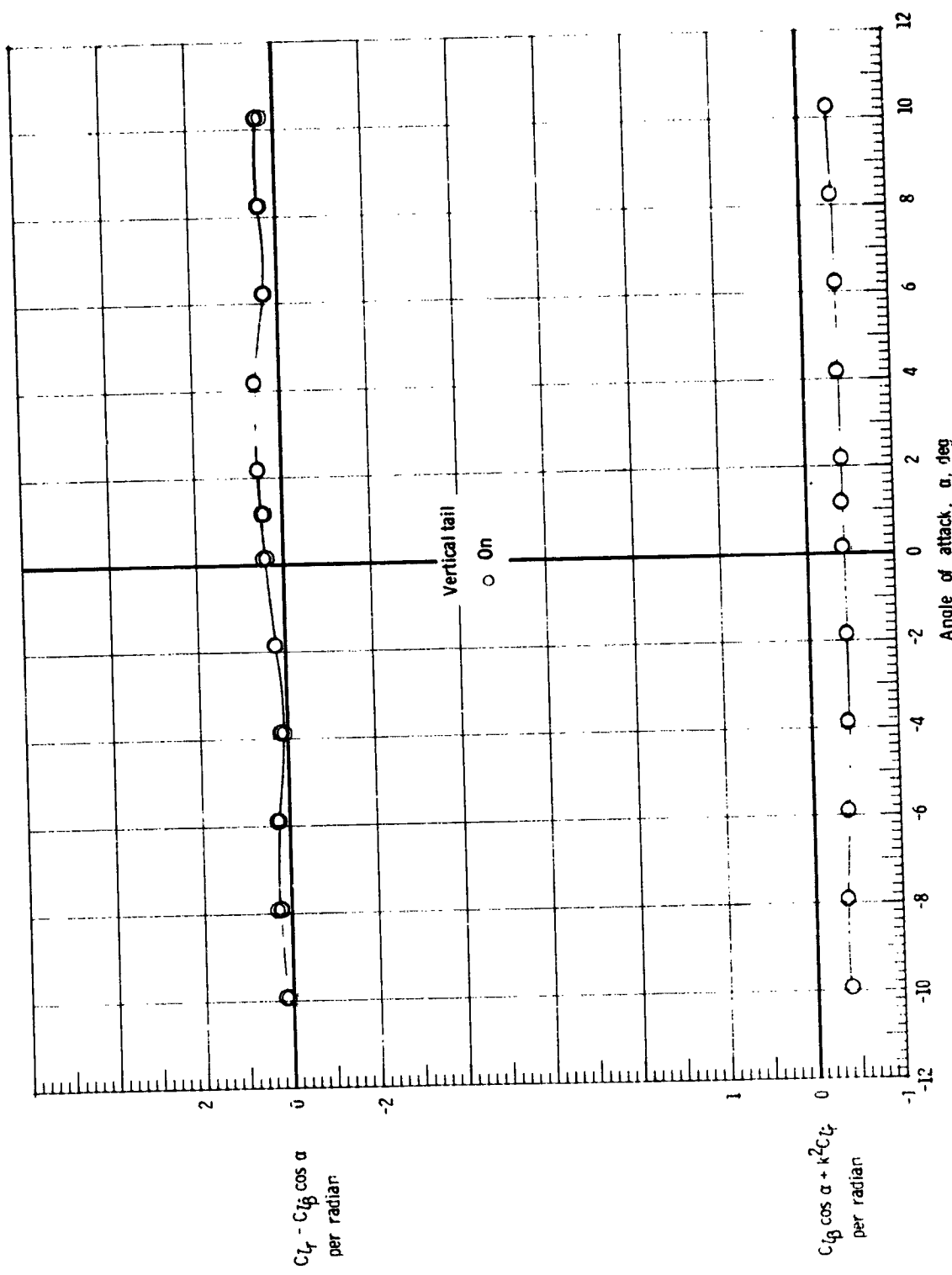


Figure 12.- Rolling moment due to yaw rate parameter and effective dihedral parameter for orbiter external-tank configuration.



(b) $M = 0.6$.

Figure 12.- Continued.



(c) $M = 0.9$.

Figure 12.- Continued.

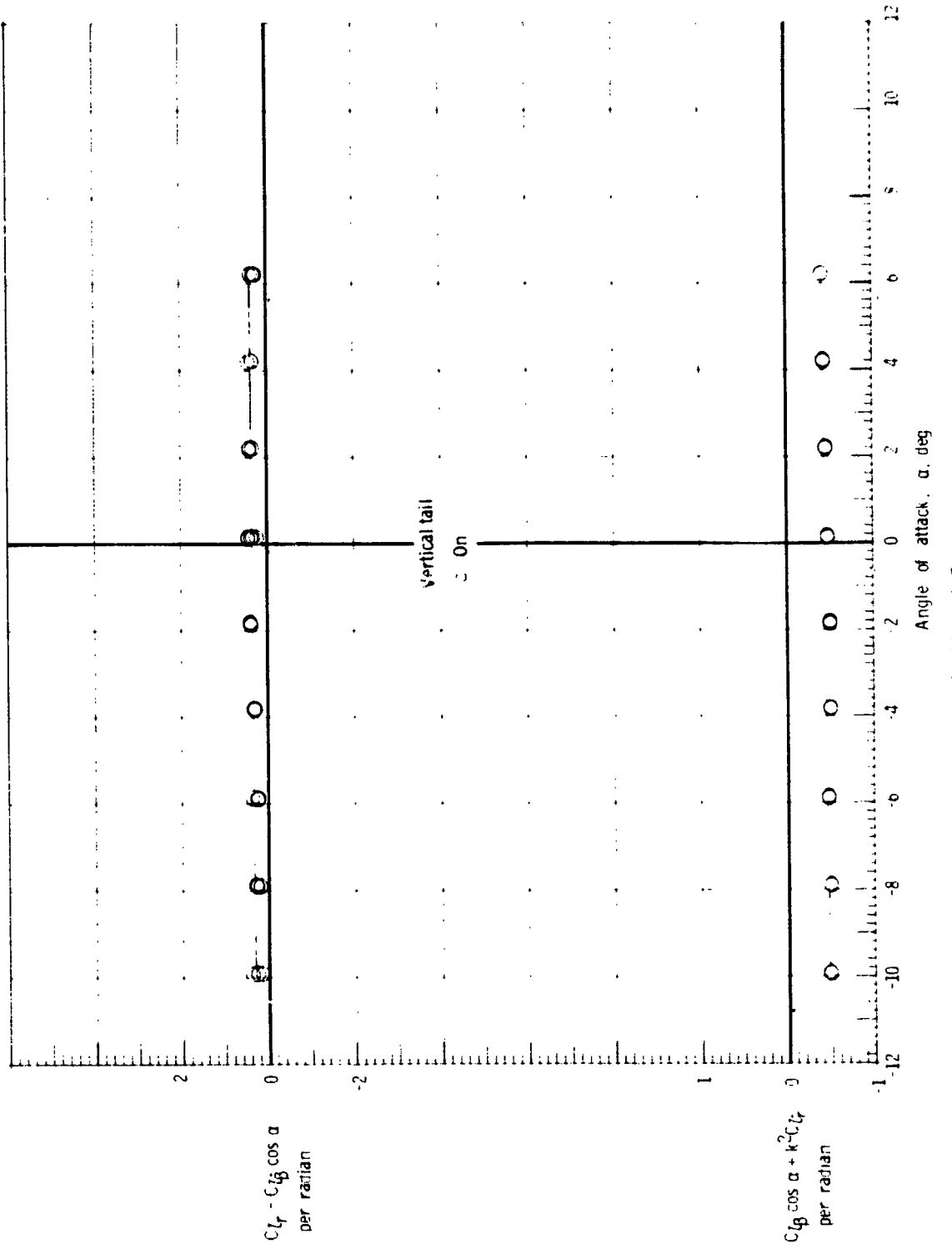
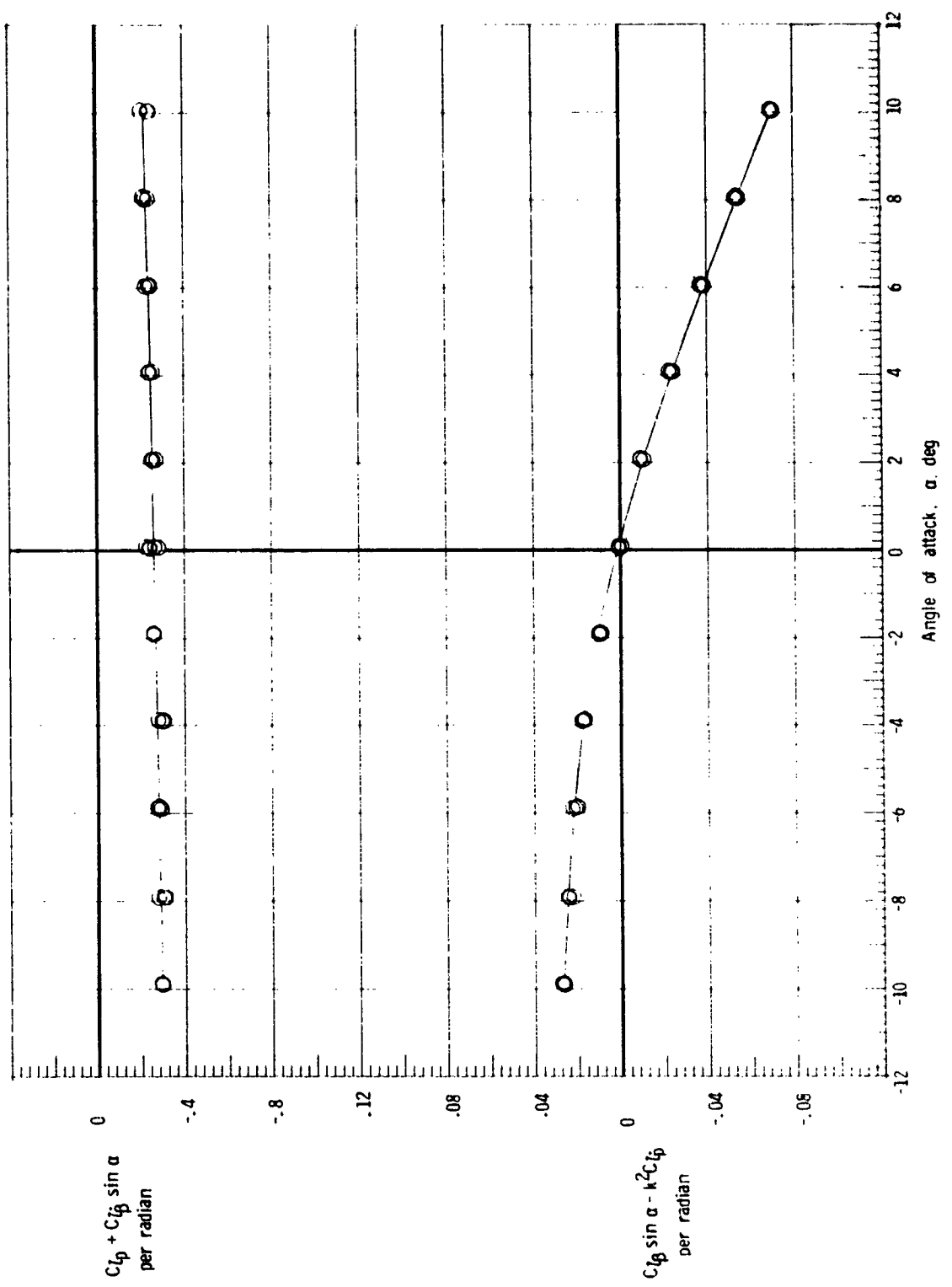
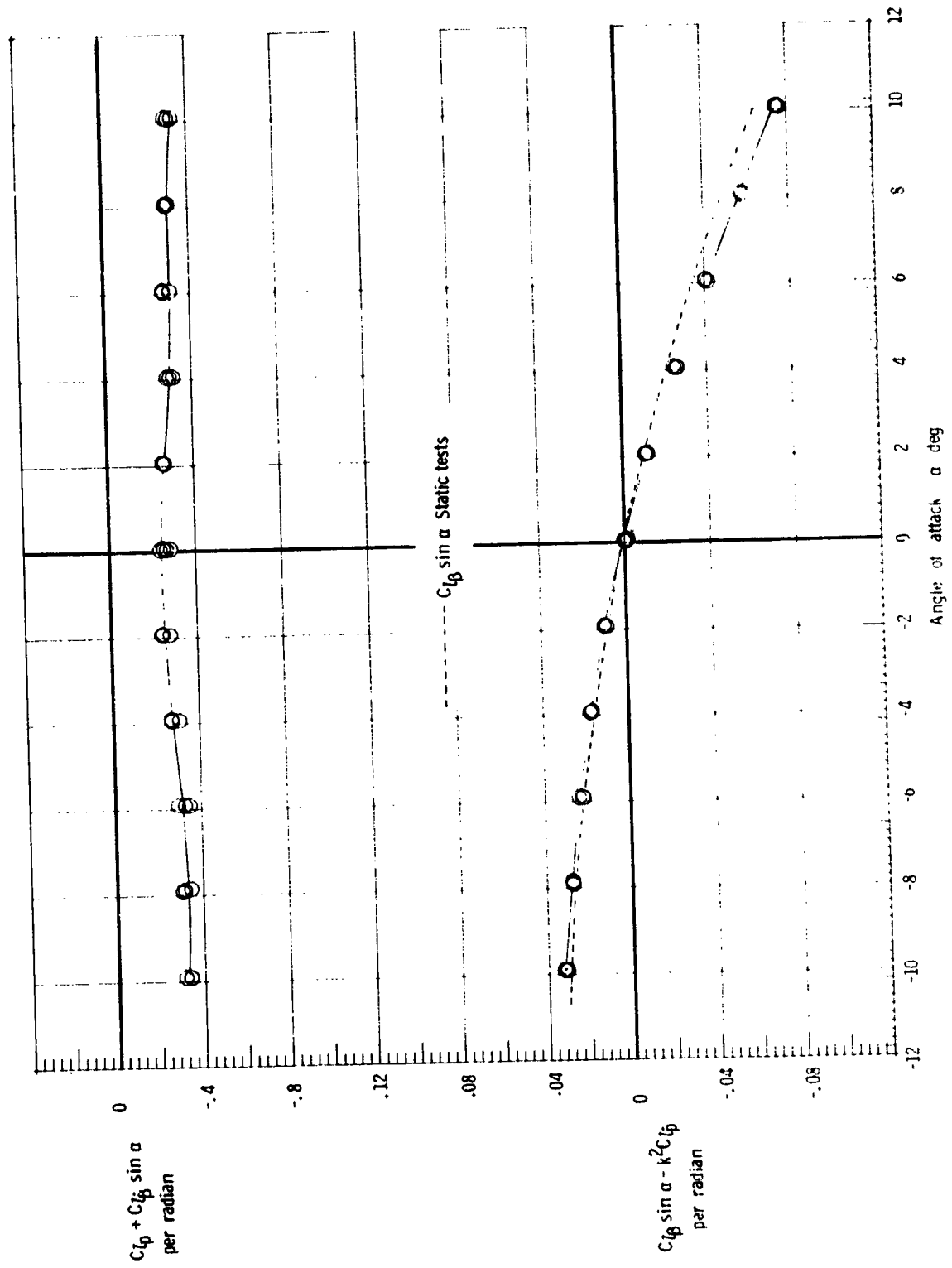


Figure 12.- Concluded.



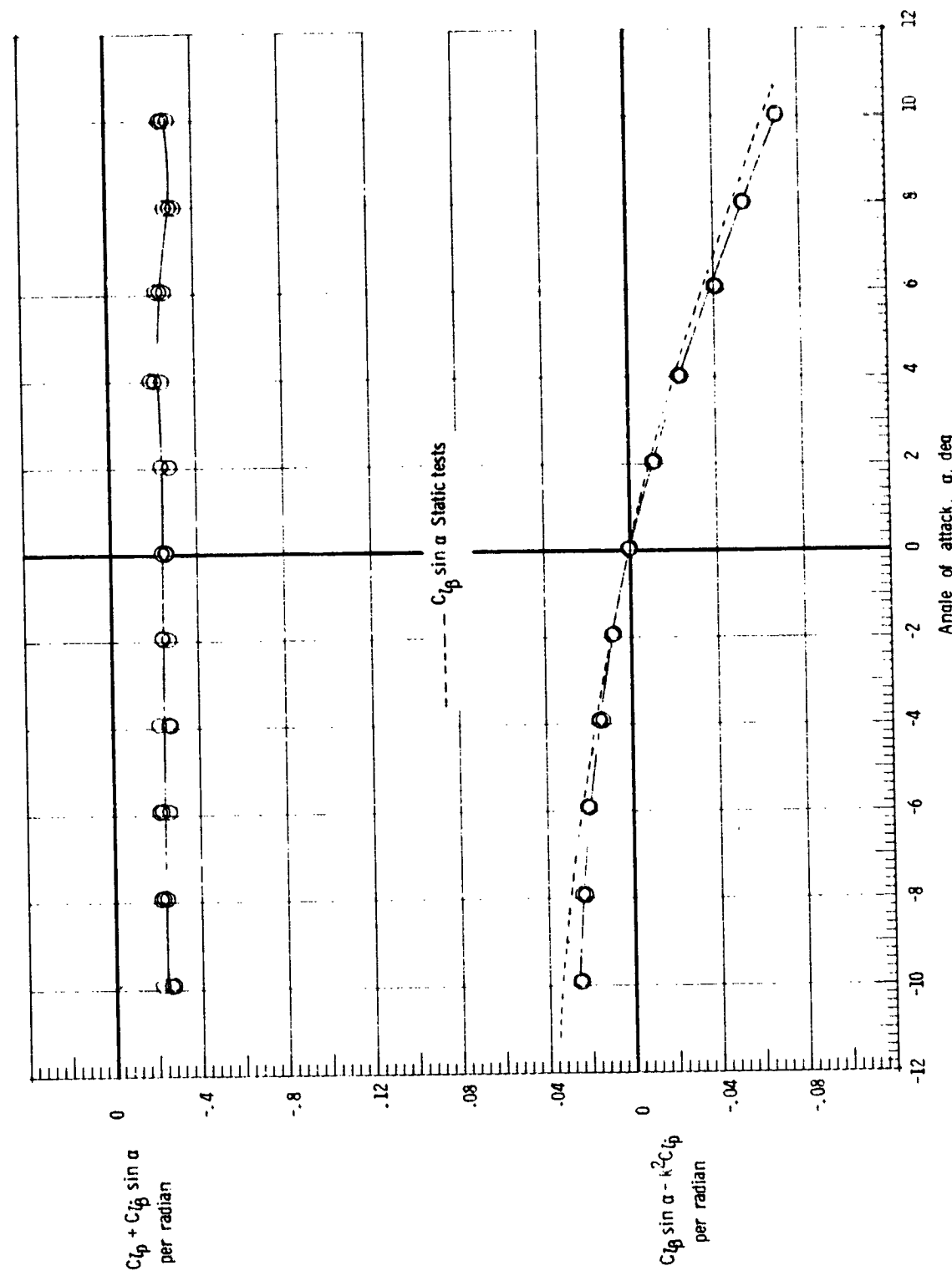
(a) $M = 0.3$.

Figure 13.- Damping-in-roll parameter and rolling moment due to roll displacement parameter for launch vehicle (Max q_x c.g.).



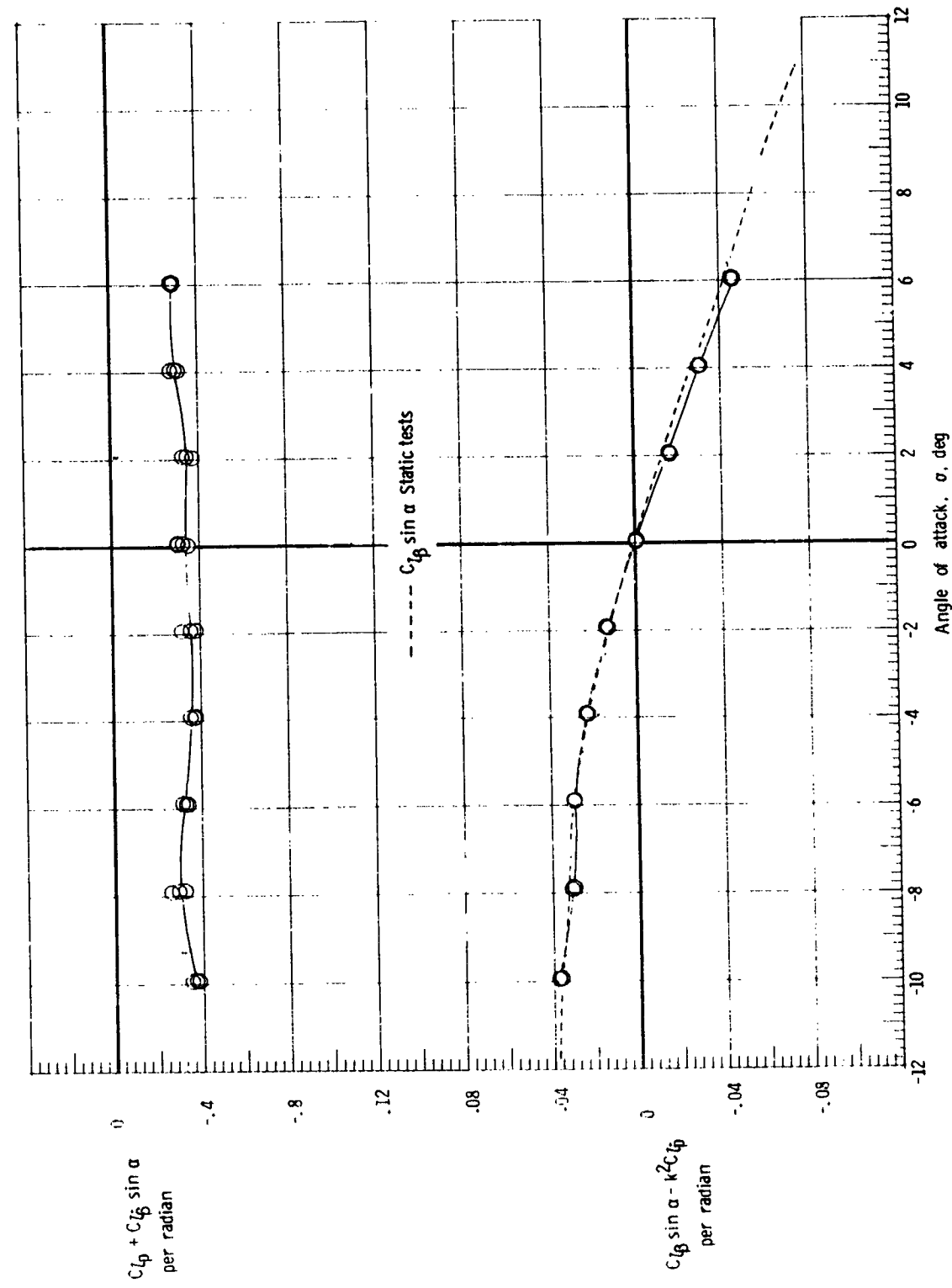
(b) $M = 0.6$.

Figure 13.- Continued.



(c) $M = 0.9$.

Figure 13.- Continued.



(d) $M = 1.2$.

Figure 13.- Concluded.

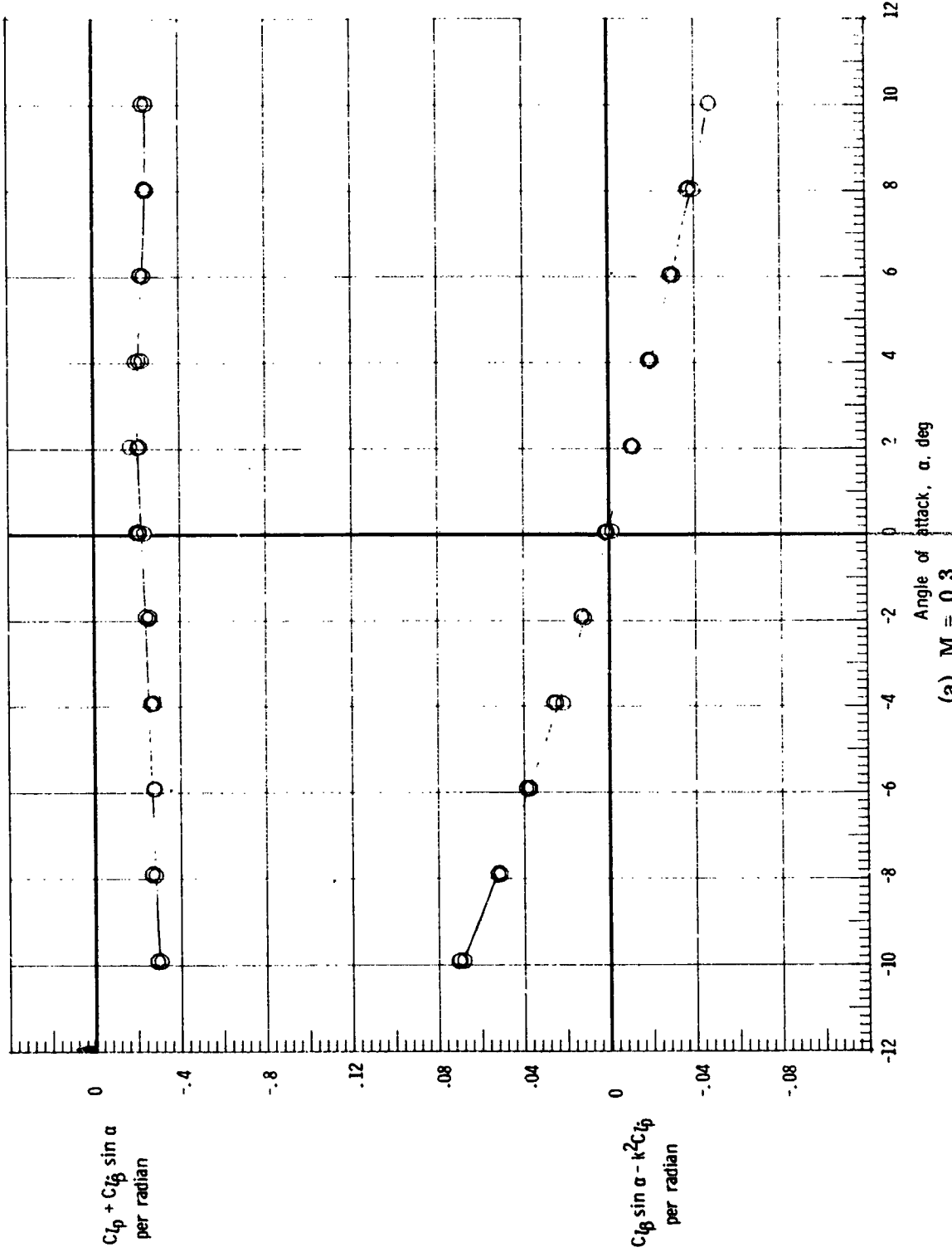
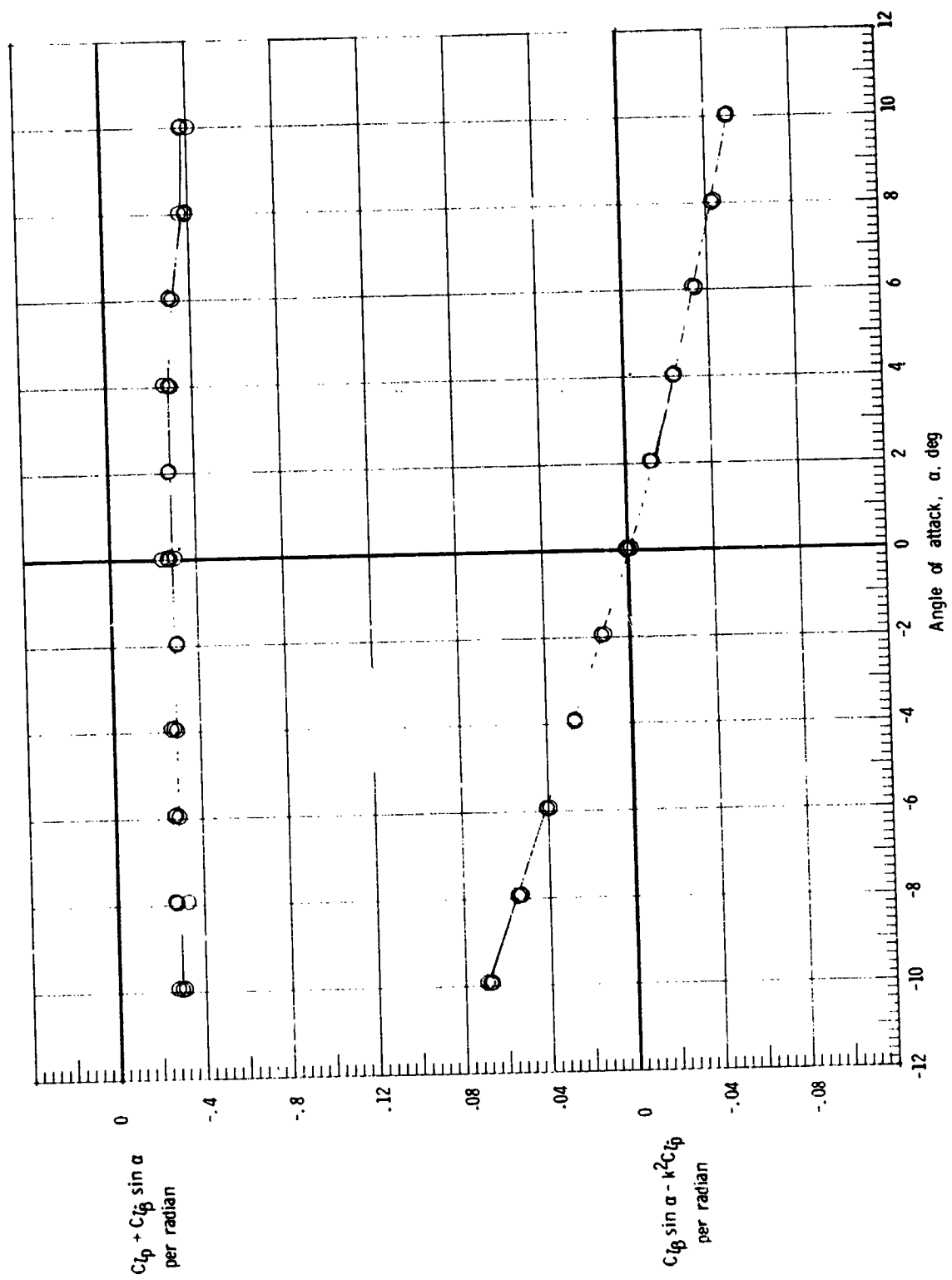


Figure 14.- Damping-in-roll parameter and rolling moment due to roll displacement parameter for orbiter external-tank configuration (Max q_∞ , c.g.).
 (a) $M = 0.3$.



(b) $M = 0.6$.

Figure 14.- Continued.

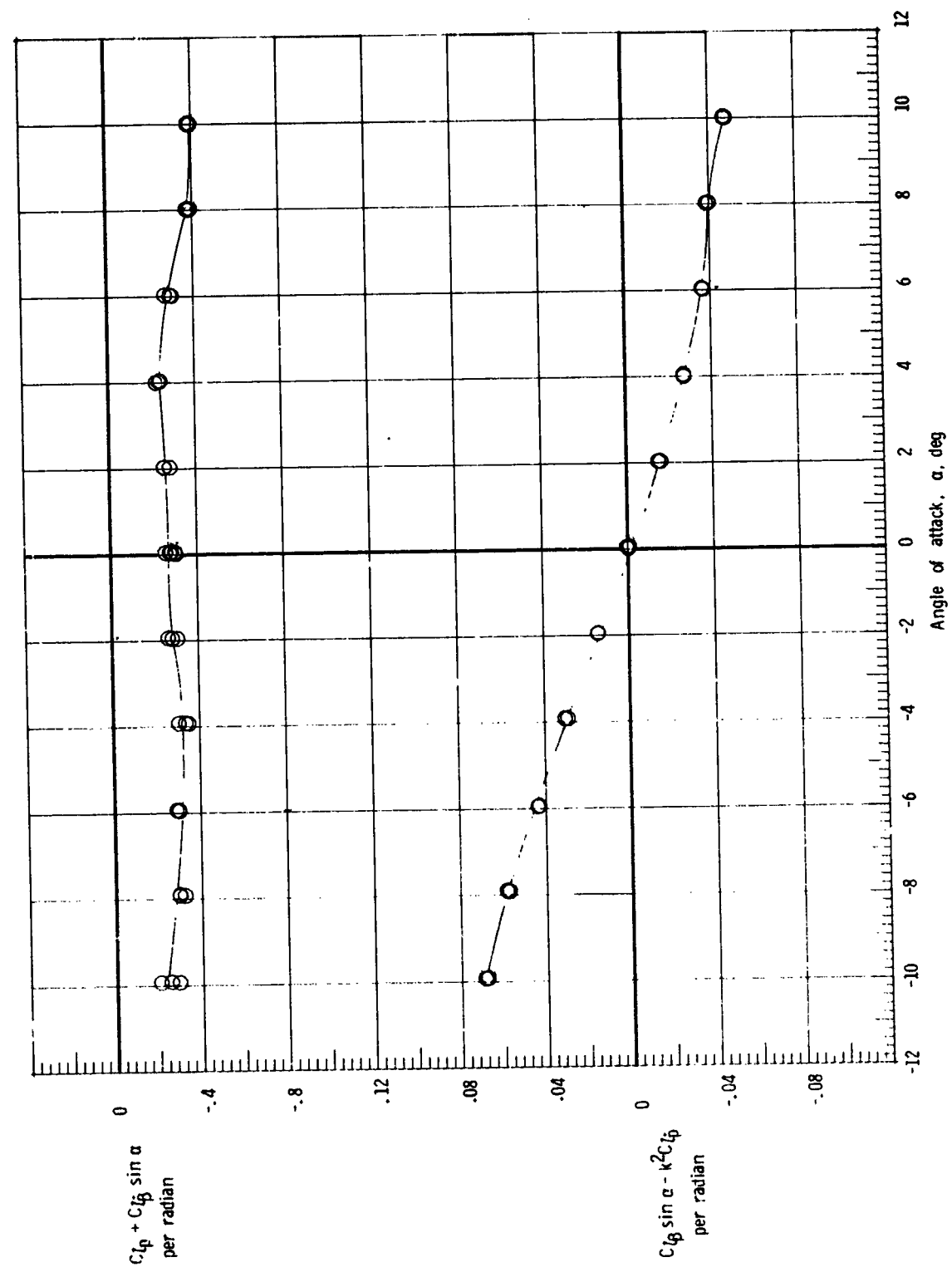


Figure 14.- Continued.
(c) $M = 0.9$.

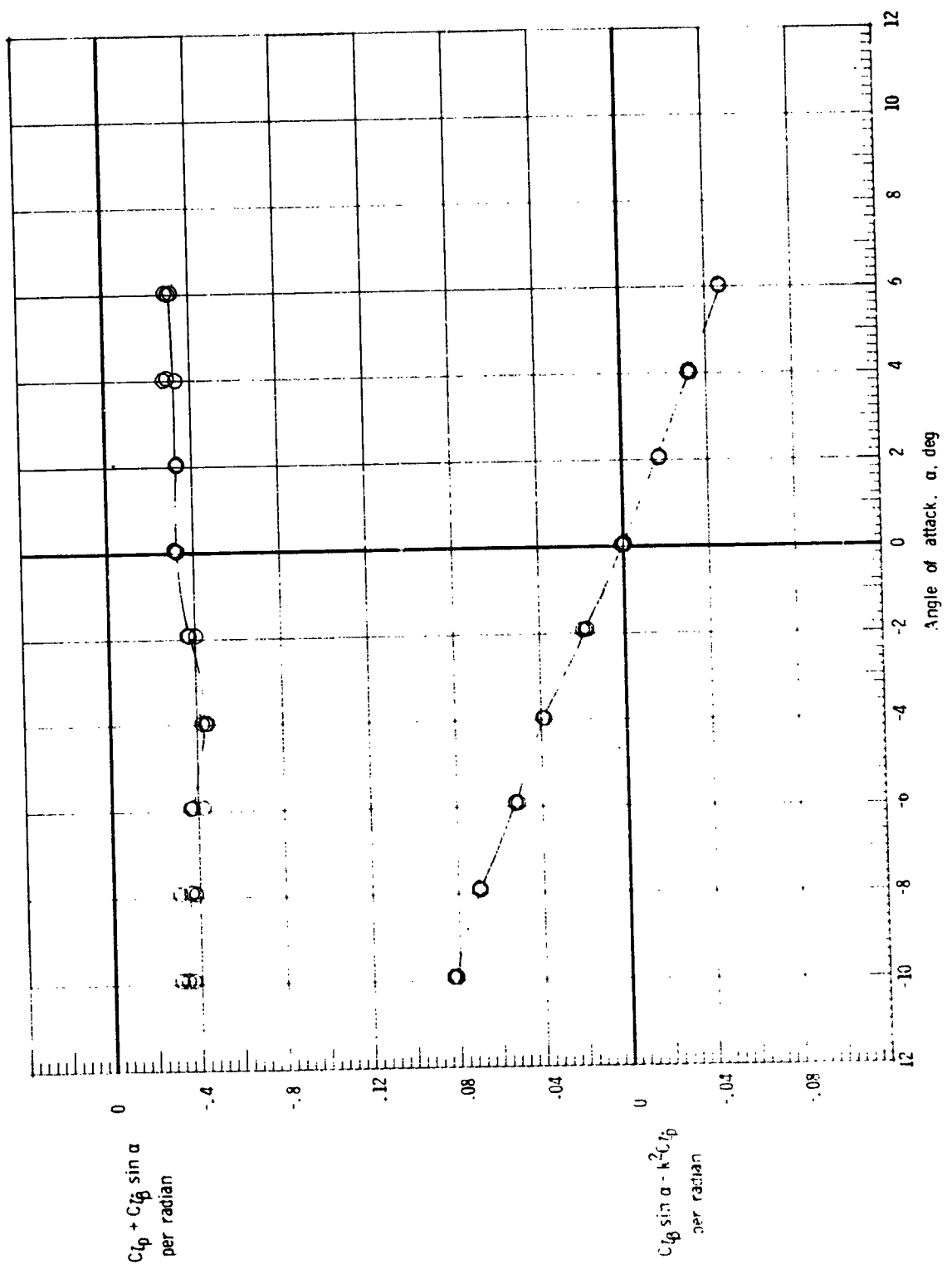


Figure 14.- Concluded.

(d) $M = 1.2$.

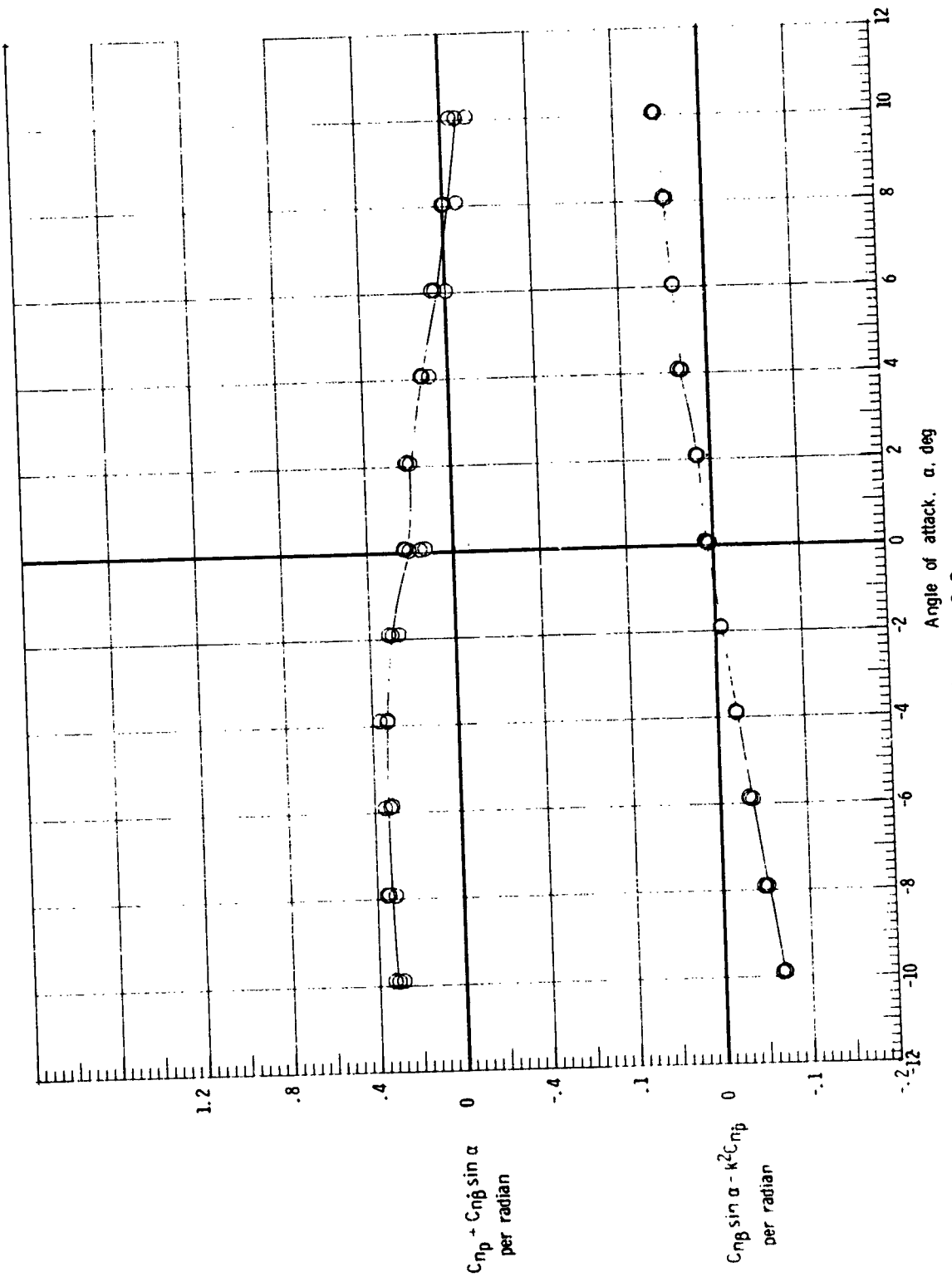
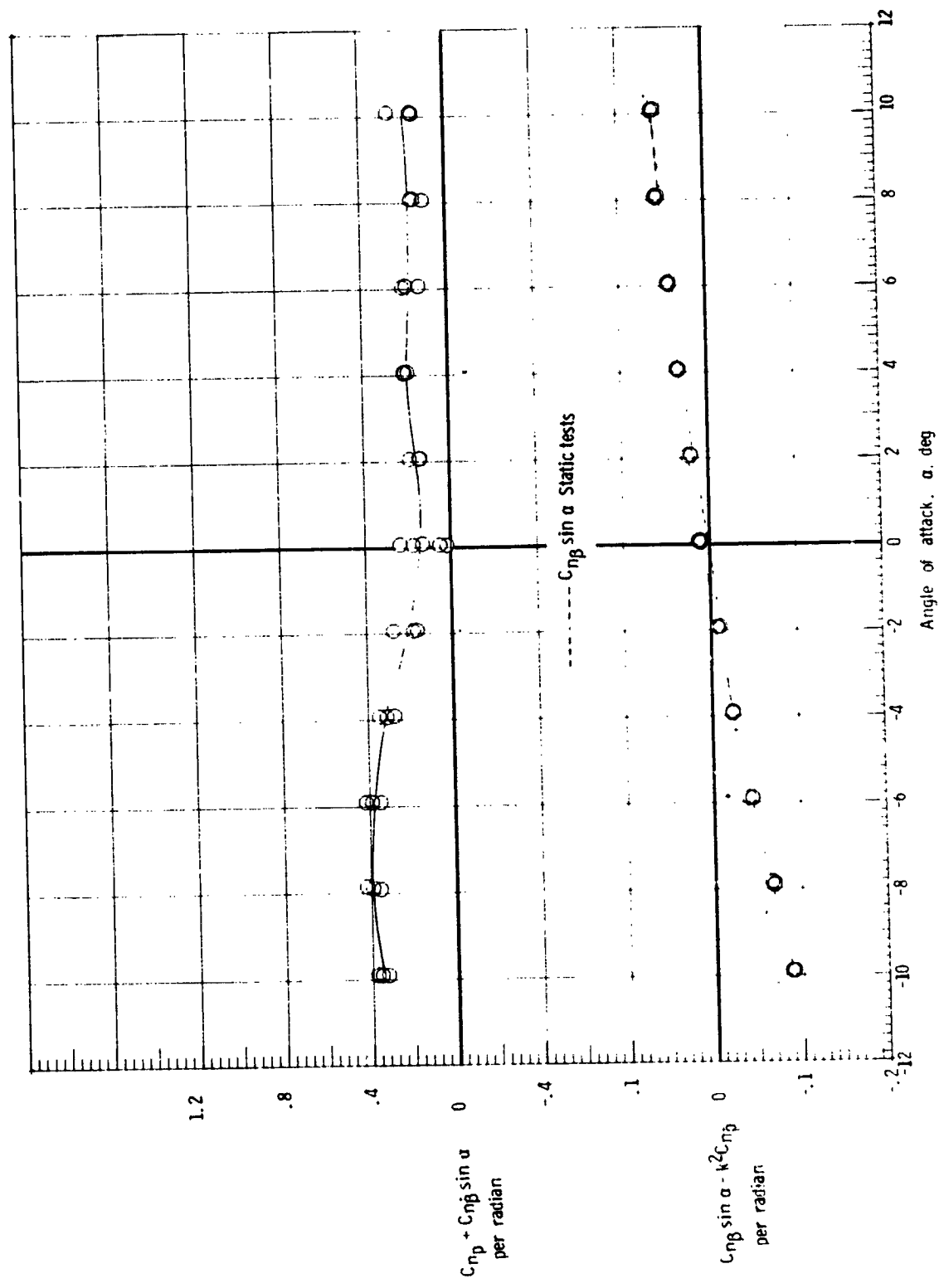


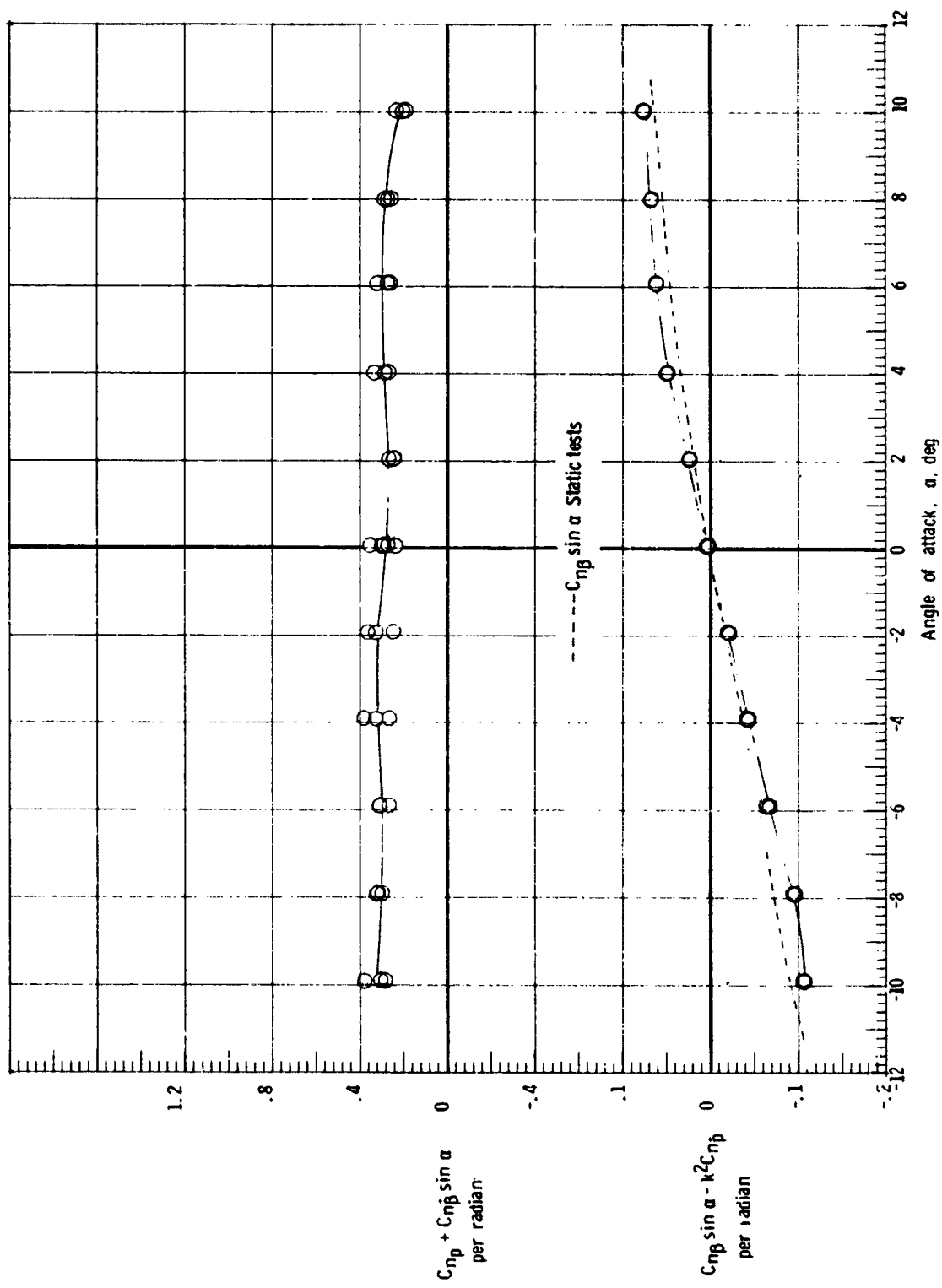
Figure 15.- Yawing moment due to roll rate parameter and yawing moment due to roll displacement parameter for launch vehicle (Max q_∞ c.g.).

(a) $M = 0.3$.



(b) $M = 0.6$.

Figure 15.- Continued.



(c) $M = 0.9$.

Figure 15.- Continued.

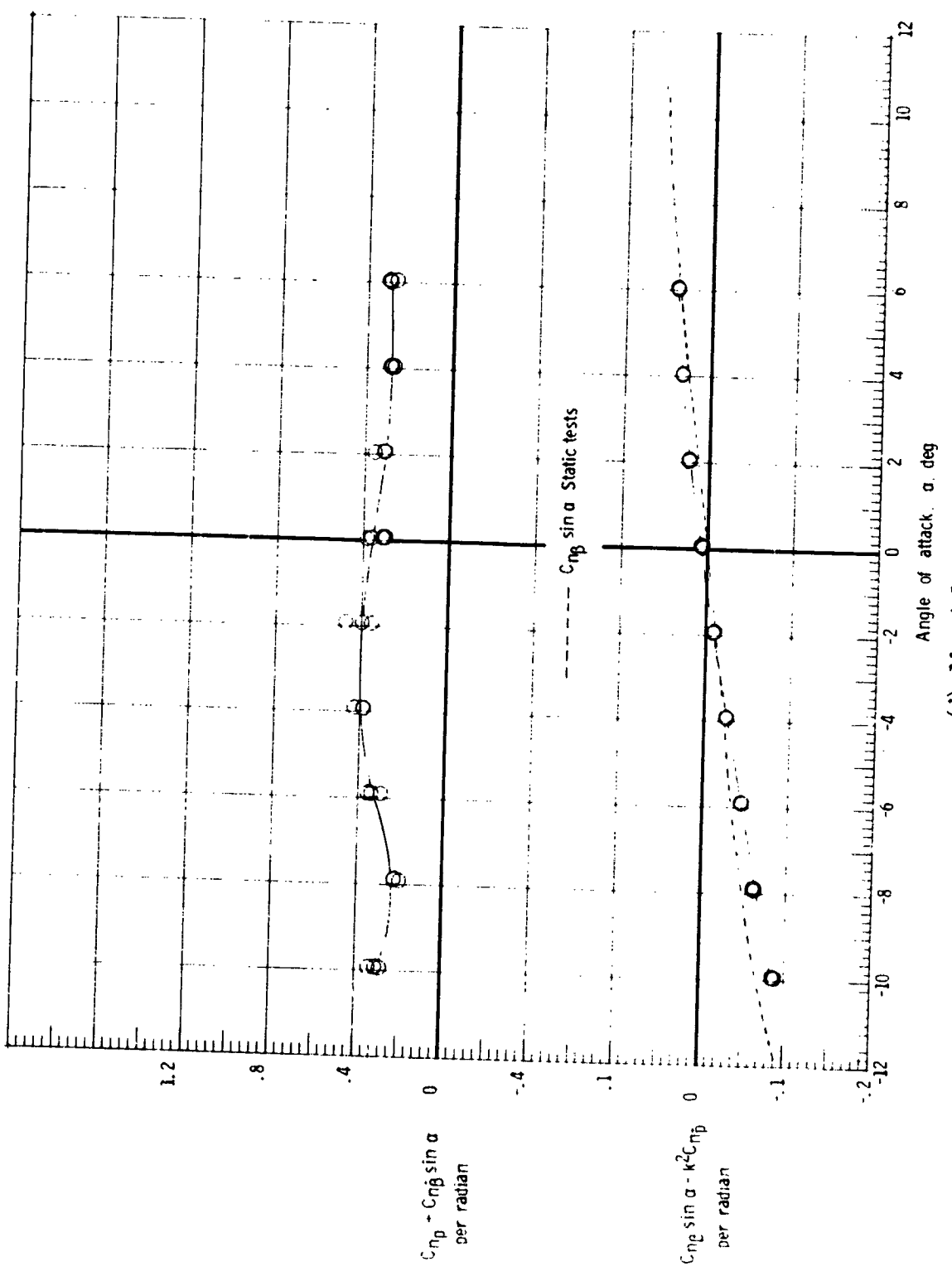
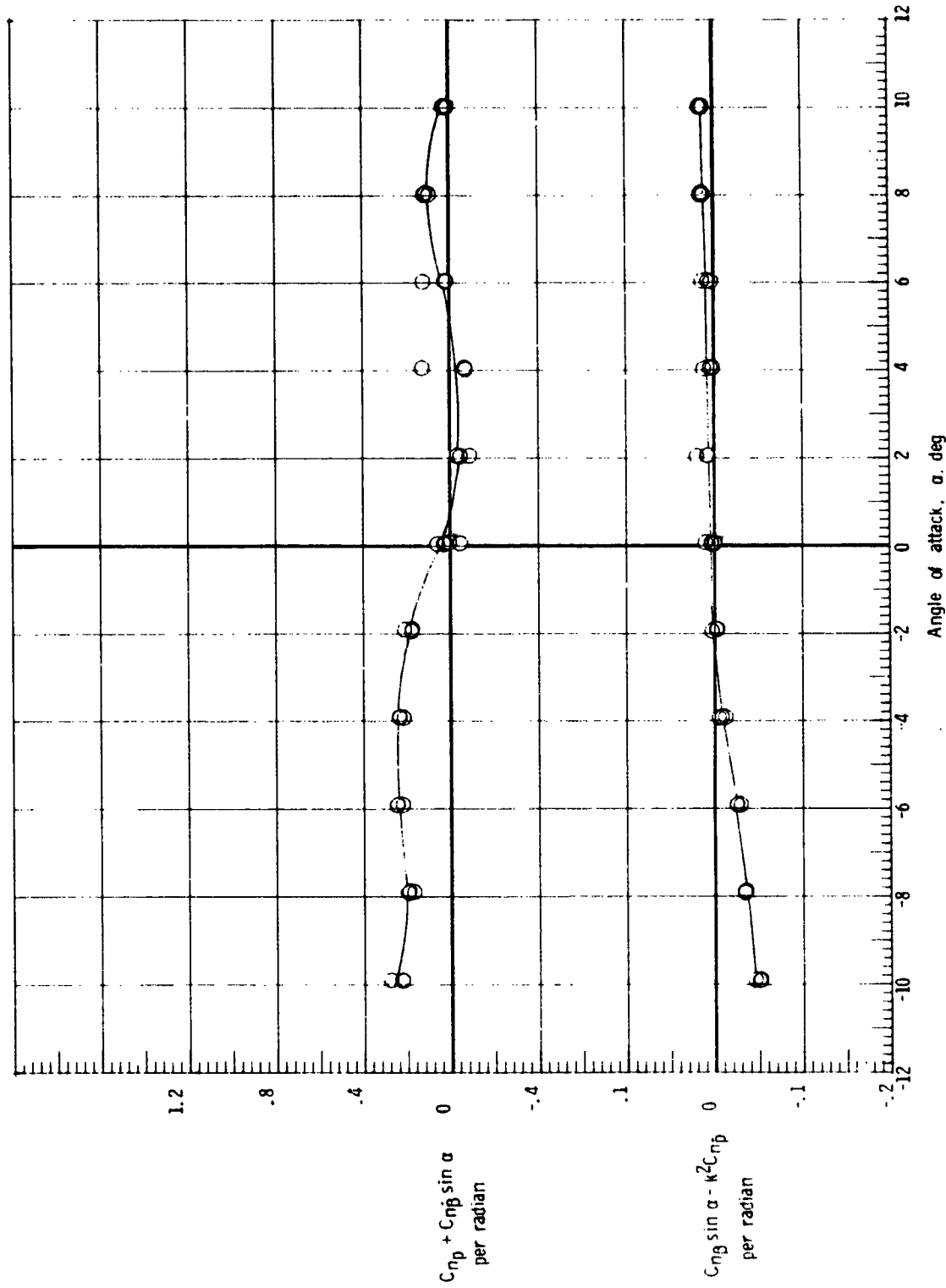
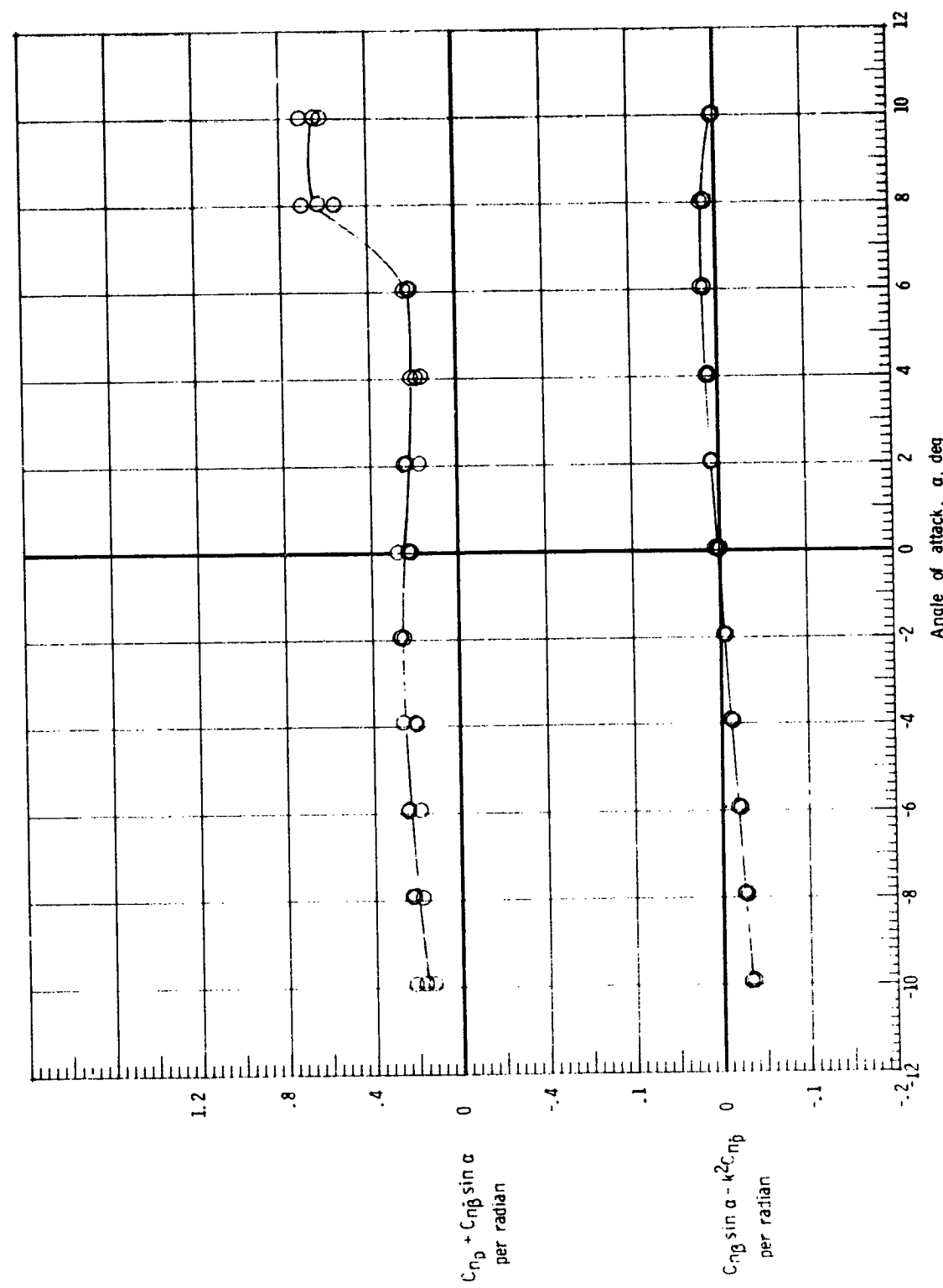


Figure 15.- Concluded.
(d) $M = 1.2$.



(a) $M = 0.3$.

Figure 16.- Yawning moment due to roll rate parameter and yawing moment due to roll displacement parameter for orbiter external-tank configuration.



(b) $M = 0.6$.

Figure 16.- Continued.

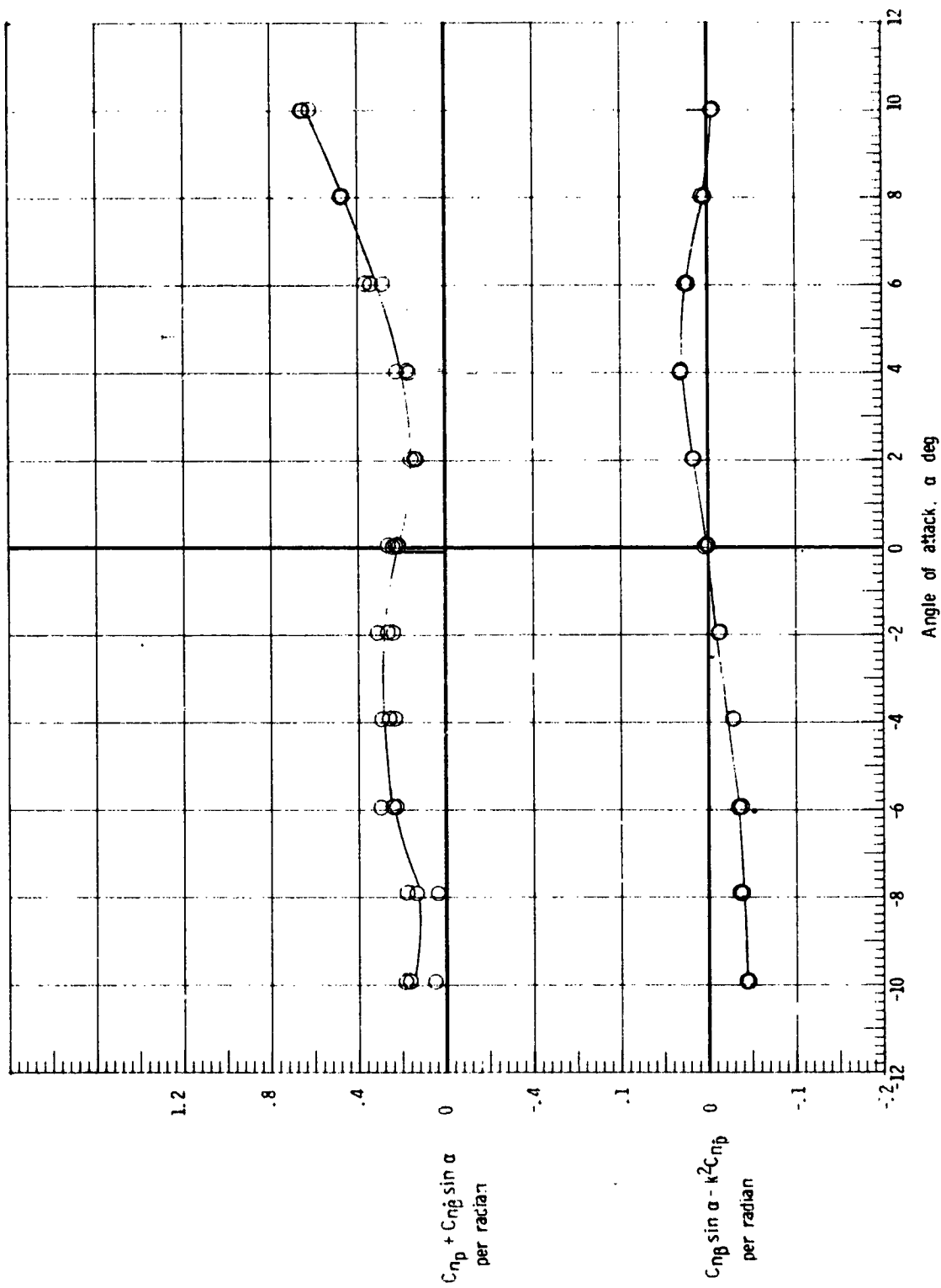


Figure 16.- Continued.

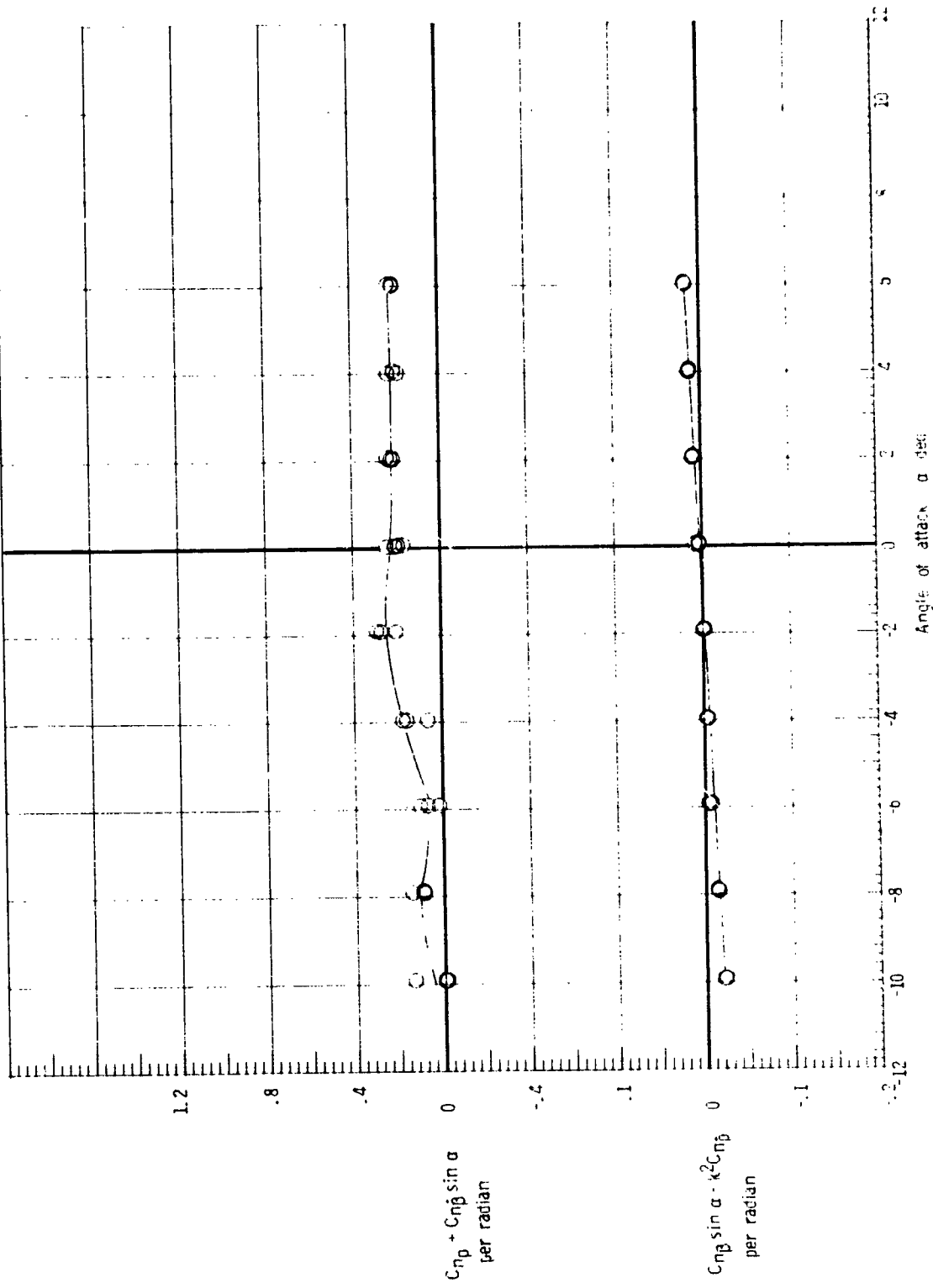


Figure 16.- Concluded.